UNIVERSIDAD MICHOACANA DE SAN NICOLÁS DE HIDALGO

FACULTAD DE INGENIERÍA ELÉCTRICA

DIVISIÓN DE ESTUDIOS DE POSGRADO

Steady State and Transient Waveforms State Estimation in Power Systems

THESIS

Presented to obtain the degree of

DOCTOR OF SCIENCE IN ELECTRICAL ENGINEERING

by

ISMAEL MOLINA MORENO

Ph.D. J. AURELIO MEDINA RÍOS

Thesis Advisor

Morelia, Michoacán, México February, 2017

STEADY STATE AND TRANSIENT WAVEFORMS STATE ESTIMATION IN POWER SYSTEMS

Los Miembros del Jurado de Examen de Grado aprueban la **Tesis de Doctorado en Ciencias en Ingeniería Eléctrica, Opción en Sistemas Eléctricos** de ***Ismael Molina Moreno.***

Dra. Elisa Espinosa Juárez
Presidente del Jurado

Dr. J. Aurelio Medina Rios
Director de Tesis

Dr. Claudio R. Fuerte Esquivel
Vocal

Dr. Antonio Ramos Paz
Vocal

Dr. Manuel Madrigal Martínez
Revisor Externo (ITM-Morelia)

Dr. Félix Calderón Solorio
Jefe de la División de Estudios de Posgrado de la Facultad de Ingeniería Eléctrica. UMSNH
(Por reconocimiento de firmas)

UNIVERSIDAD MICHOACANA DE SAN NICOLÁS DE HIDALGO
Febrero 2017

Dedicatoria

A Dios:

Por haberme permitido llegar hasta este punto y haberme dado salud para lograr mis objetivos y por fortalecer mi corazón e iluminar mi mente y por haber puesto en mi camino a aquellas personas que han sido mi soporte y compañía durante esta estancia de estudios doctorales, además de su infinita bondad y amor.

A mis papás, Francisco y Magdalena:

Por darme la vida, quererme mucho, creer en mí y porque siempre me han apoyado.

A mis dos hijos, Carlos Eduardo y Ángel David:

Que son mi orgullo y mi gran motivación.

A mi compañera de vida, Karla Patricia:

Que ha estado a mi lado todo este tiempo en que he trabajado para lograr esta meta. Para ti, amada esposa, que siempre has creído en mí, que en los duros momentos me has apoyado y tenido paciencia. Para ti, mi amor, que eres mi fuente de inspiración.

Acknowledgments

I wish to sincerely thank my Director of Thesis, Ph.D. J. Aurelio Medina Ríos. His great guidance, his knowledge, his way of working, his persistence, his patience and motivation have been fundamental for my training as a researcher.

I also want to thank my co-adviser, Ph.D. Rafael Cisneros Magaña, his guidance and his patience to conduct research papers developed during the course of this doctoral research.

I would like to thank Professors: Antonio Ramos Paz, Norberto Garcia Barriga, Claudio Ruben Fuerte Esquivel, J. Jesús Rico Melgosa, Fernando Ornelas Téllez, Roberto Tapia Sánchez, Elisa Espinosa Juárez and Manuel Madrigal Martínez for helping me to achieve this aim, my Ph.D. Your work often underestimated, focuses on taking care of the world's knowledge, and allows others to expand their knowledge. You, dear Professors, have helped me to live the dream of surpassing my selves and fulfilling my expectations, and always continue finding the constant improvement, to be a better human being.

I would also like to thank the administrative staff of the UMSNH, especially Ph.D. Felix Calderon Solorio and Mrs. Ma. Guadalupe Mercado Hernández for all the attentions I so kindly received

I specially want to thank Ph.D. Olimpo Anaya Lara for give me the opportunity to conduct a study leave under your guidance at the Department of Electronic & Electrical Engineering, University of Strathclyde, Glasgow, UK.

I also wish to thank the study leave granted by the Instituto Tecnológico de Morelia and to the Consejo Nacional de Ciencia y Tecnología of México (CONACYT) for finance assistance to doctoral studies at the Facultad de Ingeniería Eléctrica, División de Estudios de Posgrado (FIE-DEP) de la Universidad Michoacana de San Nicolás de Hidalgo.

Resumen

Esta tesis propone un marco de referencia en el dominio del tiempo para evaluar fenómenos adversos de la calidad de la energía, particularmente, el contenido armónico y el estado transitorio de sistemas eléctricos de potencia.

El objetivo principal es desarrollar una metodología usando la representación discreta de las ecuaciones diferenciales, definidas por la teoría de circuitos, que modelan a un sistema eléctrico de potencia, que estime las formas de onda con contenido armónico o en estado transitorio en nodos que no estén instrumentados.

Una vez estimada las formas de onda, sea de voltaje o de corriente, el contenido armónico es determinado explícitamente utilizando la transformada de Fourier.

La metodología propuesta aprovecha la propiedad de la simetría de media onda de las formas de onda de voltajes y corrientes en estado estacionario bajo estudio. De este modo, el tiempo computacional empleados en el proceso de estimación, es reducido de uno a medio ciclo.

La formulación del problema de estimación se basa en métodos numéricos de diferenciación en lugar de los de integración de modo que no sea necesario tener conocimiento del estado estacionario para definir un estado inicial. Como consecuencia, el esfuerzo computacional requerido para la estimación, es reducido.

La metodología propuesta incorpora un método que determina el número mínimo de dispositivos de medición que generen una observabilidad completa del sistema eléctrico de potencia. De esta manera se tiene una referencia para optimizar la instrumentación usada en el sistema.

Las mediciones obtenidas del sistema eléctrico de potencia generalmente están contaminadas por ruido aleatorio el cual, es resultado de los márgenes de exactitud de los dispositivos de medición. El proceso de medición filtra las mediciones ruidosas antes de que sean utilizadas en la obtención de la solución final de estimación. Para la estimación de estado armónico, dado que las variables están en estado cuasi-estacionario, se propone utilizar un filtro basado en la transformada de Fourier. Por otro lado, para la estimación de estado transitorio se propone emplear un filtro basado en la respuesta infinita al impulso.

La metodología propuesta es validada mediante la comparación directa de los resultados obtenidos en diferentes casos de estudio para la estimación de estado armónico y de estado transitorio del sistema de prueba con los datos simulados obtenidos utilizando la herramienta SimPowerSystems de Simulink®. Adicionalmente, la metodología es validada usando un sistema de prueba experimental construido en el laboratorio. Los resultados obtenidos son comparados con datos tomados del sistema de prueba.

Finalmente se presentan conclusiones sobre la investigación realizada y se sugieren direcciones para continuar el trabajo de investigación desarrollado en el campo de la estimación de estado de la calidad de energía.

Palabras clave: Estado estacionario, estimación de estado armónico, estimación de estado estacionario, filtro de Kalman, simetría de onda.

Abstract

This thesis proposes a framework in the time domain to evaluate adverse phenomena to power quality, particularly, the harmonic content and the transient state in power systems.

The main aim is to develop a methodology using the discrete representation of the differential equations, defined by circuit theory, which models a power system in order to estimate waveforms with harmonic content or in transient state at unmonitored buses.

Once the waveforms are estimated, be voltage or current, the harmonic content can be determined explicitly using Fourier transform.

The proposed methodology exploits the half-wave symmetry property in voltage and current waveforms. Hence, computational time needed by the estimation process is reduced from one to half cycle.

The formulation of the estimation problem is based on numerical differentiation rather than on integration methods. Therefore, it is not required of an accurate steady state to define an initial state. As a consequence, the computational effort required for estimation is reduced.

The proposed methodology includes a method to determine the minimum number of measuring devices that achieve full observability of the power system. Thus, there is a reference to optimise the instrumentation used in the system.

Measurements obtained from the power system are usually contaminated by random noise which is the result of the margins of accuracy of the measuring devices. The measuring process filters noisy measurements before they are used to obtain the final estimation solution. A filter based on Fourier transform is proposed for the harmonic state estimation. On the other hand, for the transient state estimation, a filter based on the infinite impulse response is proposed.

The proposed methodology is validated through direct comparison against the results obtained in different case studies for the harmonic state estimation and transient state estimation of the test system using the simulated data obtained by the SimPowerSystems tool of Simulink®. In addition, the methodology is validated against an experimental test system built in the laboratory. The obtained results are compared against recorded data taken from the test system.

Finally conclusions about the research work are presented and directions are suggested for further research work in the field of power quality state estimation.

Table of Content

List of Acronyms and Symbols

Acronyms:

A.....Ampere
ATP.....Alternative transients program
BF.....Brute Force
DAQ.....Data acquisition
DFT.....Discrete Fourier Transform
EMTDC.....Electromagnetic Transients with direct current
EMTP.....Electromagnetic Transient Program
END.....Enhanced numerical differentiation
FFT.....Fast Fourier Transform
GPS.....Global positioning system
H.....Henry
HSE.....Harmonic state estimation
Hz.....Hertz
IIR.....Infinite impulse response
ILP.....Integer linear programming
KCL.....Kirchhoff's current law
KF.....Kalman filter
KV.....Kilovolt
KVL.....Kirchhoff's voltage law
KW.....Kilowatt
LS.....Least squares
MVA.....Megavolt-ampere
MW.....Megawatt
ND.....Numerical differentiation
Ω.....Ohm
PCC.....Point of common coupling
PQ.....Power quality
PQSE.....Power quality state estimation
PSCAD.....Power system computer aided design
RMSD.....Root-mean-squared deviation
SVD.....Singular value decomposition
TDHSE.....Time Domain Harmonic State Estimation
THD.....Total Harmonic Distortion
TSE.....Transient state estimation

V .....Volt

VA.....Volt-ampere

VSSE.....Voltage sag state estimation

WLS .....Weighted Least Squares

ZIB .....Zero injection bus

Symbols

a .....Relation of the ideal transformer

$\mathbf{A}$.....State matrix

A_h .....Harmonic order amplitude

$\mathbf{B}$.....Input matrix

$\mathbf{C}$.....Outputs matrix

C_{eq} .....Equivalent capacitance

C_l .....Line capacitance

C_s.....Capacitance at node *s*

$\mathbf{C}_s$ .....Capacitance at busbar s matrix

C_{sj} .....*j-th* capacitance at bus *s*

C_r .....Capacitance at busbar *r*

C_{rj} .....*j-th* capacitance at bus *r*

$\mathbf{D}$.....Direct transmission matrix

$\mathbf{G}$.....Conductance matrix

$\mathbf{e}$ .....Measurement error vector

$\mathbf{E}$.....Measurement noise covariance matrix

E.....Rms generator voltage

f.....Fundamental frequency

$\mathbf{F}$ .....Discrete input matrix

F_{S}.....Sample frequency

g .....General function

h .....Harmonic order

$\mathbf{H}$ .....Measurements matrix

i .....Instantaneous current

$\mathbf{i}$.....Instantaneous current vector

i_{C_s} .....Instantaneous branch current in C_s

i_{C_r} .....Instantaneous branch current in C_r

$\mathbf{i}_{\mathrm{C}}$ .....Instantaneous capacitive branch current vector

$\mathbf{i}_{\mathrm{G}}$ .....Instantaneous conductive branch current vector

i_s .....Instantaneous sending end current from *s*

$\mathbf{i}_s$ .....Instantaneous sending end current vector from *s*

i_r .....Instantaneous receiving end current to *r*

$\mathbf{i}_r$ .....Instantaneous receiving end current vector to *r*

i_{sr} .....Instantaneous branch current from *s* to *r*

$\mathbf{I}$.....Identity matrix

I_h .....Harmonic order current

$I_{h\mathrm{T}}$ .....Harmonic total current

I_{p} .....Peak current

I_T .....Terminal current

k .....Sample number

$\mathbf{K}$ .....Kalman filter gain

$\mathbf{L}$ .....Inductance matrix

L_1.....Primary wind leakage inductance

L_2 .....Secondary wind leakage inductance

L_g .....Generator inductance

L_l .....Line inductance

L_L .....Linear load inductance

L_p .....Transformer inductance referred to primary side

m .....Number of measurements

M .....Order filter

n .....Number of state variables

n_{ch}.....Number of communication channels

N.....Samples per cycle

p .....Number of transmission lines connected at *s*

$\mathbf{P}$.....Error covariance matrix

$\overline{\mathbf{P}}$.....A priori error covariance

P_g.....Real power of generator

P_L.....Real power load

$\mathbf{q}$.....Process noise vector

$\mathbf{Q}$.....Process noise covariance matrix

Q_g.....Reactive power of generator

Q_l.....Line quality factor

Q_L .....Linear load inductance quality factor

r .....Busbar *r*

rad .....Radian

$\mathbf{R}$ ..... Resistance matrix

R_1 ..... Primary wind resistance

R_2 ..... Secondary wind resistance

R_g ..... Generator resistance

R_l ..... Line resistance

R_L ..... Linear load resistance

R_p ..... Transformer resistance referred to primary side

s ..... Busbar *s*

t ..... Time

T ..... Period

T_i ..... Transient index

T_S ..... Sample period

$\mathbf{u}$ ..... Input variable vector

v ..... Instantaneous voltage

v_g ..... Instantaneous voltage at generator

v_r ..... Instantaneous voltage at *r*

$\mathbf{v}_r$ ..... Instantaneous voltage vector at *r*

v_s ..... Instantaneous voltage at *s*

$\mathbf{v}_s$ ..... Instantaneous voltage vector at *s*

v_{sz} ..... Instantaneous voltage measurement at *s*

V_p ..... Peak voltage

V_{pf} ..... Rms voltage in post-fault time interval

V_{tr} ..... Rms voltage in transient time interval

V_T ..... Terminal voltage

T_i ..... Transient index

$\mathbf{x}$ ..... State variable vector

$\hat{\mathbf{x}}$ ..... Estimate state vector

$\dot{\mathbf{x}}$ ..... Derivative of state variable vector

$\bar{\mathbf{x}}$ ..... A priori estimate state vector

$\mathbf{x}_0$ ..... Initial state

$\hat{\mathbf{x}}_\mathrm{h}$ ..... Half-cycle estimated state

X_g ..... Generator reactance

$\mathbf{y}$ ..... Output variable vector

$\mathbf{z}$ ..... Measurement vector

$\tilde{\mathbf{z}}$ ..... Filtered measurement vector

Z_l ..... Line impedance

α.....Thyristor firing angle

θ_h .....Harmonic order angle

$\emptyset$.....Internal angle of generator voltage

η_{sa} .....Saving index

∞ .....Infinite

ω .....Angular frequency

$\mathbf{\Phi}$.....State transition matrix

List of Figures

List of Tables

List of Contributions

Published papers conference Papers indexed by ISI Thomson:

1. **Experimental time domain harmonic state estimation using partial measurement,** Ismael Molina-Moreno, Aurelio Medina, Rafael Cisneros-Magaña, IEEE North American Power Symposium (NAPS 2014), Pullman, Washington, USA, September 07-09, 2014

2. **Time-domain harmonic state estimation using filtered measurements based on Fourier transform,** Ismael Molina-Moreno, Aurelio Medina, Rafael Cisneros-Magaña, IEEE North American Power Symposium (NAPS 2015), Charlotte, North Caroline, USA, October 04-06, 2015.

3. **Methodology for optimal bus placement to integrate wind farm optimizing power flows,** Ismael Molina-Moreno, Aurelio Medina, Rafael Cisneros-Magaña, IEEE International Autumn Meeting on Power, Electronics and Computing (ROPEC), Ixtapa, Guerrero, México, November 04-06, 2015.

4. **Harmonic and transient state assessment in the time-domain,** Ismael Molina-Moreno, Aurelio Medina, Rafael Cisneros-Magaña, Olimpo Anaya-Lara, IEEE International Autumn Meeting on Power, Electronics and Computing (ROPEC), Ixtapa, Guerrero, México, November 09-11, 2016.

Paper in journals Indexed by Journal Citation Reports (JCR), under review:

1. **Time domain harmonic state estimation in unbalanced power networks based on optimal number of meters and the principle of half-wave symmetry,** Ismael Molina-Moreno, Aurelio Medina, Rafael Cisneros-Magaña, Olimpo Anaya-Lara, *IET Generation, transmission & distribution*.

2. **A methodology for transient state estimation based on numerical derivatives using optimal number of measuring devices and filtered measurements,** Ismael Molina-Moreno, Aurelio Medina, Rafael Cisneros-Magaña, Olimpo Anaya-Lara, *IEEE Transactions on Power Delivery*.

Chapter 1 An introduction to power quality state estimation

1.1 Introduction

Power quality (PQ) is the general term to describe the quality of power supply. However, it is actually the quality of the voltage that is being addressed in most cases since the power supply system can only control the quality of the voltage; it has no control over the currents that particular loads might draw. However, a PQ problem can be defined as any power problem revealed in voltage, current, or frequency deviations that result in failure or misoperation of customer equipment [Kusko and Thompson 2007].

Ideal power quality for the source of energy to an electrical load is represented by a sinusoidal single-phase waveform or the three-phase voltage waveforms. In practical terms, the amplitude, frequency, and any distortion of the waveforms must remain within prescribed limits to consider good power quality [Kusco and Thompson 2007].

Power quality problems encompass a wide range of different phenomena, as follows [Dugan *et al.* 2002]:

- Transients
  - Impulsive transient
  - Oscillatory transient
- Long-duration voltage variations
  - Over-voltage
  - Under-voltage
  - Sustained interruptions
- Short-duration voltage variations
  - Interruption
  - Sags
  - Swells
- Voltage unbalanced
- Voltage fluctuation
- Power frequency variations
- Waveform distortion
  - DC offset
  - Harmonics
  - Inter-harmonics
  - Notching
  - Noise

Electric utilities, manufactures and end users of electric power are becoming increasingly concerned about the PQ delivered to factories, commercial establishments, and residences. The ultimate reason why they are interested in power quality is mainly of financial type. There are economic impacts on utilities, customers, and suppliers of load equipment [Dugan *et al.* 2002], [Kusko and Thompson 2007].

Measurements play an important role for almost any PQ issue. This is the primary method of characterizing the problem that is being evaluated. When performing measurements, it is important to record impacts of the PQ variations at the same time so problems can be appropriately correlated with possible causes. Solutions need to be evaluated using a system perspective, and the economic and technical limitations must be both considered. Possible solutions are identified at all levels of the system from utility supply to the end-use equipment that is being affected [Dugan *et al.* 2002], [Kusko and Thompson 2007].

PQ assessment is not carried out regularly and systematically; instead an ad hoc measurement procedure is used to ensure that the point of common coupling (PCC) voltage meets the specified distortion limits, but the local area solution affects the rest of the system. The global assessment has practical limitations owing to the restricted number of monitoring points and insufficient knowledge of the system parameters. As an alternative to obtain a global assessment, the power quality state estimation (PQSE) has been addressed [Arrillaga *et al.* 2000], [Watson 2010], [Farzanehrafat and Watson 2013]. In [Farzanehrafat and Watson 2013], PQSE is presented as a class of techniques as shown in Fig. 1.1. Despite the different formulation and quantities they use, the common feature is that they are applying state estimation techniques to PQ problems, such as: harmonic state estimation (HSE), identification of harmonic sources, transient state estimation (TSE), and voltage sag state estimation (VSSE). Therefore, PQSE is not one particular type of analysis but covers many different types in PQ issues. Hence, the main objective of PQSE is to determine the magnitude of phenomena that adversely affect PQ and as consequence the associated PQ indices at unmonitored busbars in power systems.

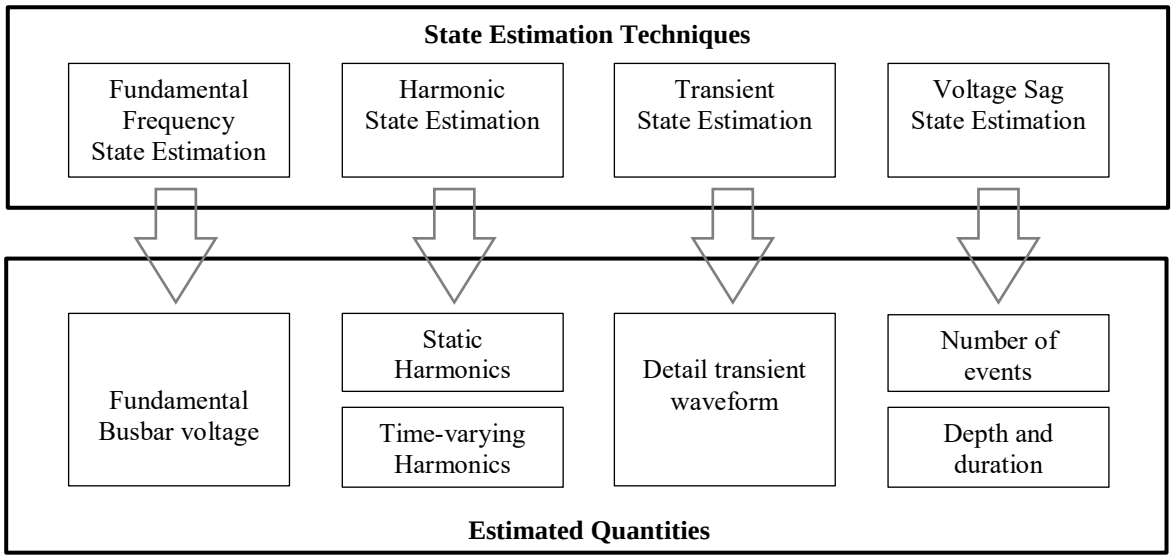

Fig. 1.1 Different type of PQSE [Farzanehrafat and Watson 2013]

1.2 State of the art

This research work focuses on HSE and TSE. Both fields of knowledge are concisely described in next subsections.

1.2.1 Harmonic state estimation

Harmonic contamination is generated by different elements of the power network such as power converters, transformer magnetic saturation and diverse nonlinear loads, which are commonly connected to power systems. Of particular concern is the voltage harmonic distortion due to nonlinear loads such as static power converters, extensively used in industry, considered as being among the largest nonlinear loads. These devices are not only useful because they can convert ac to dc, dc to dc, dc to ac, and ac to ac but they also inject harmonic currents into the power system; hence, nonlinear loads can be represented as an injection of current sources and the network by its electrical parameters [IEEE 1995].

It is necessary to maintain the monitoring of the harmonic levels to verify they meet the specified limits established by standards [IEEE 1995].

HSE can be classified into two types, i.e.

a. Static HSE. It occurs in a steady state or static conditions, the state is a harmonic state snapshot.

b. Dynamic HSE. It is presented when the harmonic state varies over time.

In 1989, Heydt started to study HSE [Heydt 1989]. He sets the inverse problem for harmonic power flows on a network, i.e. given the harmonic currents in certain lines and harmonic voltages at certain busbars, find the sources of such harmonics. To solve this problem, Heydt proposed a static harmonic estimator. The problem is formulated in the frequency domain where voltage and current measurements are not performed on all the busbars. Hence, each harmonic component is partitioned in observable and unobservable. Due to there are more variables than equations, the under-determined matrix must be inverted using its pseudo inverse [Monticelli 1999], [Abur and Exposito 2004].

In 1991, Beides and Heydt proposed a dynamic HSE using the Kalman filter (KF) [Beides and Heydt 1991]. The system is considered quasi-static, i.e. it has a small variation. The network is not modelled, i.e. it is considered that the next state is the same with a small variation. However, it is necessary determine an initial condition. A computer program called HARFLOW calculates the harmonic flow to determine the initial conditions. Then for a period of 24 hours, the HSE is performed; estimations are obtained every 15 minutes. Harmonic busbar voltages were used as state variables, provided by harmonic measuring instruments.

In 1994, Meliopoulos *et al*. included the synchronised measurements using the global positioning system (GPS) [Meliopoulos *et al*. 1994]. In each instrumented busbar, the voltage and current waveforms are obtained, which in turn are converted to the frequency domain. The harmonic component are measured and sent to a central station to make the corresponding estimation.

In 1996, Du *et al*. reported a summary of relevant criteria to judge which estimation algorithm is the "best" and claimed that under certain conditions; these criteria are equivalent to each other. A system-wide continuous harmonic state estimator of three-phase asymmetric power systems, with development of its

reduced mathematical models and algorithm, as well as its application to a New Zealand test system has been proposed [Du *et al*. 1996]. The method is extended to account for unbalance conditions and synchronized measurements. The main contribution is that converts an under-determined problem in an over-determined problem when the concept of suspected busbars and busbars that do not inject harmonics are included.

In 2000, Matair *et al*. addressed the problem of remote estimating where not necessarily the power system is fully observable [Matair *et al.* 2000]. If the measuring matrix is ill conditioned, the pseudo inverse based on least squares (LS) method generates a considerable error. The method is based on the singular value decomposition (SVD). The SVD can be used for computing the pseudoinverse of a matrix.

In 2005, Yu *et al*. proposed an adaptive filter for dynamic HSE and harmonic injection tracking to switch between two basic process noise covariance matrix models [Yu *et al*. 2005]. The method is an improved version of [Beides and Heydt 1991] since considered sudden changes in the harmonic tracking. The method replaces the optimal noise covariance matrix with one of two basic process noise covariance matrices, one for steady state and other for sudden change in operation conditions. Hence a difference in measurement is evaluated each step and using student's t statistical model, the noise covariance matrix is selected.

So far, HSE can be defined as a methodology that uses a set of harmonic measurements taken from a power system to estimate the harmonic content in unmonitored buses. Thus, the meters used have been power quality meters, and the state variables have been the magnitude and phase of each harmonic component.

In 2012, Medina and Cisneros-Magaña proposed an alternative methodology for HSE assessment of power networks [Medina and Cisneros-Magaña 2012]. The method formulates the HSE problem in the time domain instead of frequency domain.

The time domain HSE (TDHSE) methodologies use voltage and current waveforms. Hence, the meters are data acquisition (DAQ) systems. DAQ systems can be synchronised using a global positioning system (GPS) reference time [National Instruments 2016]. The waveforms are sampled generating a set of points that form the waveforms. Then, the TDHSE can be defined as a methodology that estimates the waveforms at unmonitored buses using voltage and current waveforms as measurements. The waveforms are distorted due to implicitly contain a harmonic content. To explicitly obtain the harmonic content, a method for that specific purpose must be used, e.g. the Fourier transform.

The time domain method in [Medina and Cisneros-Magaña 2012] is based on the application of the KF. If considers the linear-time-invariant case by means of a first-order ordinary differential equation (ODE) set and defining the appropriate state variables, the model is written in the classical form. The formulated continuous model is discretised. The method requires of an initial condition which is determined using Poincare´ map and extrapolation to the limit cycle using a numerical differentiation (ND) procedure [Semlyen and Medina 1995], [Medina *et al*. 2003], [Segundo and Medina 2010].

The KF theory is widely explained in [Grewal and Andrews 2001], [Moreno *et al*. 2009]. The KF and its variants evaluate the state estimation in the frequency domain [Chen *et al.* 2010], [Ray and Subuchi 2012]. The KF has been applied to assess the dynamic HSE [Beides and Heydt 1991], [Ma and Girgis 1996], [Chen *et al.* 2010], [Ghahremani and Kamwa 2011]. However, all these methodologies use phasor quantities.

The KF algorithm is summarised in Fig. 1.2. A project state and a project covariance are computed using the ODE set that models the power network. The first projection needs an initial condition. A measurements set is taken from the power network and are fed back to update the state and the covariance. The current estimation is taken as initial condition for the next estimation. The process is repeated until all data is analysed.

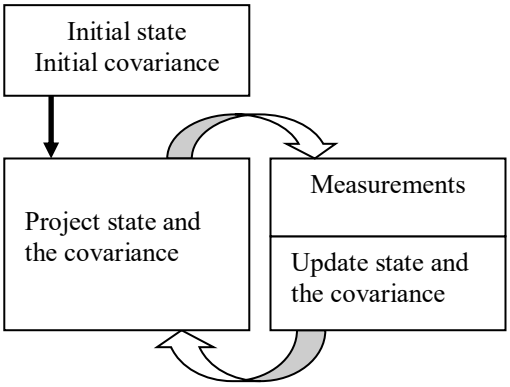

Fig. 1.2 Kalman filter algorithm

In 2014, Cisneros-Magaña *et al.* proposed an improvement to the methodology in [Medina and Cisneros-Magaña 2012]; the method exploits the property of half-wave symmetry in voltage and current waveforms, [Cisneros-Magaña *et al.* 2014]. The method uses this feature to make more efficient the ND method, named enhanced numerical differentiation (END), to obtain the periodic steady state solution of a power network taken as the initial state to the KF method. Then, with the periodic steady state as initial condition, the estimation of harmonics is evaluated by means of the KF as in [Medina and Cisneros-Magaña 2012].

1.2.2 Transient State Estimation

Electromagnetic transients or simply transients are severe short-time variations of voltage and current in a power system. Transients are mainly generated by switching events and system disturbances such as faults or sudden load and generation variations. The energy exchanges, due to transients, subject the circuit components to higher stresses, resulting in excessive currents or voltage variations. Computational programs such EMTDC [EMTDC 2005], EMTP [EMTPTB 1981], ATP [ATP 2002] or similar programs have been used to compute the solution during a specific disturbance event. Thus, the adverse effects of transients in the power system can be adequately predicted.

In 2007, Yu and Watson introduced the concept of TSE as a reverse function to transient simulation, i.e. the main objective of TSE is to determine the origin of the disturbances taking a limited number of measurements as shown in Fig. 1.3 [Yu and Watson 2007]. The power system, represented by its discrete equivalent RLC branches, is described by a set of current and voltage state equations. Each capacitive and

inductive component of the power system is taken as state variable and they are modelled by their differential equations which are discretized using backward Euler integration formula. By combining these equations with appropriate state variables, the complete state model of the power system is achieved. Hence, the model of the system is large and complex due to the number of lines and busbars. Considerable computational effort for the solution may be needed.

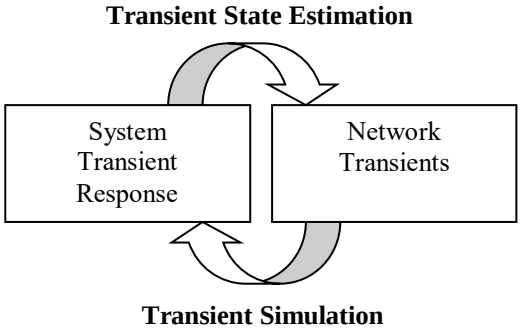

Fig. 1.3 Reverse process relating the transient simulation and transient state estimation

[Cisneros-Magaña and Medina 2013] formulate the TSE problem as in [Yu and Watson 2007], i.e. the busbar voltages and line current are again taken as state variables and the SVD is the base to solve the TSE. The SVD advantages are that can generate a solution of ill conditioned matrices and under-determined cases and also can make the intrinsic observability analysis during the state estimation [Moghadasian *et al*. 2010], [Arefi *et al*. 2011]. To solve the problem of initial condition, which is usually zero and takes time to reach the steady state, the numerical differentiation method is added to obtain faster the periodic steady state of the power system.

[Farzanehrafat and Watson 2013], [Watson and Farzanehrafat 2014] present a problem formulation for the TSE where the busbar voltages are taken as state variables. The algorithm is based on the numerical integrator substitution method. However, numerical integration methods have the disadvantage that requires of an initial condition. If the analysis begins when the power system is energized, then the initial conditions can be zero and the initial transients can be observed. However, if the power is already energized, the initial condition cannot be zero.

[Cisneros-Magaña *et al.* 2014] exploit the half wave symmetry in the voltage and current waveforms to minimize the computational effort to evaluate the pre-fault condition, i.e. the periodic steady state. Then, with the periodic steady state as initial condition, the estimation of transients is evaluated by means of the KF as in [Cisneros-Magaña and Medina 2013].

1.2.3 Optimal placement of measuring devices to evaluate HSE and TSE

The methods to evaluate HSE have a particular characteristic; they do not take in count the use of optimal number of measuring devices and their optimal placement. This challenge task has been addressed as an

independent task. Since measuring devices used in conventional HSE have been PQ meters, the methods to optimise the number of them have been in the frequency domain. Several contributions have been reported, these are concisely describe next:

[Farach *et al*. 1993] utilises the sensitivity analysis and the minimum variance criterion to solve this problem. In this setting, the best choice of instrumented busbars is the one which results in bus-admittance submatrix being as well-conditioned as possible. The brute force (BF) method can always be used to compute a comparative measure for all possible combinations of sensor placement. Using ta sequential procedure, a reduction in the number of possible combinations is obtained. This method uses *m* available meters.

[Madtharad *et al*. 2005] follows a similar procedure than in [Farach *et al*. 1993] but the analysed matrix is the measurement matrix.

[Ketabi *et al*. 2011] reports a seeker optimization algorithm which is a relatively new intelligent algorithm that may be used to find optimal (or near optimal) solutions to numerical and qualitative problems. The method is used to find the optimal placement of PQ meters for HSE.

[Almeida and Kagan 2013] proposes a method based on the network topology evaluation. The method introduces the concept of optimal monitoring, defined as a monitoring system that can fully observe the power network and its cost is as low as possible. The measuring devices are PQ meters; a modified Genetic Algorithm is used to solve the optimization problem.

[Saxena *et al*. 2014] introduces a methodology to identify the multiple harmonic sources along with their harmonic injection levels in a power system using optimally placed harmonic measurement devices. Binary particle swarm optimization is used to find the optimal locations of meters. The measuring devices are PQ meters.

There are no reported methods to obtain the optimal number of measuring devices and their optimal placement to evaluate TSE.

1.3 Motivation of this research work

Power quality is a matter of concern to utilities, end users, and equipment suppliers. The main reason is the economic part; it is estimated that poor PQ causes considerable economic losses [Dugan *et al*. 2002], [Kusko and Thompson 2007]. The disturbances that affect adversely the PQ are harmonics, electromagnetic transients, voltage sags, voltage swell, voltage notch, and flicker, among others [Kusko and Thompson 2007], [Dugan *et al.* 2002], [Arrillaga *et al.* 2000]. Harmonics and electromagnetic transients are of particular interest.

Harmonic distortion is one of the issues that adversely affects the PQ since it causes losses, e.g. heating and vibration [Kusko and Thompson 2007]. Today, the progressive increase in nonlinear loads is notorious. Because switched systems tend to be more efficient, its use has been increased. Despite operation efficiency of switched systems, which has resulted in the increase of its use in practical electric networks, they are identified as being one of the main harmonic sources of the network. Although the amount of harmonics that can be injected to the grid is regulated, monitoring is needed in order to meet established standards [IEEE

1995]. The simplest solution to this problem is the placement of power quality meters at each bus of the network. However this is not always possible. There are several reasons for this lack of monitoring. One reason can be the non-feasibility due to the size of the network [Arrillaga et al. 2000]. Another reason can be due to unexpected events, e.g. damage to the equipment or failure in the communication. Or simply, it can be the need to optimise resources in the monitoring implementation. Thus, to face the problem of lack of monitoring, the HSE has been arisen. Hence, HSE can be defined as a methodology which deals with a limited number of measuring devices to estimate the harmonic content in unmonitored buses. HSE has continuously been reported in the literature, e.g. [Heydt 1989], [Beides and Heydt 1991], [Meliopoulos *et al*. 1994], [Du *et al*. 1996], [Matair *et al*. 2000], [Yu *et al*. 2005], [Medina and Cisneros-Magaña 2012], [Cisneros-Magaña *et al*. 2014].

Electromagnetic transients or simply transients are very common in a power system. Transients are mainly generated by disturbance events such as faults in lines or switching operation among other intentional or unintentional disturbance events. Transients can damage prematurely the isolation of system components or mistakenly activate a protection component or damage a system load. Computational programs such EMTDC [EMTDC 2005], EMTP [EMTPTB 1981], and ATP [ATP 2002] or similar programs have been used to compute the transient state under a disturbance event located at specific place. However, it is necessary to monitor such transients in the power system generated by a real disturbance event to verify that these transient values are within the standards. A similar situation to the harmonic assessment issue arises, i.e. the number of measuring devices is limited and most of the busbars of interest are not monitored. Hence, TSE which is defined as the inverse problem, where the response of the power system is given and the fault location must be located, has been addressed to treat this problem [Yu and Watson 2007], [Cisneros-Magaña and Medina 2013], [Farzanehrafat and Watson 2013], [Watson and Ali 2014], [Cisneros-Magaña *et al*. 2014].

The TDHSE is a recently alternative methodology to face HSE [Medina and Cisneros-Magaña 2012], [Cisneros-Magaña and Medina 2013], [Cisneros-Magaña *et al.* 2014]. On the other hand, by its proper nature, TSE is analysed in the time domain. However, it is an opportunity to continue conducting research taking advantages of achievements in the TDHSE.

Therefore, it is necessary to continue conducting research in the field of state estimation both for harmonics and transients to generate new contributions which, inter alia,

- Optimise the instrumentation implementation.
- Increase the accuracy of estimation.
- Reduce the complexity of the methodology used.
- Implement lab prototypes to deal with experimental data instead of synthetic data.

1.4 Aims

1.4.1 Main aim

To develop a time domain mathematical formulation based on voltage and current waveform measurements taken from a power system that can estimate the corresponding waveforms, which can implicitly contain a harmonic content or be in the transient state, at unmonitored buses in power system; the methodology should be efficient respect to instrumented resources and the computational effort needed to obtain the state estimation assessment.

1.4.2 Particular aims

- To conduct research on the state of the art concerning power quality state estimation, particularly waveforms which implicitly contain harmonic content or is in transient state at unmonitored buses in power systems.
- To extend the concept of the optimal measuring system defined for HSE in the frequency domain to the TDHSE.
- To develop an experimental test system to conduct case studies to validate the methodologies proposed in this research work.
- To formulate in the time domain, a mathematical model to estimate steady and transient waveforms that can be used to implicitly determine the harmonic state of a power system using a limited number of measurements taken from power system under balanced conditions.
- To extend the above methodology to unbalanced operation conditions and to reduce the computer effort needed to determine the steady state using an arbitrary initial state, and exploiting the half-wave symmetry property.
- To develop an alternative mathematical formulation to estimate the harmonic state of power systems through waveforms and using filtered measurements. The filter used will be one based on the Fourier transform. Here, it is assumed that the waveforms under study are periodic and quasi-stationary. The case studies will be under balanced conditions.
- To extend the methodology, defined in the previous particular aim, to unbalanced conditions and to reduce the execution time exploiting the half-wave symmetry property.
- To develop an alternative mathematical formulation to estimate the transient state of power systems using filtered measurements. The filter used will be one based on the infinite impulse response. The case studies will be under balanced and unbalanced conditions.

1.5 Contributions

The main contributions of this research work can be summarized as follows:

- The development of an experimental test laboratory set-up to validate, using practical data instead of synthetic ones, the methodologies proposed in the field of estimation, among others.
- A methodology based on Kalman filter to estimate the harmonic state using not only partial measurements but also an under-determined condition.
- A methodology to estimate the harmonic state based on Kalman filter that can find itself the initial state and exploits the half-wave symmetry in voltage and current waveforms to reduce the computer effort.
- A methodology to estimate the harmonic state without a priori knowledge of the harmonic sources.
- A methodology to estimate the harmonic state not only without a priori knowledge of the harmonic sources but also exploiting the half-wave symmetry in voltage and current waveforms to reduce the computer effort.
- The development of a methodology based on analytical tools in the time domain that allows determines the estimation of transient state using a limited number of filtered measurements.
- The proposed methodology includes a method based on topological analysis to obtain the minimum number of measuring devices that generates full observability optimising the instrumentation implementation.
- Digital tools for HSE and TSE analysis.

1.6 Methodology

The methodology of this research work is the implementation of the power quality state estimator using both synthetic and experimental data for the following processes and their use in different case studies:

- Generate the appropriate mathematical background for the proposed methodologies
- To implement the methodologies for HSE and TSE assessment.
- Conduct case studies under balanced conditions.
- Extend the balanced case studies to unbalanced ones.
- Determine the adequate theoretical test systems to conduct case studies.
- Validate the obtained results with those obtained by commercial software for simulation
- Use the experimental test system to extend the validation using practical data.

1.7 Thesis outline

Chapter 1 presents the motivation to conduct research in the field of power quality state estimation and a review of the state of the art associated with the state estimation in power systems with particular reference to harmonic and transient state estimation. As a result, the general and particular objectives and the main contributions to be achieved are established. The methodology to this research work is addressed as well as the description of the rest of the chapters is given.

Chapter 2 presents an alternative methodology based on Kalman filter and the design of a prototype to conduct experimental study cases in the field of harmonic and transient state estimations.

Chapter 3 describes an enhanced methodology to estimate the harmonic state based on Kalman filter that can find itself the initial state.

Chapter 4 presents a formulation for harmonic state estimation using derivative methods instead of integration ones. It presents a filter based on Fourier transform to mitigate the noise in measurements used in the methodology. It also presents case studies under balanced condition to validate the proposed methodology.

Chapter 5 extends the previous methodology to estimate the harmonic state. It explains how the principle of half-wave symmetry is exploited in the evaluation of the state estimation problem.

Chapter 6 describes an alternative methodology to estimate the transient state in power systems. It details how the method finds the initial state taken from the measurements as well as how methodologies to find the optimal number of measuring devices in the frequency domain can be extended to the time domain framework.

Chapter 7 gives the general conclusions drawn from this research work, addresses and suggests ideas for further research work to be conducted in the same field of knowledge.

Chapter 2 Harmonic state estimation using waveform measurements

2.1 Introduction

The harmonic state estimation analysis has been conventionally developed in the frequency domain. This methodology needs to measure the amplitude and phase angle of the harmonic components of the related waveforms. This chapter presents a time domain methodology based on a simplified network model and KF to estimate waveforms at unmonitored buses in power systems. The estimate waveforms implicitly contain a harmonic content that distorts the waveforms. Thus, measurements are sampled voltage and current waveforms registered by a DAQ system. The HSE is explicitly determined by applying the Fourier transform to the estimated waveforms. This indirect way to obtain the HSE is defined as TDHSE.

The proposed methodology is tested on an experimental electric power test system developed in the laboratory. The reported case study consists of a three-phase balanced system with a nonlinear load. An under-determined measurement model case is tested.

The results are validated by direct comparison of the state estimation response against the data taken from laboratory experimental measurements.

2.2 Methodology

The TDHSE based on the KF algorithm encompasses four parts: initial condition, model definition of the plant, measuring process to take data from the plant, and KF method to obtain the harmonic state [Medina and Cisneros-Magaña 2012], [Cisneros-Magaña *et al.* 2014]. The steps of this methodology are shown in Fig. 2.1. In addition, to change from time domain to frequency domain, the fast Fourier transform (FFT) is used.

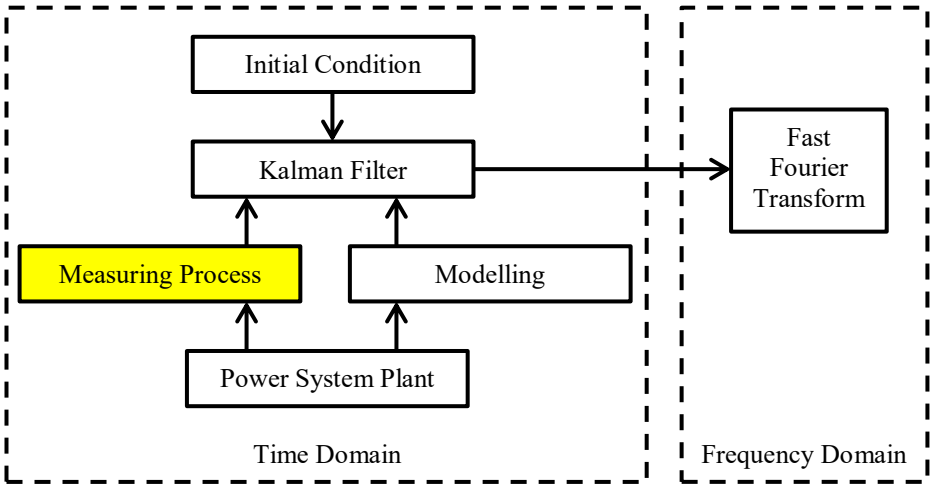

Fig. 2.1 Time domain harmonic state estimation methodology

2.2.1 Modelling

The solution of the TDHSE requires the definition of a network model in order to be applied in the KF algorithm as shown in Fig. 2.1.

An electrical power system can be represented in the state space through first-order ODE set in the continuous time as,

$$\dot{\mathbf{x}}(t) = \mathbf{A}\mathbf{x}(t) + \mathbf{B}\mathbf{u}(t) \tag{2.1}$$

$$\mathbf{y}(t) = \mathbf{C}\mathbf{x}(t) + \mathbf{D}\mathbf{u}(t) \tag{2.2}$$

where $\mathbf{x} \in \mathbb{R}^{n}$ is the state variable, $\mathbf{A} \in \mathbb{R}^{n\times n}$ is the state matrix, $\mathbf{u} \in \mathbb{R}^{r}$ is the input vector, $\mathbf{B} \in \mathbb{R}^{n\times r}$ is the input matrix, $\mathbf{y} \in \mathbb{R}^{m}$ is the output vector, $\mathbf{C} \in \mathbb{R}^{m\times n}$ is called the output matrix, and $\mathbf{D} \in \mathbb{R}^{m\times r}$ is called the direct transmission matrix which is usually zero.

The continuous time model formulated by (2.1) and (2.2) can be transformed into the discrete time by several methods [Ogata 1995]. The discrete transform of $\dot{\mathbf{x}}$ can be obtained if t is approximated by kT_S, where T_S is the sampling period and k is the number of sample.

If the notation of kT_S is represented by k, the continuous model formulated in (2.1) and (2.2) can be discretised as,

$$\mathbf{x}[k] = \mathbf{\Phi}\mathbf{x}[k-1] + \mathbf{F}\mathbf{u}[k] \tag{2.3}$$

$$\mathbf{z}\,[k] = \mathbf{H}\mathbf{x}[k-1] \tag{2.4}$$

Please note that (2.2) is exchanged by the measurement model defined in (2.4) where $\mathbf{z} \in \mathbb{R}^{m}$ is the vector that contains the *k-th* sampled measurements taken from the plant of the system. $\mathbf{H} \in \mathbb{R}^{m\times n}$ is the measurement matrix.

The discrete model formulated in (2.3) and (2.4) is ideal; it means that it does not contain error. In practical cases both plant and measurements present errors, these are represented as follows,

$$\mathbf{x}[k] = \mathbf{\Phi}\mathbf{x}[k-1] + \mathbf{F}\mathbf{u}[k] + \mathbf{q}[k] \tag{2.5}$$

$$\mathbf{z}\,[k] = \mathbf{H}\mathbf{x}[k-1] + \mathbf{e}[k] \tag{2.6}$$

where $\mathbf{\Phi} \in \mathbb{R}^{n\times n}$ is the transition state matrix, $\mathbf{F} \in \mathbb{R}^{n\times r}$ is the discrete input matrix, $\mathbf{q} \in \mathbb{R}^{n}$ represents the error vector associated to the plant and $\mathbf{e} \in \mathbb{R}^{m}$ is the error associated to measuring devices.

2.2.2 Measuring process

The main contribution to this methodology is in the measuring process, shown in Fig. 2.1 as highlighted block. In [Medina and Cisneros-Magaña 2012], the KF is applied for an over-determined measurement state estimation equation with an observable system condition. The number of measurement is greater than the number of state variables, i.e. $m > n$. In [Cisneros-Magaña *et al.* 2014] the $\mathbf{z}$ vector takes all line currents and their derivatives as measurements. Hence, the contribution in this methodolgy is to explore the behaviour of the KF when is applying not only partial measurements but also an under-determined condition are applied to estimate the state variables that are not monitored, i.e. $m < n$.

2.2.3 Kalman filter

The KF theory is widely explained in [Grewal and Andrews 2001], [Moreno *et al*. 2009]. It evaluates the state estimation based on minimizing the squared error defined as,

$$\mathbf{e}[k] = \mathbf{x}[k] - \hat{\mathbf{x}}\,[k] \tag{2.7}$$

where $\hat{\mathbf{x}}\,[k]$ is defined as an estimated state at *k-th* sample.

The KF is a recursive algorithm, i.e. it is required the state from the previous time step (a priori state) and the current measurement to compute the estimate for the current state (a posteriori state). The KF algorithm assumes that $\mathbf{x}[1]$ is known, i.e. the initial state at $k = 1$. The KF oscillates between the a priori state named prediction and the a posteriori state named update as shown in Fig. 1.2.

In this methodology the KF is applied in the time domain. A waveform cycle is divided in *N* samples. Each sample is processed by KF in two steps:

First, using (2.3) a priori state $\bar{\mathbf{x}}$ and a priori error covariance matrix $\bar{\mathbf{P}}$ are predicted, i.e.

$$\bar{\mathbf{x}}[k+1] = \mathbf{\Phi x}[k] + \mathbf{Fu}[k+1] \tag{2.8}$$

$$\bar{\mathbf{P}}\,[k+1] = \mathbf{\Phi P}[k]\mathbf{\Phi}^{\mathrm{T}} \tag{2.9}$$

The error covariance at $k = 1$ is defined as $\mathbf{P}[1] = \mathbf{q}$.

Second, once the measurement are taken from the power system, the state is update as,

$$\hat{\mathbf{x}}\,[k+1] = \bar{\mathbf{x}}\,[k+1] + \mathbf{K}[k+1](\mathbf{z}\,[k+1] - \mathbf{H}\bar{\mathbf{x}}\,[k+1]) \tag{2.10}$$

where $\mathbf{K}$ is define as,

$$\mathbf{K}\,[k+1] = \mathbf{H}\,\bar{\mathbf{P}}\,[k+1](\mathbf{H}\bar{\mathbf{P}}\,[k+1]\mathbf{H}^{\mathrm{T}} + \mathbf{R}\,)^{-1} \tag{2.11}$$

The current state is taken as a previous state and the process is repeated until all cycle is processed.

After *N* iterations, a waveform cycle is estimated.

2.2.4 Initial condition

The mathematical modelling of a physical system is frequently made by an ODE set that requires an initial condition known as initial value problem. Given the initial state, the system model will evolve to a steady state or could diverge to an unstable state. It is common to set the initial state to zero. As an alternative, the method described in [Semlyen and Medina 1995] can be used to obtain the periodic steady state to be used as the initial state for the ODE set.

The KF require the initial error covariance. It is common to take the process noise as initial error covariance. Therefore, the initial condition $\mathbf{x}[1]$ and $\mathbf{P}[1]$ must be given.

2.2.5 Root-mean-squared error

The root-mean-squared error value of the difference between the actual and the estimate voltage or current waveforms is defined as the RMS error (RMSE) given by,

$$RMSE = \sqrt{\frac{\sum_{k=1}^{N}(x[k]-\hat{x}[k])^2}{N}} \tag{2.12}$$

2.3 Experimental 5-bus test system

Solutions to the harmonic state problem have been suggested in several contribution reported in the open literature. However, it is virtually impossible to select one for practical implementation due to the complexity and unique characteristics of power systems. Hence, digital simulations are often used as a way of validating the proposed methodologies, which are typically based on synthetic data, i.e. simulated data plus Gaussian noise, as opposed to practical data [Saini and Kapoor 2012]. These validations have been questioned due to the fact that simulations use system models, which are usually of low-order and based on ideal parameter values. Therefore, the synthetic data is always dependent on the model; this in practice does not occur. Therefore, an experimental test system is needed to validate methodologies using practical data. In this contribution, the results obtained from the TDHSE assessment will be validated against practical laboratory experimental data.

Test systems for harmonic analysis have been proposed in [IEEE 1996a], [IEEE 1996b], [Chang et al. 2004]. However, in this research work, an experimental test system based on the classic 5-bus test system [Stagg and El-Abiad 1968], [Acha and Madrigal 2001] is proposed to evaluate the proposed methodology. The test system has been modified to include harmonic sources. It has been chosen due to practical feasibility to physically implement the network. Fig. 2.2 shows the single-phase network.

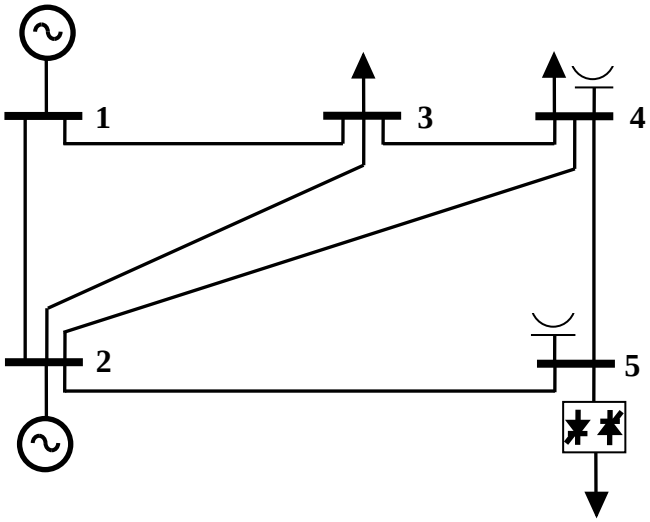

Fig. 2.2 Modified 5-bus test system

2.3.1 Parameters of the experimental 5-bus test system

The first step to design the experimental test system is to obtain the parameters of the test system according to the manufacturer specifications. The synchronous generators, transmission lines and linear electrical loads will be implemented with modules of the Lab-Volt 2KW Electromechanical Training Systems, model 8013 [Festo 2015].

2.3.1.1 Impedance of the transmission line

According to manufacturer specifications of the Lab-Volt 2KW Electromechanical Training Systems, model 8013 [Festo 2015], $Z_l = 5\Omega$ and $Q_l = 10$. According to circuit theory,

$$Z_l = X_l + R_l \tag{2.13}$$

$$Q_l = \frac{X_l}{R_l} \tag{2.14}$$

Substituting (2.14) in (2.13) and solving for X_l gives,

$$X_l = \frac{Z_l}{1+\frac{1}{Q_l}} \tag{2.15}$$

Substituting data in (2.13), (2.14), and (2.15) $X_l = 4.5454\Omega$, $R_l = 0.4545\Omega$, and $L_l = 12.057\text{mH}$. An external capacitance $C_l = 0.22\mu\text{F}$ is used.

2.3.1.2 Inductive load

According to manufacturer specifications of the Lab-Volt 2KW Electromechanical Training Systems, model 8013 [Festo 2015], $Z_{L1} = 60\Omega$ and $Z_{L2} = 120\Omega$ with $Q_L = 10$. Using (2.13), (2.14) and (2.15), it is obtained:

$X_{L1} = 54.5454\Omega$ $R_{l1} = 5.45454\Omega$ $L_{L1} = 144.6861\text{mH}$

$X_{L2} = 109.0909\Omega$ $R_{l2} = 10.90909\Omega$ $L_{L2} = 289.3725\text{mH}$

2.3.1.3 Resistive load

According to manufacturer specifications of the Lab-Volt 2KW Electromechanical Training Systems, model 8013 [Festo 2015] defines two resistive loads:

$R_{L1} = 60\Omega$

$R_{L2} = 120\Omega$.

2.3.1.4 Synchronous generator parameters

According to manufacturer specifications of the Lab-Volt 2KW Electromechanical Training Systems, model 8013 [Festo 2015], the synchronous generator parameters are:

$X_g = 18.5\Omega$ $R_g = 0.6\Omega$

$L_g = 49.0727$ mH ($f = 60$ Hz)

2.3.1.5 Parameters in per unit values

The voltage base is defined as the rate value of the generator, i.e. $V_{\text{base}} = 208$ V. In order to obtain similar parameter defined in [Acha and Madrigal 2001], an apparent power base of $VA_{\text{base}} = 900$ VA is used. Hence, the parameter values in per unit are given in Table 2.1; the load values in per unit are given in Table 2.2; and the injected Vars are given in Table 2.3.

Table 2.1 Per unit impedances and line charging

Line	Impedance	Line charging
1–2	0.02 + j0.06	j0.030
1–3	0.08 + j0.27	j0.025
2–3	0.06 + j0.18	j0.020
2–4	0.06 + j0.18	j0.020
2–5	0.04 + j0.12	j0.010
3–4	0.01 + j0.03	j0.010
4–5	0.08 + j0.27	j0.025

Table 2.2 Per unit load

Busbar	Watts	Vars
1	0	0
2	0	0
3	0.4	0.2
4	0.8	0.4
5	0.6	0

Table 2.3 Per unit injected Vars

Busbar	Vars
4	0.4
5	0.2

2.3.1.6 Nonlinear load

The nonlinear load has been connected to busbar 5 of the experimental test system. Fig. 2.3 shows the diagram of the per phase nonlinear load. Since the main aim of the nonlinear load is inject a harmonic content, a nonlinear load is implemented with parallel resistive incandescent lights controlled by dimmers. An AC-AC converter controlled by the α angle can represent a nonlinear load. [Rashid 1993] states that the output power for a resistive load can be determined by,

$$P_L = \frac{V_p^2}{2R_L}\left(1 - \frac{\alpha}{\pi} + \frac{\sin 2\alpha}{2\pi}\right) \tag{2.16}$$

The α angle can be adjusted to control the load power flow; according with the firing angle adjustment. These loads can inject a range of wide harmonics spectrum to the power system [Acha and Madrigal 2001].

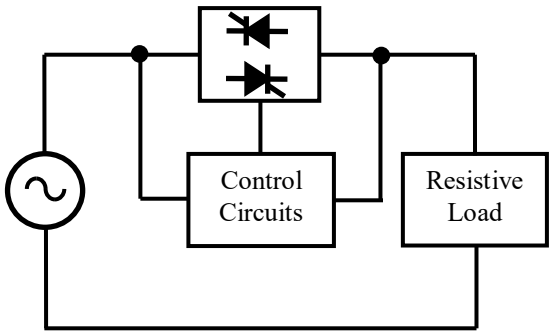

Fig. 2.3 Thyristor single-phase control

2.3.2 Model of the experimental 5-bus test system

The main components of power system are synchronous generators, transmission lines, transformers and linear and nonlinear loads. These components can be modelled as follows:

2.3.2.1 *Synchronous generator*

Generators can be modelled in several ways [Vilchis-Rodríguez and Acha 2009], [Despalatovic *et al*. 2012]. In this research work they are modelled by means of sinusoidal voltage sources behind impedances as shown in Fig. 2.4, with an $f = 60$ Hz and $V_{\mathrm{p}} = \sqrt{2}$ per unit. The state variables are the terminal voltages, in this particular case v_r and the series branch current i_r.

The series branch current through the RL components, in the continuous time, is defined by,

$$v_g - v_r = R_g i_r + L_g i_r' \tag{2.17}$$

where $v_g = V_{\mathrm{p}} \sin(\omega t)$ and the apostrophe in i_r' indicates the first derivative. Solving for i_r' from (2.17) yields,

$$i_r' = L_g^{-1}\left(v_g - v_r - R_g i_r\right) \tag{2.18}$$

Equation (2.18) gives the first-order ODE that represents the electric synchronous generator.

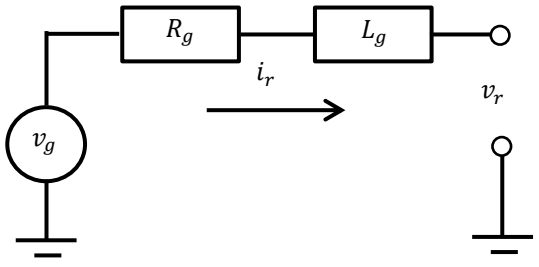

Fig. 2.4 Synchronous generator modelled as a source behind impedance

2.3.2.2 Two busbars are connected through a transmission line

The transmission line is modelled as a nominal π-circuit. Fig. 2.5 shows the transmission line represented by the nominal π-circuit. The state variables are the voltages at s and r, i.e. v_s and v_r, and the series branch current i_{sr} in RL components. In the continuous time, they are related by,

$$v_s - v_r = R_l i_{sr} + L_l i'_{sr} \tag{2.19}$$

Solving for i'_{sr} from (2.19) gives,

$$i'_{sr} = L_l^{-1}(v_s - v_r - R_l i_{sr}) \tag{2.20}$$

The voltage at busbar is related by the current in the equivalent capacitor C_{eq} connected to s, i.e.

$$i_{C_s} = C_{eq} v'_s \tag{2.21}$$

where $i_{C_s} = \sum i$, i.e. the incident currents at s and $C_{eq} = \sum C_l$. Hence, solving for v'_s yields,

$$v'_s = C_{eq}^{-1} i_{C_s} \tag{2.22}$$

In a similar way,

$$v'_r = C_{eq}^{-1} i_{C_r} \tag{2.23}$$

Equations (2.20), (2.22), and (2.23) give the first-order ODE set to model a transmission line.

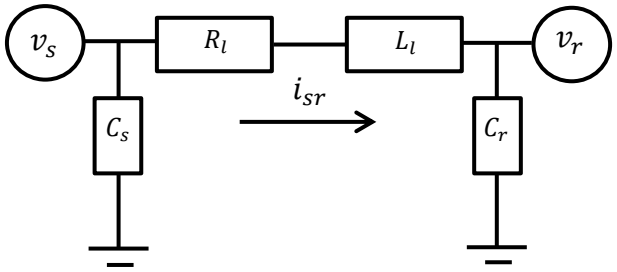

Fig. 2.5 Transmission line modelled as a nominal-π circuit

2.3.3.3 Transformer

To analyse the transformer, it is necessary to refer the equivalent circuit to either the primary side of the transformer or its secondary side. Fig. 2.6 shows the simplified transformer equivalent circuit referred to the primary side. The transformer model includes the following parameters: a, R_1, R_2, L_1, and L_2. The state variables are the voltages, at the input v_s and at the output v_r of the transformer as well as i_s. The series branch current through the RL components, in the continuous time, can be obtained from,

$$v_s - a v_r = R_p i_s + L_p i'_s \tag{2.24}$$

Solving for i'_s from (2.24) gives,

$$i'_s = L_p^{-1}\left(v_s - v_r - R_p i_s\right) \tag{2.25}$$

where $R_p = R_1 + a^2 R_2$ and $L_p = L_1 + a^2 L_2$.

Equation (2.25) gives the first-order ODE to model the power transformer dynamic operation.

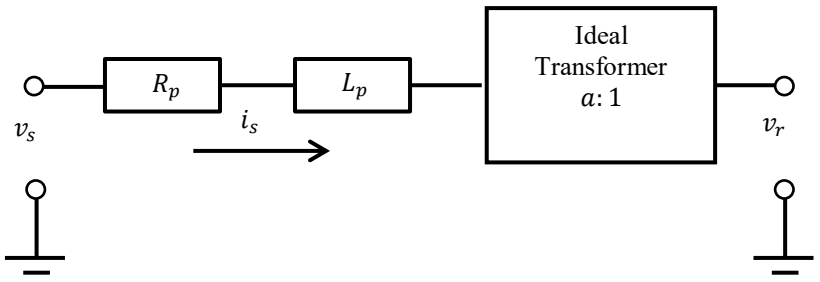

Fig. 2.6 Transformer modelled by impedance and an ideal transformer

2.3.4.4 *Linear load*

A linear load can be modelled by a parallel RL circuit as shown in Fig. 2.7. The state variables are the voltage v_s that supplies the linear load and the current in the inductive part L_L.

The series branch current in the inductor L in the continuous time is defined by,

$$v_s - 0 = L_L i_L' \tag{2.26}$$

Solving for i_L' from (2.26) gives,

$$i_L' = L_L^{-1} v_s \tag{2.27}$$

Equation (2.27) gives the ODE to represent a linear load.

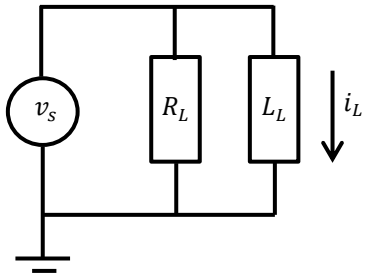

Fig. 2.7 Linear load represented as a parallel RL circuit

2.3.2.5 *Nonlinear load*

Nonlinear load can be modelled as injected current sources [Acha and Madrigal 2001]. Hence,

$$i_{h\mathrm{T}} = \sum_{h=1}^{\infty} i_h \tag{2.28}$$

where $i_h = A_h * cos(h\omega t + \theta_h)$. It can be noticed that (2.27) can be bounded by the harmonics of interest.

Equations (2.18), (2.20), (2.22), (2.23), (2.25), and (2.27) are the first-order ODEs to model the interconnection of components representing the entire power system.

2.3.2.6 *Model of the experimental 5-bus test system*

The experimental 5-bus test system shown in Fig. 2.2 has 5 busbars, 7 transmission lines, 2 linear loads, and 2 generators. Hence, the experimental 5-bus test system model is modelled by a set of 16 ODE's. Table 2.4

relates the state variable vector to the corresponding physical network variables. The nonlinear load connected to busbar 5 is modelled as current sources. The injected harmonics are given in Table 2.5.

Table 2.4 Single-phase state and physical variables

State Variable	Physical Variable
x_1	Voltage at Node 1
x_2	Voltage at Node 2
x_3	Voltage at Node 3
x_4	Voltage at Node 4
x_5	Voltage at Node 5
x_6	Current Generator 1
x_7	Current Generator 2
x_8	Branch Current in Line 1–3
x_9	Branch Current in Line 1–2
x_{10}	Branch Current in Line 2–3
x_{11}	Branch Current in Line 2–4
x_{12}	Branch Current in Line 2–5
x_{13}	Branch Current in Line 3-4
x_{14}	Branch Current in Line 4–5
x_{15}	Branch Current in Inductive Load 1
x_{16}	Branch Current in Inductive Load 2

Table 2.5 Harmonic injected at node 5

h	(%) A-Phase Fundamental	Angle (rad)
1	100.0000	-2.2310
3	18.5478	0.0744
5	15.5699	-2.2461
7	4.3456	1.6723
9	5.1431	-0.2693
11	5.4663	2.9610
13	5.4105	0.2483
15	4.3324	-2.2391
17	3.7660	1.2486

The ODE set to model the experimental 5-bus test system is defined by,

$$\begin{cases} \frac{dx_1}{dt} = (C_1 + C_2)^{-1}(x_6 - x_8 - x_9) \\ \frac{dx_2}{dt} = (C_1 + C_4 + C_5 + C_6)^{-1}(x_7 + x_9 - x_{10} - x_{11} - x_{12}) \\ \frac{dx_3}{dt} = (C_2 + C_3 + C_4)^{-1}(x_8 + x_{10} - x_{13}) \\ \frac{dx_4}{dt} = (C_3 + C_5 + C_7 + C_{b4})^{-1}(x_{13} + x_{11} - x_{14}) \\ \frac{dx_5}{dt} = (C_5 + C_7 + C_{b5})^{-1}(x_{12} + x_{14} - i_{h\mathrm{T}}) \\ \frac{dx_6}{dt} = {L_{g1}}^{-1}(v_{g1} - x_1 - x_6 R_{g1}) \\ \frac{dx_7}{dt} = {L_{g2}}^{-1}(v_{g2} - x_2 - x_7 R_{g2}) \\ \frac{dx_8}{dt} = {L_{l2}}^{-1}(x_1 - x_3 - x_9 R_{l2}) \\ \frac{dx_9}{dt} = {L_{l1}}^{-1}(x_1 - x_2 - x_9 R_{l1}) \\ \frac{dx_{10}}{dt} = {L_{l4}}^{-1}(x_2 - x_3 - x_{10} R_{l4}) \\ \frac{dx_{11}}{dt} = {L_{l5}}^{-1}(x_2 - x_4 - x_{11} R_{l5}) \\ \frac{dx_{12}}{dt} = {L_{l6}}^{-1}(x_2 - x_5 - x_{12} R_{l6}) \\ \frac{dx_{13}}{dt} = {L_{l3}}^{-1}(x_3 - x_4 - x_8 R_{l3}) \\ \frac{dx_{14}}{dt} = {L_{l7}}^{-1}(x_4 - x_5 - x_{14} R_{l7}) \\ \frac{dx_{15}}{dt} = {L_{L1}}^{-1}(x_3 - x_{15} R_{R1}) \\ \frac{dx_{16}}{dt} = {L_{L2}}^{-1}(x_4 - x_{16} R_{R2}) \end{cases} \tag{2.29}$$

where $v_{g1} = 170 \sin \omega t$ and $v_{g2} = 170 \sin \omega t$. The fundamental frequency is $f = 60$Hz.

2.4 Results

2.4.1 Steady state for the experimental 5-bus test system

The experimental 5-bus test system modelled by (2.29) is numerically integrated according to [Medina and Cisneros-Magaña 2012]. The steady state is achieved after 4 cycles. For illustrative purposes, the voltage at node 5 is shown in Fig. 2.8.

The steady state response of the experimental 5-bus test system is taken as initial state for KF.

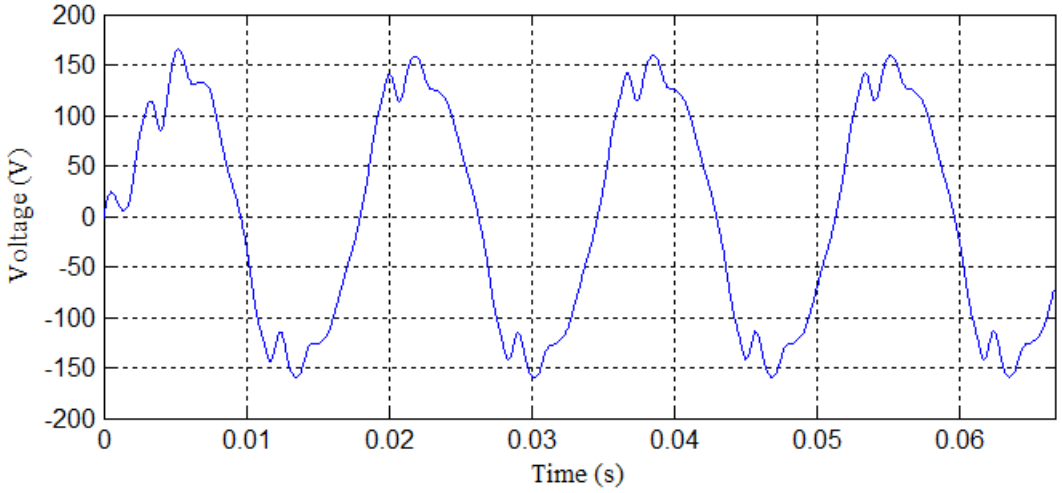

Fig. 2.8 Voltage at node 5; the steady state is obtained after 4cycles

2.4.2 Time domain harmonic state estimation

The parameters found in Section 2.3.1 have been verified. Appendix A details the verification process.

The experimental 5-bus test system has been implemented in the laboratory. The wiring test power system is shown in Fig. 2.9.

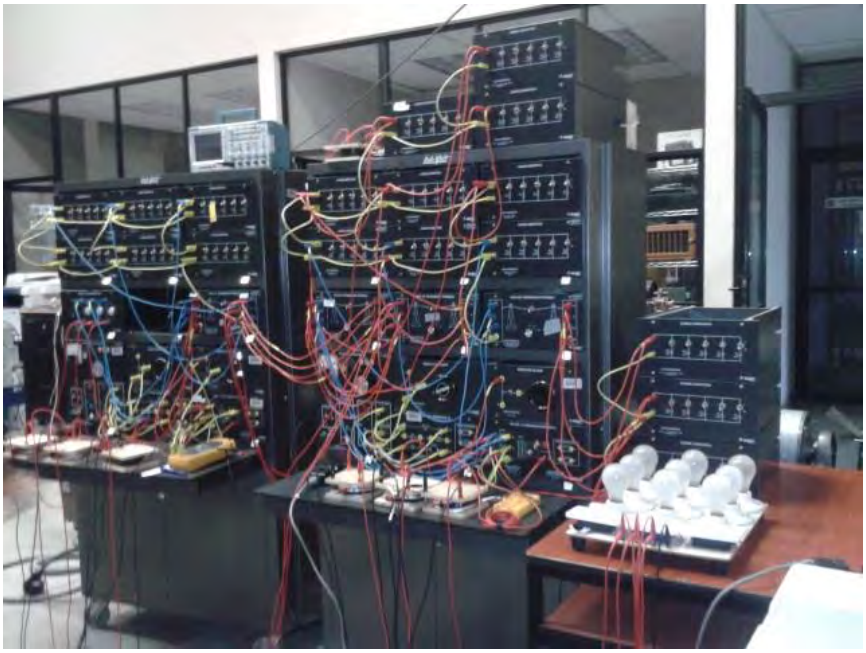

Fig. 2.9 Wired test power system

Eleven experimental measurements are taken from the test system according to Fig. 2.10. Please observe that nodes 3 and 4 are not monitored. Hence, an under-determined condition is used ($n = 16$ and $m = 11$). Measurements have been taken from the scale-down test system set up detailed in Fig. 2.10. A digital oscilloscope set to $F_S = 50{,}000$ samples per second has been used to record node voltages and branch currents. From these practical measurements, the harmonic content is defined.

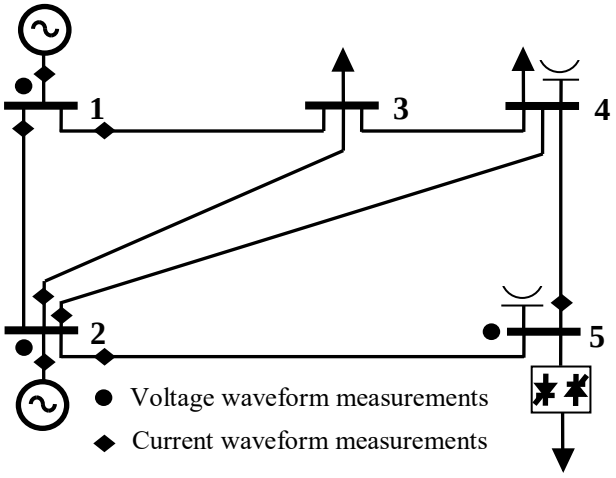

Fig. 2.10 Laboratory implementation of modified 5-bus test system

By using (2.10), the TDHSE assessment has been performed. The software where the algorithms have been implemented has been MATLAB®. The personal computer has been a MacBook Pro from Apple® which has an i5 core processor. For illustrative purposes, Fig. 2.11 shows and compares the estimated voltage waveform at unmonitored node 3 against the corresponding experimental waveform. A close agreement between the experimental and estimated values is observed since the RMSE has been 1.3V or 0.7%.

Once the waveforms are estimated, the FFT is applied to the estimated waveform to transform time domain data to frequency domain data. Fig. 2.12 shows the harmonic content corresponding for the estimated voltage at node 3. It can be noticed that the harmonic spectrum for estimated voltage at unmonitored nodes 3 is close to the one for the experimental waveform.

The error for the harmonic state is given in detail in Table 2.6. The maximum absolute error was of 0.26% presented in 3-*th* harmonic. However the average absolute error has been 0.15%. The maximum relative error has been 12.9% presented in 7-*th* harmonic whereas the average relative error has been 7.1%. Thus, despite of slight errors on modelling and parameter values, the TDHSE obtained has been adequate.

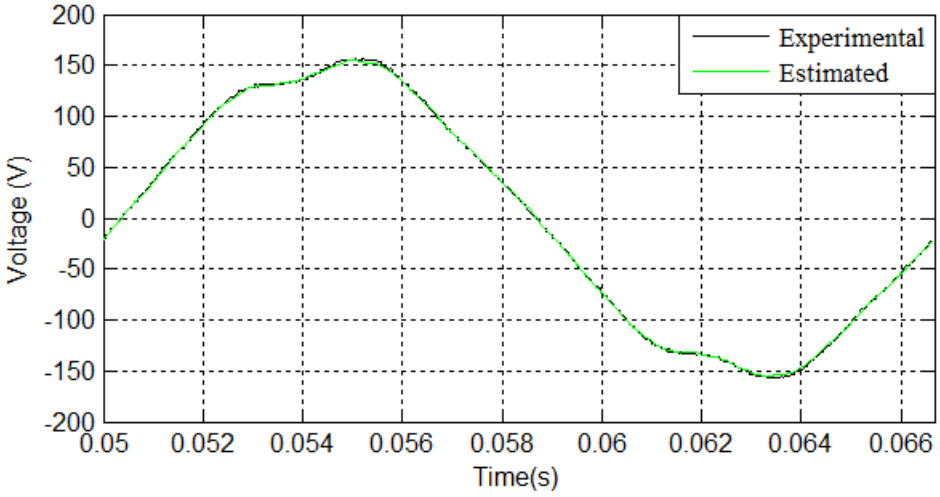

Fig. 2.11 Voltage waveforms at unmonitored node 3

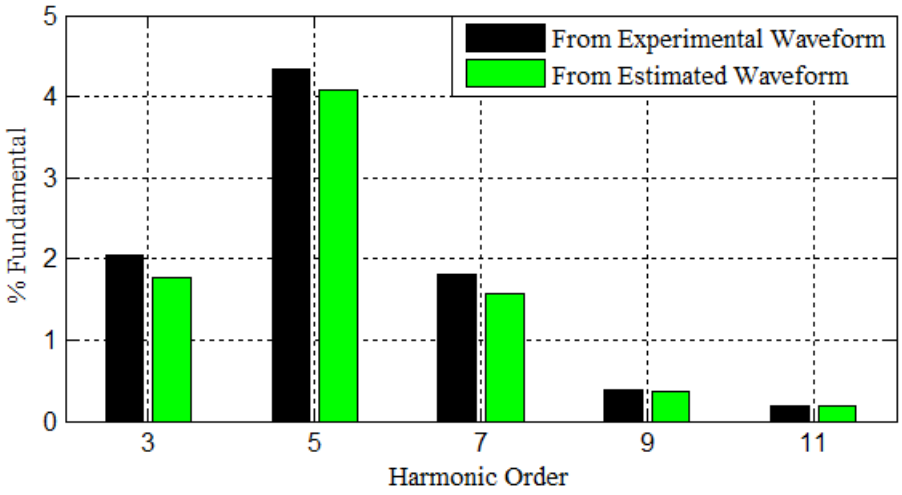

Fig. 2.12 Spectra for the experimental and estimated voltage waveform at unmonitored node 3

Table 2.6 Estimated error in the HSE assessment for unmonitored voltage at node 3

Harmonic Order	Experimental (%)	Estimated (%)	Absolute Error	Relative Error (%)
3	2.0398	1.7769	0.2629	12.8885
5	4.3351	4.0748	0.2602	6.0034
7	1.8035	1.5708	0.2327	12.9029
9	0.3863	0.3707	0.0156	4.0449
11	0.1860	0.1861	0.0001	0.0651

2.4.3 Filtering measurements

Measurements can be contaminated through natural measuring process. In addition, measurements can be more easily contaminated as they are smaller. For illustrative purposes, Fig. 2.13, 2.14, and 2.15 show three noisy branch current waveforms and their corresponding filtering. The selected branch currents are the state variables x_6, x_{10}, and x_{14}, defined in Table 2.4. The selected state variables are of different magnitude. The pick current values are 3.22, 1.54, and 0.38A corresponding to state variables x_6, x_{10}, and x_{14}, respectively. Please observe that as amplitude magnitude decreases, the noise increases is more notorious. These measurements are used by KF, once KF algorithm has been applied, the noisy measurements are filtered.

Fig. 2.13(a) shows the noisy measurement corresponding to x_6. Since the peak current is 3.22, the adverse effect of the noise is little. The level noise has been 0.62%. However, this noise is mitigated as shown in Fig. 2.13(b).

Fig. 2.14(a) shows the noisy measurement corresponding to x_{10}. The noisy is greater than one in x_6, i.e. the noise level has increased from 0.62 to 1.32%. The KF algorithm has mitigated the noise as shown in Fig. 2.14(b).

Fig. 2.15(a) shows the noisy measurement corresponding to x_{14}. The magnitude of x_{14} is the lowest, around 0.38A; hence, the noise is more notorious as shown in Fig. 2.15(a), around 5.41%. Fig. 2.15 (b) shows the filtered measurement waveform. Again, the KF has adequately mitigated the noise.

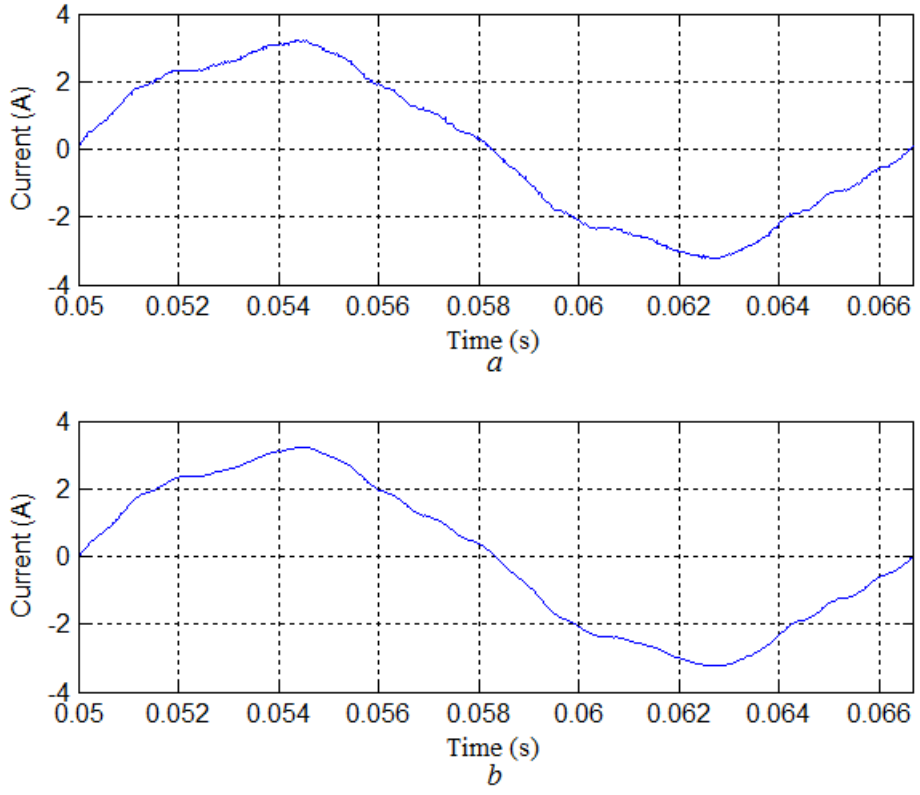

Fig. 2.13 Measurement for x_6, (a) taken from the experimental test system and (b) filtered using the KF

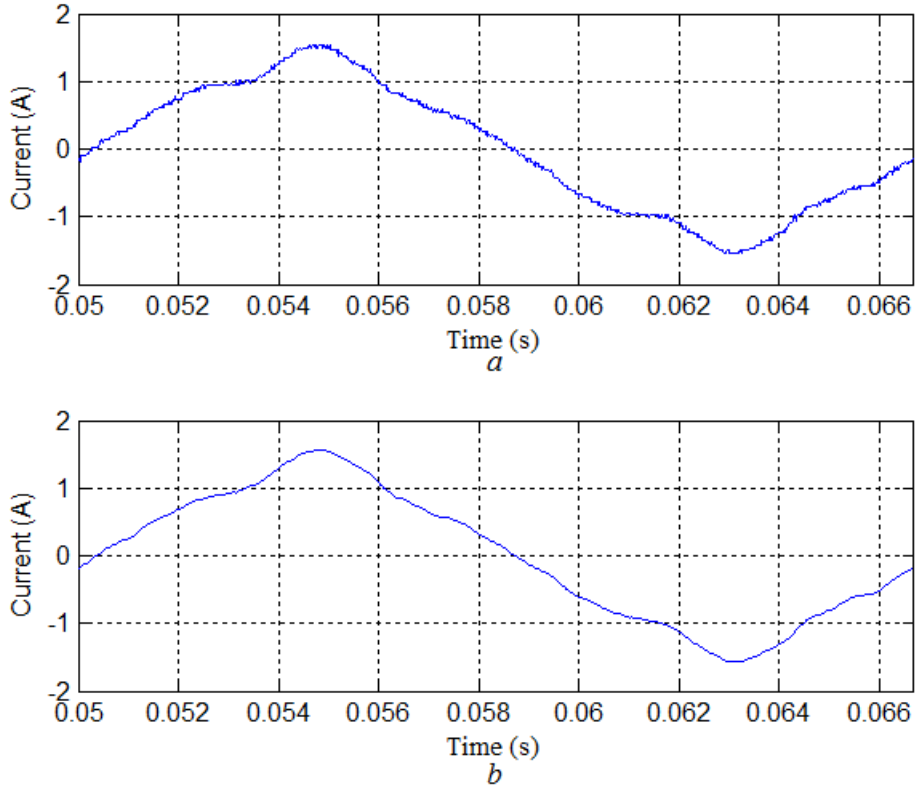

Fig. 2.14 Measurement for x_{10}, (*a*) taken from the experimental test system and (*b*) filtered using the KF

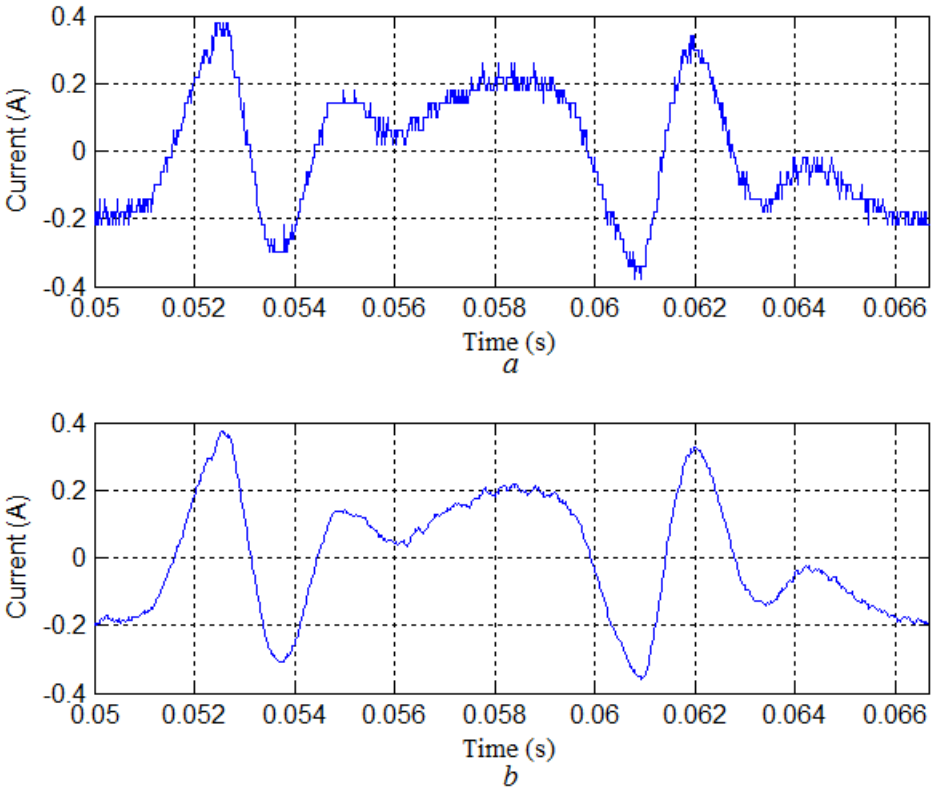

Fig. 2.15 Measurement for x_{14}, (*a*) taken from the experimental test system and (*b*) filtered using the KF

2.4.4 Global assessment for harmonic state

A global assessment for harmonic state has been conducted using the proposed formulation. The assessment is based on the THD. Voltage waveform measurements at nodes 1, 2 and 5 have been estimated by applying the KF to filter the measurements. The voltage waveform estimation of the unmonitored voltages at nodes 3 and 4 has been obtained using the KF algorithm. After waveforms are estimated, the THD corresponding to simulated and estimated waveforms are obtained by using the Fourier transform. Table 2.7 details the THD for the voltages at all nodes of the power system. An adequate agreement between experimental values and the estimated ones by the proposed methodology can be observed. The maximum difference between the THD for the experimental and estimate waveforms is 0.44%.

Table 2.7 THD for waveforms at all nodes (% Fundamental)

Node	THD for experimental	THD for estimated	Absolute Estimated Error	Relative Estimated Error (%)
1	1.4729	1.3372	0.1357	9.21
2	2.3465	2.5636	0.2170	9.24
3	5.1371	4.7330	0.4042	7.80
4	6.0329	5.6977	0.3352	5.50
5	11.3187	10.8721	0.4466	3.94

2.5 Conclusions

In this chapter, a methodology based on the Kalman filter formulation in the time domain to estimate voltage waveforms, which have implicitly a harmonic content, has been detailed. Its practical application has been successfully validated against an experimental 5-bus test system laboratory set-up. The performance of the proposed methodology has been satisfactory for the under-determined measurement model case. A direct comparison between the estimated voltage waveforms to the same physical variables directly measured in the laboratory set-up has been satisfactorily achieved since RMSE has been 1.3V. The harmonic content has explicitly obtained by applying the Fourier transform to the estimated waveforms where the maximum difference between the THD for the experimental and estimate waveforms has been 0.44%.

Minor inaccuracies are present due to error of some physical parameters, reflected in the conducted simulation. Despite of these inaccuracies, it is possible to adequately assess the harmonic state estimation with the proposed methodology.

Therefore, it can be concluded that by using the TDHSE based on Kalman filter, is feasible to obtain an accurate global assessment of the harmonic state in power systems.

Chapter 3 Harmonic state estimation based on Kalman filter using an arbitrary initial state and the half-wave symmetry property

3.1 Introduction

This chapter details a time domain methodology to indirectly estimate the harmonic state in power systems. The proposed methodology is again based on the Kalman filter, but a difference of the Chapter 2, an arbitrary initial state is used which allows the KF itself to find the steady state. The half-wave symmetry property in voltage and current waveforms is exploited to reduce from one to half cycle, the execution time needed by the Kalman filter in the estimation process. In addition, the use of sending and receiving end line currents instead of branch current for the case of transmission lines as branch current measurement are not available for practical cases, is detailed.

A case study for two unbalanced operation in a power network is analysed. The resulting estimated waveforms obtained by the proposed methodology are validated through direct comparison against the waveforms registered from an experimental laboratory test system. The harmonic state for experimental and estimated waveforms is evaluated by using the Fourier transform.

3.2 Methodology

The complete scheme for the HSE problem in the time domain is shown in Fig. 3.1. The main contributions in this methodology are highlighted. The function of the blocks is detailed next.

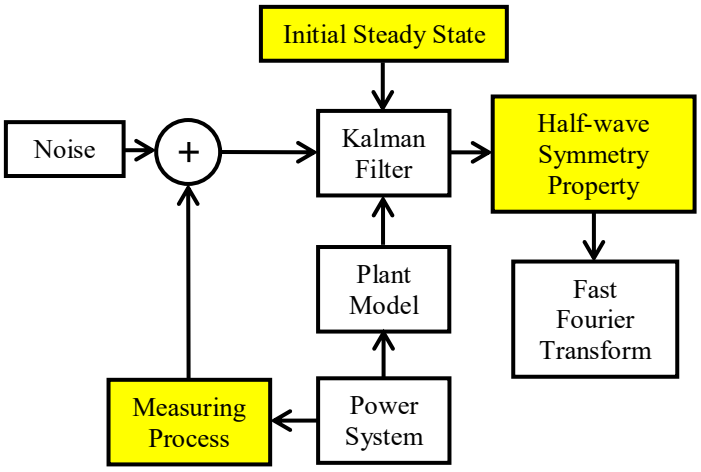

Fig. 3.1 Complete scheme for the HSE problem

3.2.1 Plant model

The model of the plant in the time domain is based on linear algebra and circuit theory [Watson and Arrillaga

2003]. The mathematical model is formulated in the state space framework through a first-order ODE set in continuous time which can be obtained according to the methodology described in Section 2.3.2.

3.2.2 Measuring process

In previous methodologies for TDHSE assessment, measurements have been busbar voltages and inductor branch currents selected as the state variables [Medina and Cisneros-Magaña 2012 and [Cisneros-Magaña *et al.* 2014]. However, inductor branch current in transmission lines modelled by an equivalent π-model or in linear load modelled by parallel RL circuit are not physically available. The next analysis describes the procedure followed to incorporate sending or receiving end line currents to construct the measurement matrix defined in (1.5).

Let p be the number of transmission lines connected at busbar s as shown in Fig. 3.2. The differential equation associated to the voltage at busbar s, x_s is,

$$\dot{x}_s = \sum_{j=1}^{p} x_j \Big/ \sum_{j=1}^{p} C_{sj} \tag{3.1}$$

The current in the particular capacitor C_{sj} is defined by,

$$i_{C_{sj}} = C_{sj}\dot{x}_s \tag{3.2}$$

Substituting (3.1) in (3.2) gives,

$$i_{C_{sj}} = C_{sj} \sum_{j=1}^{p} x_j \Big/ \sum_{j=1}^{p} C_{sj} \tag{3.3}$$

Hence, the sending end line current for a particular line is,

$$i_{s_j} = x_j + C_{sj} \sum_{j=1}^{p} x_j \Big/ \sum_{j=1}^{p} C_{sj} \tag{3.4}$$

In a similar way, the receiving end line current for a particular line is,

$$i_{r_j} = x_j - C_{rj} \sum_{j=1}^{p} x_j \Big/ \sum_{j=1}^{p} C_{rj} \tag{3.5}$$

Please note that the sending and receiving end line currents are function of the state variables.

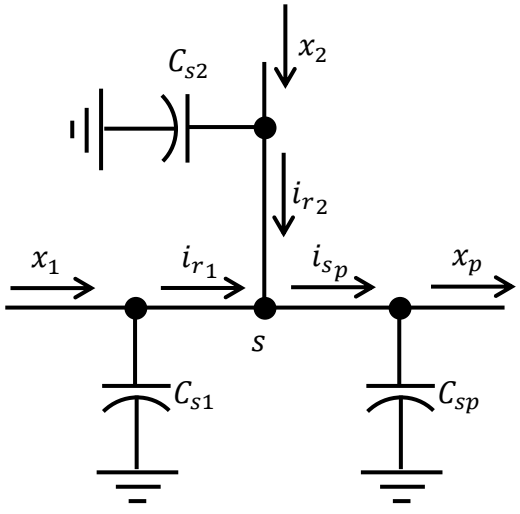

Fig. 3.2 Transmission lines connected at busbar *s*

3.2.3 Half-wave symmetry property

It is assumed that the power system is operating in steady state. Hence, distorted voltage waveforms are periodic. Symmetry of waveforms with respect to the origin of coordinates is called half-wave symmetry [Suresh 2009]. A periodic waveform $v(t)$ is half-wave symmetrical if it satisfies,

$$v(t) = -v\left(t + \frac{1}{2}T\right) \; \forall \, t \tag{3.6}$$

Once the steady initial state is determined using the algorithm shown in Fig. 3, in order to exploit the half-wave symmetry property, the KF is executed for a half-cycle. If a cycle is divided into *N* samples it is only necessary to process *N*/2 samples.

Let $\hat{\mathbf{x}}_{\mathrm{h}}$ be the half-cycle estimated state. Exploiting the half wave symmetry in voltage and current waveforms, a completed cycle can be formed using,

$$\hat{\mathbf{x}} = \hat{\mathbf{x}}_{\mathrm{h}} \cup -\hat{\mathbf{x}}_{\mathrm{h}} \tag{3.7}$$

where the operator ∪ is used to indicate the concatenation of $\hat{\mathbf{x}}_{\mathrm{h}}$ and $-\hat{\mathbf{x}}_{\mathrm{h}}$.

As a consequence, the time processing needed to estimate the HSE is reduced by approximately 50% as it only estimates half-cycle of the waveforms.

3.2.4 Kalman filter algorithm

The Kalman filter algorithm has been summarised in Section 2.2.3. In this research work, the half-wave symmetry property in voltage and current waveforms is exploited. In this way, the KF is applied in the time domain during a half cycle to evaluate the HSE without loss of accuracy.

3.2.5 Initial steady state

The KF requires a steady initial state $\mathbf{x}_0 \in \mathbb{R}^n$. [Medina and Cisneros-Magaña 2012] and [Cisneros-Magaña *et al.* 2014] use a numerical differentiation (ND) and an enhanced numerical differentiation (END), respectively to find the steady state. In this research work, an alternative method to find the steady initial state for KF is proposed. The idea is to stablish an arbitrary initial state and take advantage of the available measurements of the power system. It is assumed that the power system is already in steady state so that the Kalman filter itself finds the steady initial state. The algorithm for this purpose is shown in Fig. 3.3.

A flag j is set to zero. When the difference between the measurements and the estimated states by KF is less than a small quantity ε, the flag j is set to one. If the next estimation satisfies the above condition, the process is finished and the final estimation is taken as steady initial state. Otherwise, the flag j is again set to zero.

3.2.6 Fast Fourier transform

The Fast Fourier Transform can be applied to (3.7) to change data from time domain to frequency domain.

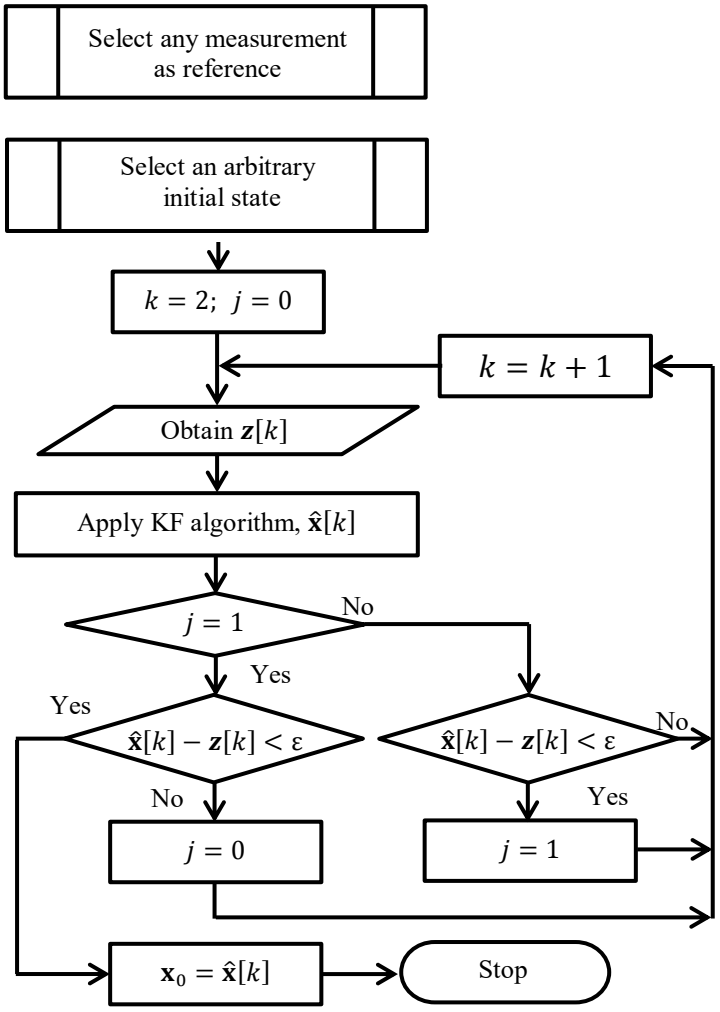

Fig. 3.3 Algorithm to find the steady state initial state

3.3 Experimental test system

3.3.1 Measuring devices placement

The experimental 5-bus test systems will be used in this part of the researching work. However, of Fig. 3.4 some details must be explained. An unbalanced three-phase 5-bus test system has been built in laboratory for experimental HSE assessment and validation of the proposed TDHSE method. The detail of the laboratory implementation for HSE assessment including the location of three-phase voltage and current measurements is shown in Fig. 2.16.

The monitored locations are at busbars 1, 2, and 5; the unmonitored locations are at busbar 3 and 4. There are 33 measuring devices installed as shown in Fig. 3.4.

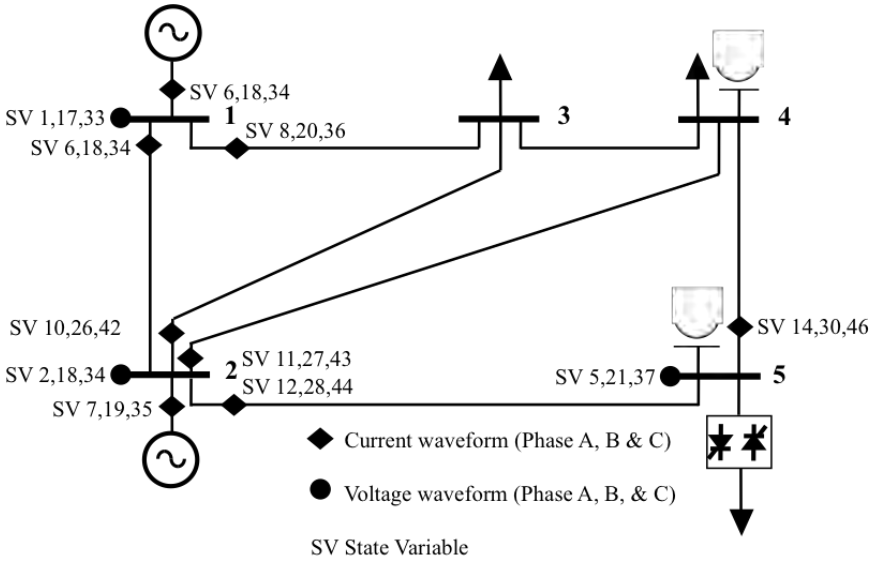

Fig. 3.4 Laboratory implementation with 33 measuring devices

3.3.2 Nonlinear three-phase load

The nonlinear load used in Chapter 2 has been single-phase. Now, in order to implement a nonlinear three-phase to can inject unbalanced harmonic current, a three single-phase nonlinear load is connected in star configuration as shown in Fig. 3.5. It consists on parallel incandescent lights with a control circuit consisting on dimmer bridge based on silicon-controlled rectifiers. The thyristor firing angle can be adjusted to control the load power flow. Each dimmer can be adjusted to different value in order to obtain an unbalanced three-phase nonlinear load. These nonlinear loads inject a wide range of harmonic components to the power system.

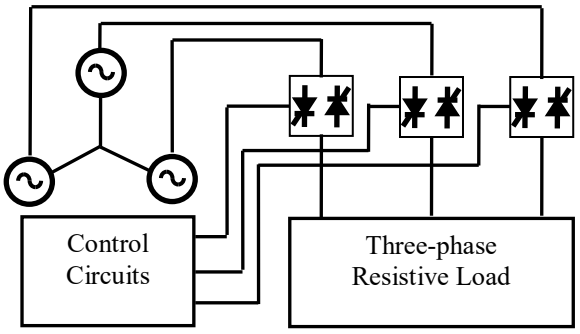

Fig. 3.5 Thyristor controlled three-phase resistive load

3.4. Results

3.4.1 Simulated TDHSE

The experimental test system shown in Fig. 2.15 has been used to conduct the case studies of this section.

Measurements have been taken from the scale-down test system set up detailed in Fig. 3.4. A digital oscilloscope set to $F_S = 50{,}000$ samples per second has been used to record busbar voltages and, sending and receiving end line currents. By applying the FFT to these practical measurements, the experimental harmonic state is defined. For illustrative purposes, the oscilloscope snapshot that displays the three-phase voltage at busbar 5 is shown in Fig. 3.6. The phase A of busbar 1 has been taken as reference and continuously measured in Channel 1 to synchronise the rest of the measurements; Channels from 2 to 4 measure phases A (channel 2), B (channel 4), and C (channel 3), i.e. positive phase sequence. Please notice that phase B waveform presents harmonic.

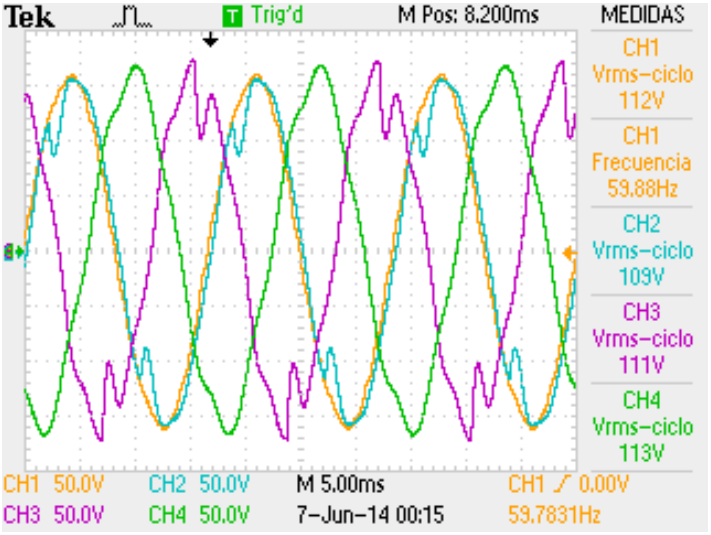

Fig. 3.6 The oscilloscope displays the three-phase voltage at busbar 5

3.4.2 Unbalanced nonlinear load

The nonlinear load shown in Fig. 3.5 is connected at busbar 5. The nonlinear load is formed by light lamps that can be controlled by independent dimmers. The unbalanced condition is obtained adjusting α to 86.4°, 0°, and 90° for phase A, phase B, and phase C, respectively. This unbalanced condition generates an average of 1.8% of unbalance between phases. The voltage and current waveforms in the unbalanced nonlinear load are shown in Fig. 3.7 where the phase A of busbar 5 is displayed on channel 2 and the load currents in phases A and C are displayed on channels 3 and 4, respectively. Then, the injected harmonic for this condition is obtained using FFT and is given in Table 3.1.

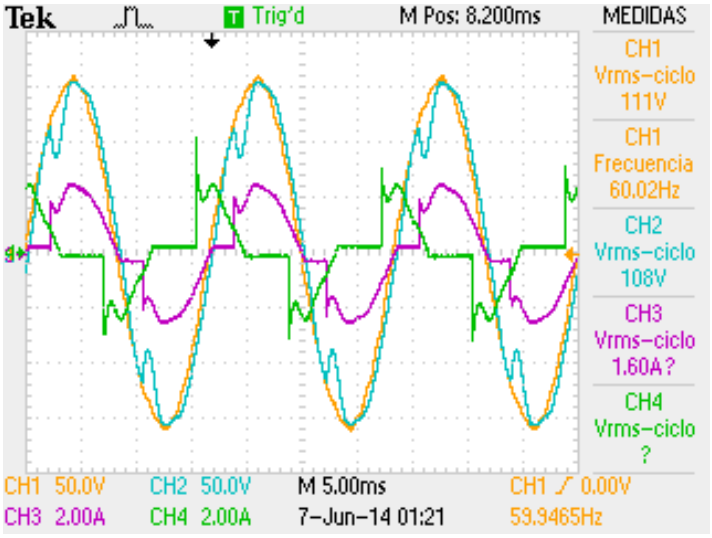

Fig. 3.7 The oscilloscope displays the nonlinear load connected at busbar 5

Table 3.1 Unbalanced harmonics injected at busbar 5

Harmonic Order	(%) Phase A fundamental	Phase A (rad)	(%) Phase C fundamental	Phase C (rad)
3	15.0225	0.2573	52.4612	-1.207
5	13.5759	-1.9159	20.3254	-1.081
7	4.2622	2.2053	10.1592	-0.957
9	5.1704	0.6350	11.8031	0.2477
11	4.5197	-2.2071	13.1627	0.0228

3.4.3 Steady initial state by numerical differentiation

The method to reach the steady state reported by [Medina and Cisneros-Magaña 2012] and [Cisneros-Magaña *et al.* 2014] use the ND and the END, respectively. Fig. 3.8 shows the evolution in time of the unbalanced three-phase voltage at busbar 5 to reach the steady state. It can be observed 4 cycles are needed to reach the steady state. Positive phase sequence has been assumed.

The obtained steady state is validated through direct comparison against the simulated response using SimPowerSystems tool of Simulink®. The unbalanced three-phase voltage at busbar 1 generated by the model defined by the ODE set is compared against the obtained by SimPowerSystems tool of Simulink®, as shown in Fig. 3.9. Please notice the excellent agreement between both responses.

The steady state can be used as the initial state for KF as the methodology described in Chapter 2. However, an alternative method is proposed for this purpose which is described next.

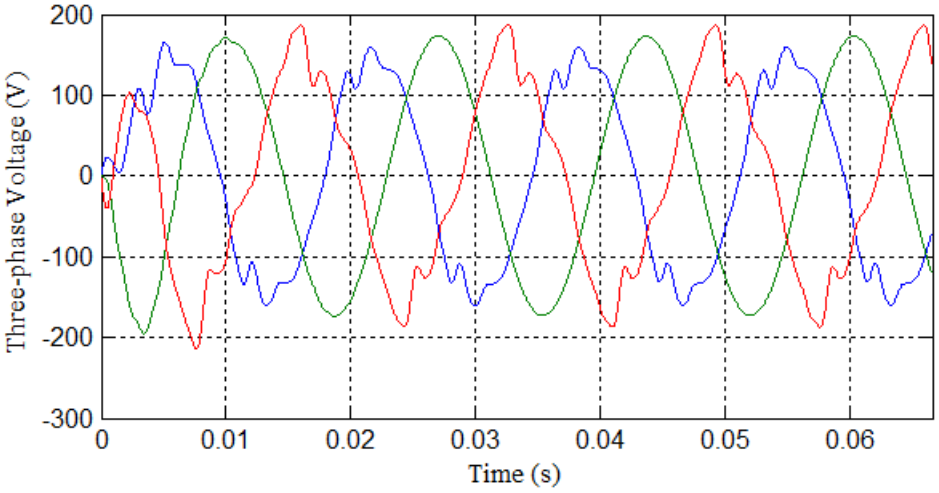

Fig. 3.8 Unbalanced three-phase voltage at bus 5 reaching the steady state after 4cycles

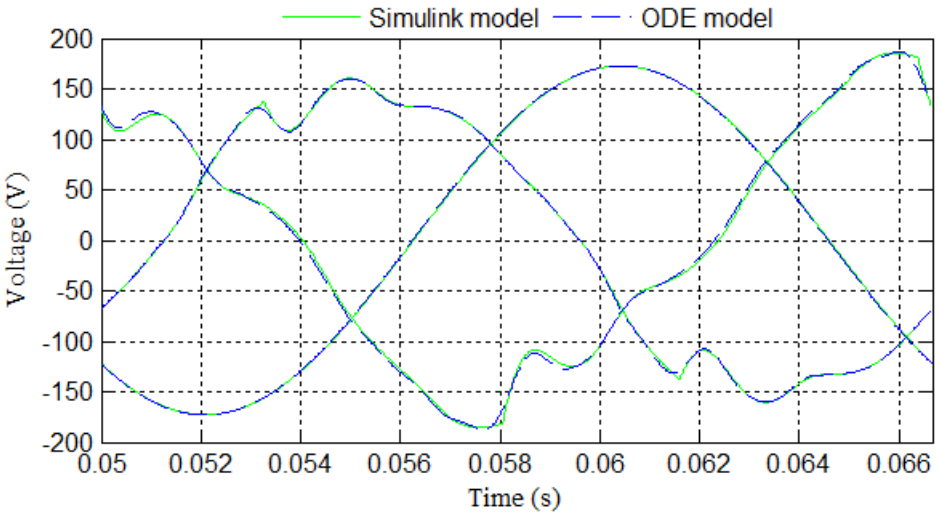

Fig. 3.9 Unbalanced three-phase voltage at bus 1 in steady state

3.4.4 Initial steady state with proposed method

The proposed methodology to estimate the harmonic state does not require accurate knowledge of the steady state to set the initial state. By applying the algorithm shown in Fig. 3.3, the KF itself finds the steady initial steady state. Different initial states have been used to evaluate the performance of the proposed algorithm. For instance, Fig. 3.10 shows the solution of the stable initial solution using different arbitrary initial states. The arbitrary initial states are : *a*) -120V, *b*) 58.2V, *c*) 0V, and *d*) 120V whose solutions are shown in Fig. 3.10(*a*), (*b*), (*c*), and (*d*), respectively. The reference measurement has been the phase A of busbar 1. The initial stable state has been reached after 335 iterations.

It is assumed that for unmonitored state variables, the steady state is reached at the same time. Fig. 3.11 shows the evolution in time to reach the steady state in the unmonitored voltage of busbar 3. It can be noticed that the steady state has been also reached at sample 335.

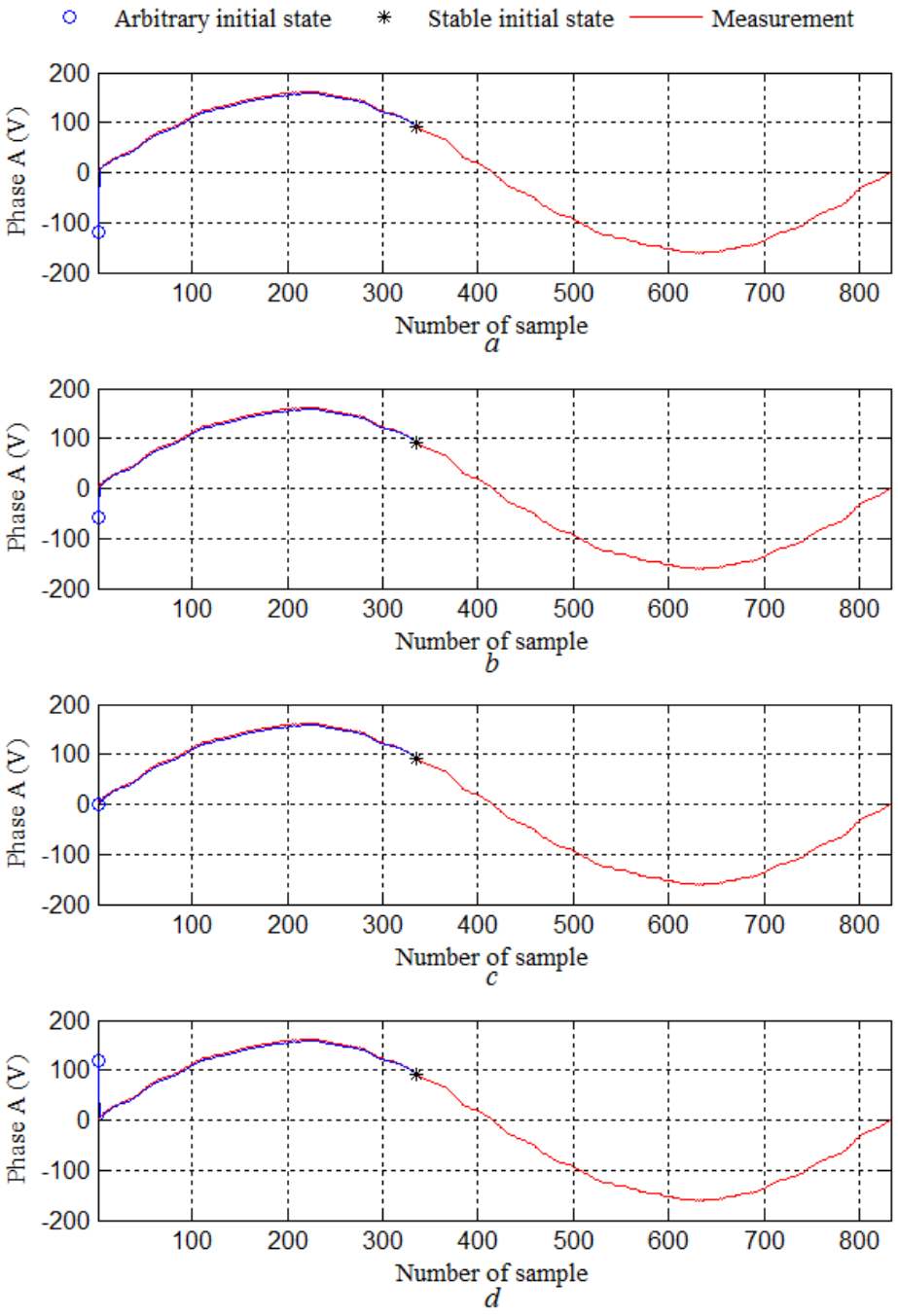

Fig. 3.10 Initial state found using measurement at busbar 1 and an arbitrary initial state: a) -120V, b) 58.2V, c) 0V, and d) 120V

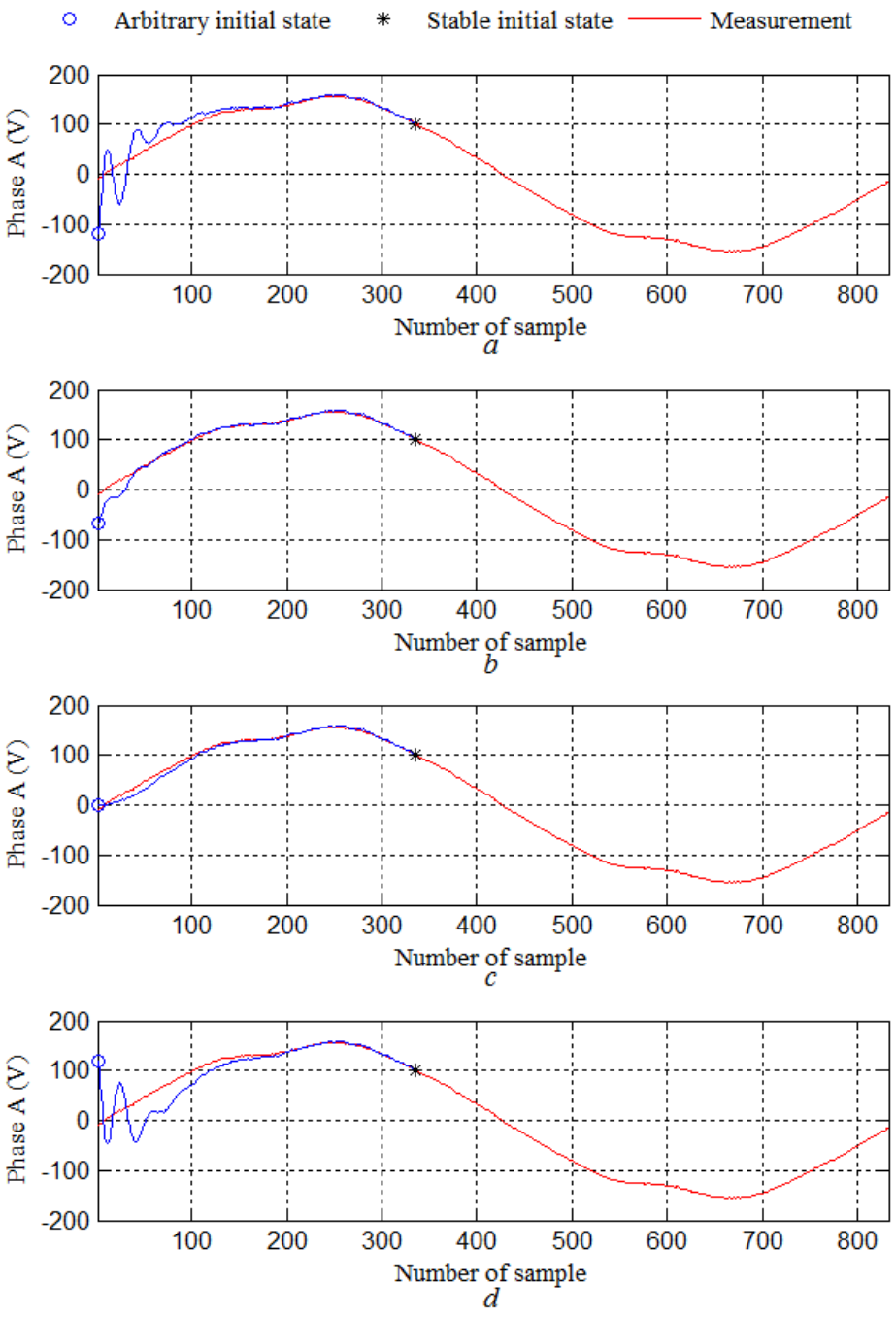

Fig. 3.11 Trajectory for initial state in unmonitored busbar 3 using an arbitrary initial state of a) -120V, b) 58.2V, c) 0V, and d) 120V

3.4.5 Half-wave symmetry property applied to TDHSE assessment

Once the stable initial state is found, the KF is executed during a half cycle to estimate the voltage at unmonitored busbars. Despite the errors on modelling and parameter values, the obtained TDHSE at unmonitored busbars is accurate. For illustrative purposes, the estimated three-phase voltage waveforms at

unmonitored busbar 3 are shown in Fig. 3.12. Please observe that after find the initial state (marked as *), the KF is executed during a half-cycle (marked as blue line).

By exploiting the half-wave symmetry, (3.7) is used to complete the estimated cycle. The estimated waveform for three-phase voltage at unmonitored busbar 3 is shown in Fig. 3.13. Then, FFT is applied to estimated and experimental waveforms to obtain the harmonic content as shown in Fig. 3.14. Please notice that the corresponding spectra is in close agreement with the simulated harmonic spectra obtained from recorded data. Table 3.2 gives the total harmonic distortion (THD) in percentage of the fundamental for the estimated and experimental voltage waveforms at unmonitored busbar 3. The maximum absolute differences between the THD measured in laboratory and THD predicted by KF are of 0.29% for the phase A, 0.11% for phase B, and 0.02% for phase C. There is not any nonlinear load connected to phase B; however, due to the wave propagation, a THD of 5.89% is generated in that phase.

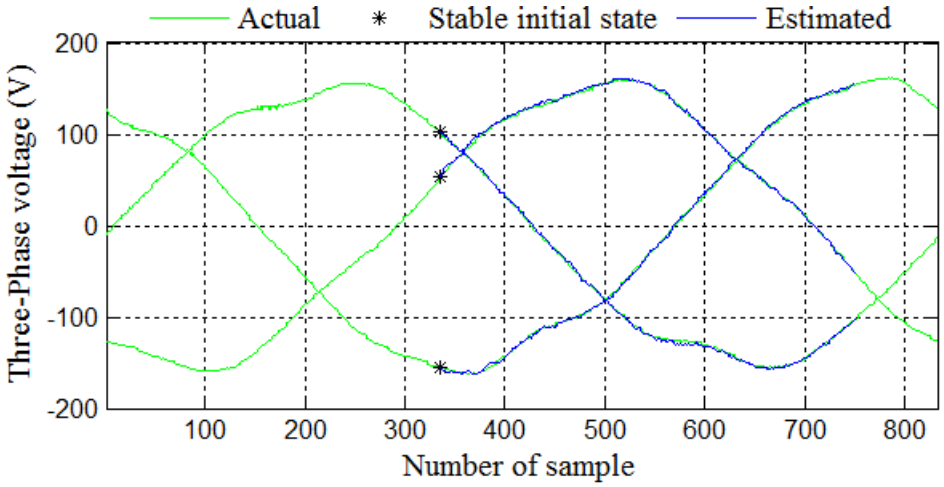

Fig. 3.12 KF estimates half cycle for voltage at unmonitored busbar 3

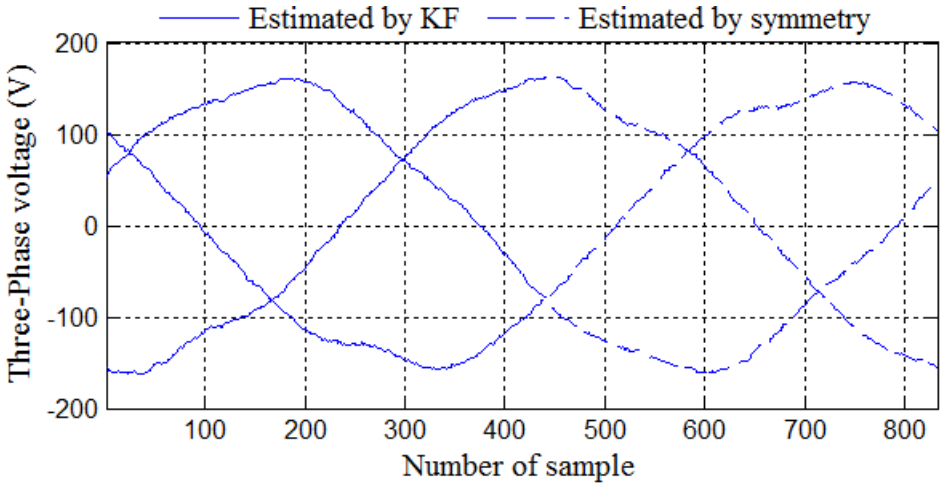

Fig. 3.13 By exploiting the symmetry property, the voltage at unmonitored busbar 3 is estimated

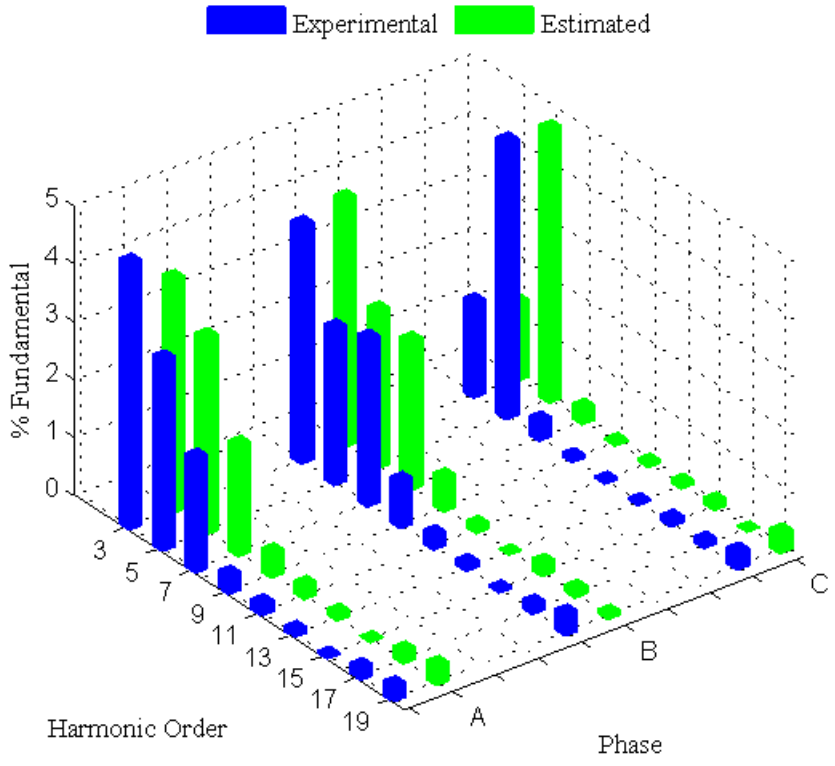

Fig. 3.14 Harmonic content at busbar 3

Table 3.2 THD (%) for voltage waveforms at unmonitored busbar 3

Phase	Experimental (laboratory)	Estimated (KF)	Absolute Error	Relative Error (%)
A	5.9204	5.6234	0.2970	5.01
B	5.8999	5.7868	0.1131	1.91
C	5.1117	4.9745	0.0268	0.52

A similar situation is observed for unmonitored busbar 4. Fig. 3.15 shows the harmonic state in the time domain. The steady state is achieved after 335 iterations. Once the stable initial state is found, the KF is applied to estimate a half cycle for the voltage at unmonitored busbar 4. Fig. 3.16 shows the result of using (3.7) to exploit the half-wave symmetry property. Table 3.3 gives the corresponding THD per phase. For this case, the maximum difference between the THD registered in laboratory and THD using the proposed methodology based on KF is 0.43%.

The harmonic contents for experimental and estimated three-phase voltage at unmonitored busbar 4 are shown in Fig. 3.17. It can be observed that estimated response is more agree with the experimental one.

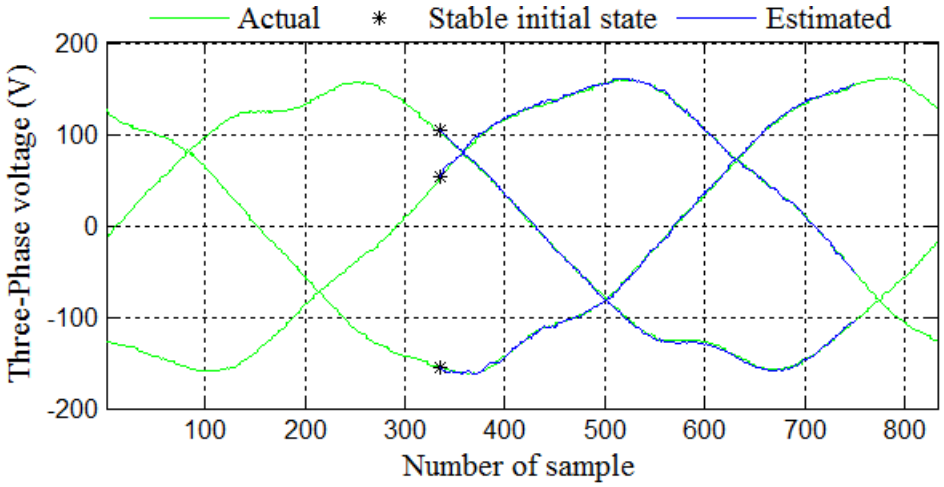

Fig. 3.15 KF estimates half cycle for voltage at unmonitored busbar 4

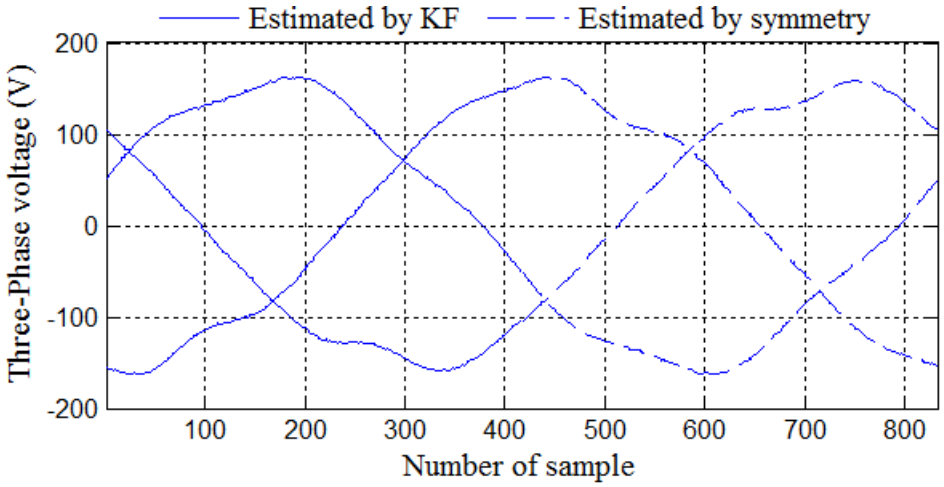

Fig. 3.16 Exploiting the symmetry property, the voltage at unmonitored busbar 4 is estimated

Table 3.3 THD (%) for voltage waveforms at unmonitored busbar 4

Phase	Experimental (Laboratory)	Estimated (KF)	Absolute Error	Relative Error (%)
A	6.9193	6.4852	0.4341	6.2
B	6.9221	6.5989	0.3232	4.6
C	6.3437	6.0102	0.3335	5.2

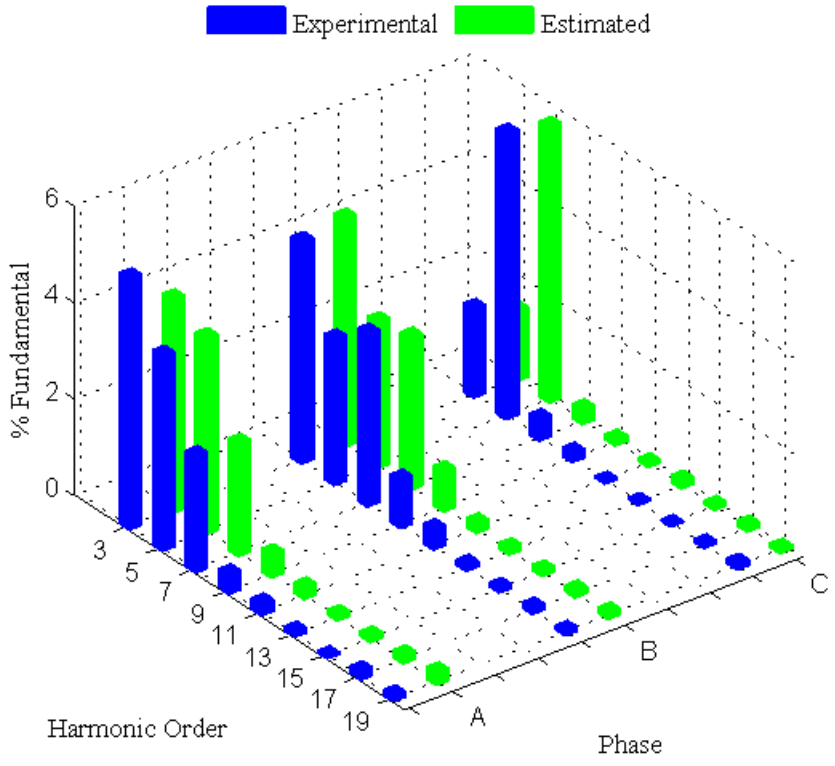

Fig. 3.17 Harmonic content at busbar 4

3.5. Conclusions

A harmonic state estimation methodology in the time domain based on the Kalman filter formulation has been successfully tested and validated against an experimental three-phase 5-bus test system with an unbalanced nonlinear load based on incandescent light dimmers controlled by thyristors and implemented in a laboratory set-up.

The computer effort for the TDHSE assessment has been reduced as proposed methodology needs only half cycle instead of a complete cycle to obtain the solution.

The KF does not need accurate knowledge of steady state to stablish an initial state as it finds itself the stable initial state. Hence, the computational effort to obtain the steady state is reduced; for the particular case study, from four cycles to less than one cycle.

The results have been validated through direct comparison of the estimated state variables (unmonitored) state variables against the corresponding physical variables directly measured in the laboratory. A close agreement between estimated and experimental responses has been obtained.

In the experimental study, common inaccuracies that are common due to uncertainty and variability on physical parameter values have been reflected in the conducted state estimation assessment.

Despite these inaccuracies, it can be concluded that the methodology for harmonic state estimation in the time domain based on Kalman filter can be used to obtain an accurate global assessment of the power system harmonic state in three-phase unbalanced power networks using a limited number of meters.

Chapter 4 Harmonic state estimation using filtered measurements based on the Fourier transform

4.1 Introduction

This chapter introduces a methodology to indirectly estimate the harmonic state using filtered measurements based on the Fourier transform, i.e. the methodology estimates the voltage waveform at unmonitored buses of power systems, and then, by applying the Fourier transform to the estimated waveforms, the harmonic state is obtained. The mathematical formulation relates the measurement vector to state variables in the time domain. Measurements are voltage and current waveforms. Measurements can be contaminated by noise. Hence, in order to assure the appropriate differentiation process needed in the time domain solution, noise in measurements is mitigated using a filter based on Fourier transform.

The proposed methodology is validated using a 5-bus test system including linear and nonlinear-balanced loads. A direct comparison of estimated waveforms against the simulated response obtained from the time domain power system simulation by the SimPowerSystems tool of Simulink® is performed. Different partial measurements sets are used to evaluate the proposed methodology.

4.2 Methodology

The proposed methodology, to evaluate the TDHSE, is shown in Fig. 4.1. A limited number of measuring devices placed at certain buses provide data of voltages and line currents. Data are waveforms sampled at frequency F_S, which meet the Nyquist theorem. Unfortunately, data may be corrupted by noise. A filter based on Fourier transform is applied for noise mitigation. The estimate error is minimised using least squares optimization.

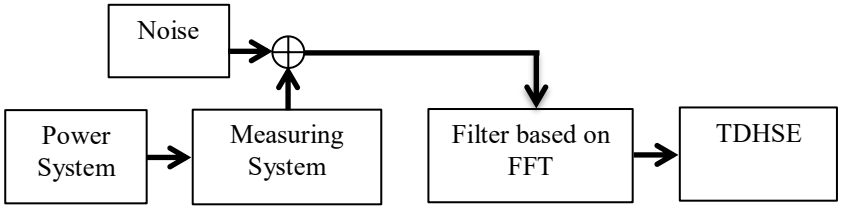

Fig. 4.1 Proposed methodology for time domain harmonic state estimation

4.2.1 Time-domain harmonic state formulation

Power system can be formulated in the discrete time domain if time t is defined as,

$$t = kT_S \tag{4.1}$$

where T_S is the inverse of F_S, called sample period, and k is the sample number. The notation of kT_S will be represented by the super index k.

The general mathematical formulation of HSE problem in the time domain given in (1.5) can be rewritten as follows:

$$\mathbf{z}^k = \mathbf{H}\mathbf{x}^k + \mathbf{e}^k \tag{4.2}$$

Least squares method is the most commonly used criterion for performance optimisation. It minimises the sum of squared deviations of estimated from actual measurements [Abur and Exposito 2004]. The solution to the optimisation problem depends on if the system is under-determined or over-determined.

In [Abur and Exposito 2004], how to obtain the pseudo inverse to an under-determined system is detailed. Be the system $\mathbf{Hx} = \mathbf{z}$ where $\mathbf{H}$ is an m x n-order matrix with $m < n$. The minimum norm problem is to find an $\mathbf{x}$ so that the norm defined by $\|\mathbf{x}\|_2 = (\mathbf{x}^T\mathbf{x})^{1/2}$ is minimum and satisfies $\mathbf{Hx} = \mathbf{z}$, i.e.

$$\begin{gathered}\text{Minimize } \|\mathbf{x}\|_2 \\ \text{Subject to } \mathbf{Hx} = \mathbf{z}\end{gathered} \tag{4.3}$$

The optimisation problem can be addressed using Lagrange function, i.e.

$$\mathfrak{L}(\mathbf{x}, \Lambda) = \frac{1}{2}\mathbf{x}^T\mathbf{x} - \Lambda^T(\mathbf{Hx} - \mathbf{z}) \tag{4.4}$$

where Λ is a scalar matrix.

Applying the derivative to obtain first order optimisation condition gives,

$$\left.\frac{\partial \mathfrak{L}(\mathbf{x},\Lambda)}{\partial x}\right|_{\mathbf{x}\Lambda} = \mathbf{x} - \mathbf{H}^T\Lambda = 0 \rightarrow \mathbf{x} = \mathbf{H}^T\Lambda \tag{4.5}$$

$$\left.\frac{\partial \mathfrak{L}(\mathbf{x},\Lambda)}{\partial \Lambda}\right|_{\mathbf{x}\Lambda} = \mathbf{Hx} - \mathbf{z} = \mathbf{0} \rightarrow \mathbf{Hx} = \mathbf{z} \tag{4.6}$$

Premultiplying (4.5) by $\mathbf{H}$ yields,

$$\mathbf{Hx} = \mathbf{H}\mathbf{H}^T\Lambda = \mathbf{z} \rightarrow \Lambda = (\mathbf{H}\mathbf{H}^T)^{-1}\mathbf{z} \tag{4.7}$$

Substitution of (4.7) in (4.5) gives,

$$\mathbf{x} = \mathbf{H}^T(\mathbf{H}\mathbf{H}^T)^{-1}\mathbf{z} \tag{4.8}$$

The estimated vector $\hat{\mathbf{x}}$ for an under-determined system at $t = kT$ is,

$$\hat{\mathbf{x}}^k = \mathbf{H}^T(\mathbf{H}\mathbf{H}^T)^{-1}\mathbf{z}^k \tag{4.9}$$

where the matrix $\mathbf{H}_R^+ = \mathbf{H}^T(\mathbf{H}\mathbf{H}^T)^{-1}$ is named right pseudo inverse.

[Abur and Exposito 2004] also describes how to obtain the pseudo inverse for an over-determined system. The least squares problem consists on finding $\mathbf{x}$ so that the index $J(\mathbf{x})$ defined as $J(\mathbf{x}) = \frac{1}{2}(\mathbf{z} - \mathbf{Hx})^T(\mathbf{z} - \mathbf{Hx})$ is minimised. The error $\mathbf{e}$ is defined as $\mathbf{e} = \mathbf{z} - \mathbf{Hx}$. Hence, the problem formulation can be defined as,

$$J(\hat{\mathbf{x}}) = \min \mathbf{e}\mathbf{e}^T \tag{4.10}$$

By applying the derivative to obtain first order optimisation condition gives,

$$\left.\frac{\partial J(\mathbf{x})}{\partial \mathbf{x}}\right|_{\mathbf{x}} = (\mathbf{z} - \mathbf{Hx})(-\mathbf{H}) = \mathbf{H}^T\mathbf{Hx} - \mathbf{H}^T\mathbf{z} \rightarrow \mathbf{x} = (\mathbf{H}^T\mathbf{H})^{-1}\mathbf{H}^T\mathbf{z} \tag{4.11}$$

where the matrix $\mathbf{H}_L^+ = (\mathbf{H}^T\mathbf{H})^{-1}\mathbf{H}^T$ is named left pseudo inverse.

The estimated vector $\hat{\mathbf{x}}$ at time $t = kT$ for an over-determined condition is defined as,

$$\hat{\mathbf{x}}^k = (\mathbf{H}^{\mathbf{T}}\mathbf{H})^{-1}\,\mathbf{H}^{\mathbf{T}}\mathbf{z}^k \tag{4.12}$$

The vector $\hat{\mathbf{x}}$ for a properly determined condition is,

$$\hat{\mathbf{x}}^k = \mathbf{H}^{-1}\mathbf{z}^k \tag{4.13}$$

4.2.2 Methodology to relate measurements to state variable

Numerical derivatives are needed to relate measurements to state variables. There are several methods suitable to determine the derivative of a function [Burden and Fires 2011]. The basic formulas are known as the forward-difference formula if $T_S > 0$ and the backward-difference formula if $T_S < 0$. These formulas generate an error $O(T_S)$. In this research work, the three-point midpoint formula is used as it generates an error $O(T_S^2)$. Hence, the derivative of the function g at $t = kT$ is,

$$g'_{(t=kT)} = \frac{g^{k+1} - g^{k-1}}{2T_S} + O(T_S^2) \tag{4.14}$$

The second derivative of the function y at $t = kT$ can be obtained using the second derivative midpoint formula. This formula also generates an error $O(T_S^2)$ and is defined as,

$$g''_{(t=kT)} = \frac{g^{k+1} - 2g^k + g^{k-1}}{T_S^2} + O(T_S^2) \tag{4.15}$$

In power systems, the most common cases where the state variables can be related to measurements are the following:

4.2.2.1 *The current in a capacitive bank placed at busbar s*

By applying circuit theory, the current in continuous time i_{C_s} in the capacitor C_s connected at busbar s, is given by,

$$i_{C_s} = C_s v'_s \tag{4.16}$$

By applying (4.14) to (4.16), the current in a capacitor connected at busbar s takes the form of,

$$i_{C_s}^k = C_s(v_s^{k+1} - v_s^{k-1})/2T_S \tag{4.17}$$

4.2.2.2 *Two busbars connected through a transmission line*

It is assumed that only one busbar is instrumented. Fig. 4.2 shows the transmission line modelled as the nominal-π circuit. The transmission line connects the busbars s and r. The instrumented busbar is s. The possible measures are the voltage v_s and the sending end line current i_{sr}.

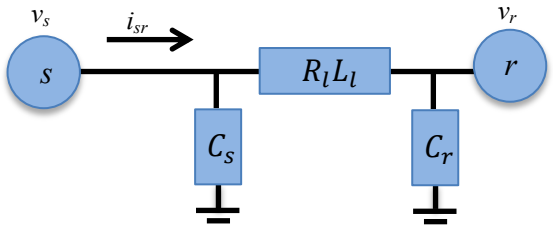

Fig. 4.2 Circuit models for two busbars connected through a line represented by a nominal-π model

The series branch currents in the RL component and in the capacitor are not possible measurements as they only exist virtually. By applying circuit theory in continuous time, buses *s* and *r* can be related as,

$$v_s - v_r = R_l i_{RL} + L_l i'_{RL} \tag{4.18}$$

By applying the KCL at bus *s*, the series branch current is defined as,

$$i_{RL} = i_{sr} - i_{C_s} \tag{4.19}$$

Substitution of (4.19) in (4.18) gives,

$$v_s - v_r = R i_{sr} - R i_{C_s} + L_l \left(i_{sr} - i_{C_s}\right)' \tag{4.20}$$

Developing (4.20), yields,

$$v_s - v_r = R_l i_{sr} - R_l i_{C_s} + L_l i'_{sr} - L_l i'_{C_s} \tag{4.21}$$

Substitution of (4.16) in (4.21) gives,

$$v_s - v_r = R_l i_{sr} - R_l C_s v'_s + L_l i'_{sr} - L_l C_s v''_s \tag{4.22}$$

By applying (4.14) and (4.15) to discretised (4.22) results in,

$$\left(1 - \frac{2L_l C_s}{T_S^2}\right) v_s^k + \left(\frac{R_l C_s}{2T_S} + \frac{L_l C_s}{T_S^2}\right) v_s^{k+1} + \left(\frac{L_l C_s}{T_S^2} - \frac{R_l C_s}{2T_S}\right) v_s^{k-1} - v_r^k = R_l i_{sr}^k + \frac{L_l}{2T_S}\left(i_{sr}^{k+1} - i_{sr}^{k-1}\right) \tag{4.23}$$

4.2.2.3 *Current in a linear load connected at busbar s*

If a linear load is represented by a RL series circuit as shown in Fig. 4.3 and by applying KVL, the voltage at busbar *s* v_s^k is,

$$v_s^k = R_L i_L^k + L_L (i_L^{k+1} - i_L^{k-1})/2T_S \tag{4.24}$$

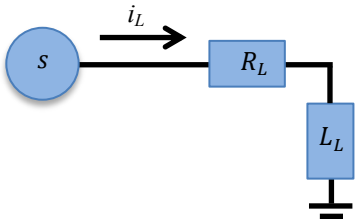

Fig. 4.3 Circuit model of a linear load represented by a RL series circuit

4.2.2.4 *Voltage at busbar s*

When the voltage at busbar s is measured v_{sz}, to obtain one estimation step, it is necessary obtain three consecutive voltage samples. Hence, the state variable must be partitioned as follows,

$$\begin{bmatrix} v_s^k \\ v_s^{k+1} \\ v_s^{k-1} \end{bmatrix} = \begin{bmatrix} 1 & 0 & 0 \\ 0 & 1 & 0 \\ 0 & 0 & 1 \end{bmatrix} \begin{bmatrix} v_{sz}^k \\ v_{sz}^{k+1} \\ v_{sz}^{k-1} \end{bmatrix} \tag{4.25}$$

Equations (4.17), (4.23) and (4.24) relate current measurements to busbar voltages, which are the state variables. Equation (4.25) adds voltage measurements to the measurement vector.

The first three samples are taken as the initial condition; hence it is not necessary to know a specific initial state.

4.2.3 Filter Based on Fourier Transform

4.2.3.1 *Fourier series*

Measurements are commonly contaminated by noise. Noise affects differently each harmonic since harmonics are of different magnitude. To select the harmonics of interest, a filter based on the Discrete Fourier Transform (DFT) is used. A summary of the proposed filter is given below:

A function $g(t)$, with period T, can be represented by Fourier series as,

$$g(t) = \frac{1}{T}\sum_{h=-\infty}^{\infty} \mathbf{c}_{\mathrm{F}}[h] e^{j2\pi ht/T} \tag{4.26}$$

The Fourier coefficients are given by,

$$\mathbf{c}_{\mathrm{F}}(h) = \frac{1}{T}\int_0^T g(t) e^{-j2\pi ht/T}\, dt \tag{4.27}$$

In the discrete time domain, the DFT can provide an approximation of the Fourier coefficients given a finite signal X sampled at N points, i.e.

$$X[k] = \begin{cases} 0 & k < 0 \\ \tilde{X}[k], & 0 \le k \le (N-1), \\ 0 & k \ge N \end{cases} \tag{4.28}$$

where $\tilde{X}[k]$ is one of the N samples of the measured signal during the time interval T. The Fourier coefficients are defined with the DFT as,

$$\mathbf{c}_{\mathrm{F}}[h] = \sum_{k=0}^{N-1} g[k]\, e^{j2\pi ht/T} \tag{4.29}$$

The Fast Fourier Transform (FFT) is an alternative algorithm to compute the Fourier coefficients. FFT transform has less computational complexity than DFT.

4.2.2.2 *Measurement model error*

The total error in (4.2) can be obtained as,

$$\boldsymbol{e}^{\boldsymbol{k}}_{\boldsymbol{total}} = \boldsymbol{e}^{\boldsymbol{k}}_{\boldsymbol{accuracy}} + \boldsymbol{e}^{\boldsymbol{k}}_{\boldsymbol{noise}} \tag{4.30}$$

The error, due to noise, affects more significantly the process of differentiation; hence, it should be removed or mitigated. For this purpose, the filter based on Fourier transform will be used.

The error presented in the harmonics of interest is called accuracy error. This error can be reduced using an over-determined condition [Abur and Exposito 2004].

4.2.2.3 *Filter based on Fourier Transform*

The procedure for noise mitigation of a measured signal is based on the following steps:

a. According to (4.28), the signal to be filtered is sampled during a time interval T to obtain N samples.
b. The FFT is applied to obtain up to the 50th harmonic coefficients.

c. To mitigate the noise spectrum, only harmonics of interest are considered. The filtered signal is reconstructed using (4.26) with the coefficients selected.

d. The selected harmonics of interest have still noise due to inaccuracy in measurements. However, the associated error to inaccuracies is mitigated by the LS method used during the estimation process.

4.3 Test power system description

4.3.1 5-Bus test power system

In this research work, the classical test system reported in [Stagg and El-abiad 1968], [Acha and Madrigal 2001] has been selected to conduct harmonic analysis. The parameter data are given in Tables 2.1, 2.2, and 2.3. The 5-bus test power system is shown in Fig. 4.4. Two possible assemblies of measuring devices, represented by the black and green colours, are shown. A black-green measuring device is added to the green set to make an over-determined system.

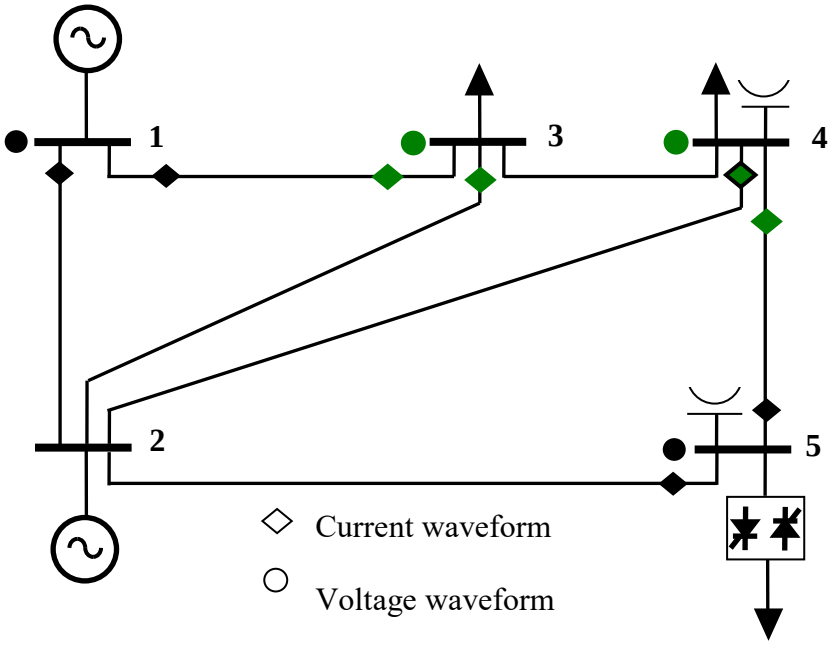

Fig. 4.4 5-bus test system where measuring devices placement are indicated

4.3.2 Simulation in the time domain

In order to conduct a simulation study closer to reality, the following considerations are observed:

- Obtain the generation conditions from a flow power study.
- Compute the parameters of the sinusoidal source model for generators

A power flow solution based on the Newton-Raphson method is a frequently used alternative [Saadat 1999]. Bus data is required for power flow algorithm. The bus data for the 5-bus test system is given in Table

4.1. The generator 1 has been defined as slack bus with $V_1 = 1.06$ and the generator 2 as PV bus with $V_2 = 1.045$ and $P_2 = 0.6$.

Table 4.1 Busbar data for 5-bus test system

			Load		**Generator**	
Busbar	**|Voltage| (pu)**	**Angle (rad)**	**MW**	**Mvar**	P_g	Q_g
1	1.06	0	0	0	0	0
2	1.045	0	0	0	60	0
3	1	0	40	20	0	0
4	1	0	80	40	0	0
5	1	0	60	0	0	0

Once power flow solution is obtained, the parameters of the sinusoidal source model, named the generation initial condition can be determined by,

$$I_T = (P_g - Q_g)/V_T^* \tag{4.30}$$

$$E = V_T + (R_g + X_g)I_T \tag{4.31}$$

The generator parameters are given in Table 4.2.

Table 4.2 Generator parameters

Generator	R_g	X_g
1	0.0125	0.3854
2	0.0125	0.3854

Data in (4.30) and (4.31) are in RMS values, i.e. they are defined in the frequency domain. In the time domain, it is necessary to define instantaneous quantities. The instantaneous generator voltage, v_g, can be defined as

$$v_g = \sqrt{2}|E|\sin(2\pi ft + \emptyset) \tag{4.32}$$

where $\emptyset$ is the angle of the phasor E.

The base value for the peak value of rated line-to-line voltage is defined as follows,

$$V_{\mathrm{p(base)}} = \sqrt{2}E_{(\mathrm{base})} \tag{4.33}$$

Dividing (4.32) by (4.33) yields,

$$\overline{v_g} = \bar{E}\sin(2\pi ft + \emptyset) \tag{4.34}$$

where $\overline{v_g}$ and $\bar{E}$ are the instantaneous and rms generator voltage, respectively, expressed in per unit notation.

4.4 Results

4.4.1 Power system simulation under linear load

The power flow solution is obtained for the test system defined in Section 4.3.1. Table 4.3 details the power flow solution.

Table 4.3 Busbar voltage and power generation

Busbar	**|Voltage| (pu)**	**Angle (degree)**	P_g **(pu)**	Q_g **(pu)**
1	1.060	0.000	1.25982	0.00012
2	1.045	-2.565	0.6000	-0.11654
3	1.019	-5.955	0	0
4	1.019	-6.637	0	0
5	1.038	-6.791	0	0

The parameters of the sinusoidal sources have been computed according to (4.29) and (4.30) which are given in Table 4.4.

Table 4.4 Per unit parameters of generator sources

Generator	$\|E\|$ (pu)	$\emptyset$ (degree)
1	1.1688	23.0732
2	1.0335	9.8783

Now, the response of the test system in the time domain can be simulated. The generation condition is tested in open circuit to measure the internal voltage. The generation conditions of both generators are shown in Fig. 4.5. From Fig. 4.5, the peak voltages for generators 1 and 2 are 1.169 and 1.033, respectively, which are agree with the theoretical values shown in Table 4.4.

Once generators are in close circuit, the voltages at busbars 1, 2, 3, 4, and 5 are generated as shown in Fig. 4.6(a). The details of peak voltages are shown in Fig. 4.6(b). These voltages are in close agreement with the voltages obtained by the power flow study summarised in Table 4.3.

Table 4.5 shows the busbar voltages, determined from the power flow study, and the corresponding in the time domain taken from the simulation response in order to compare them. The resulting difference is negligible.

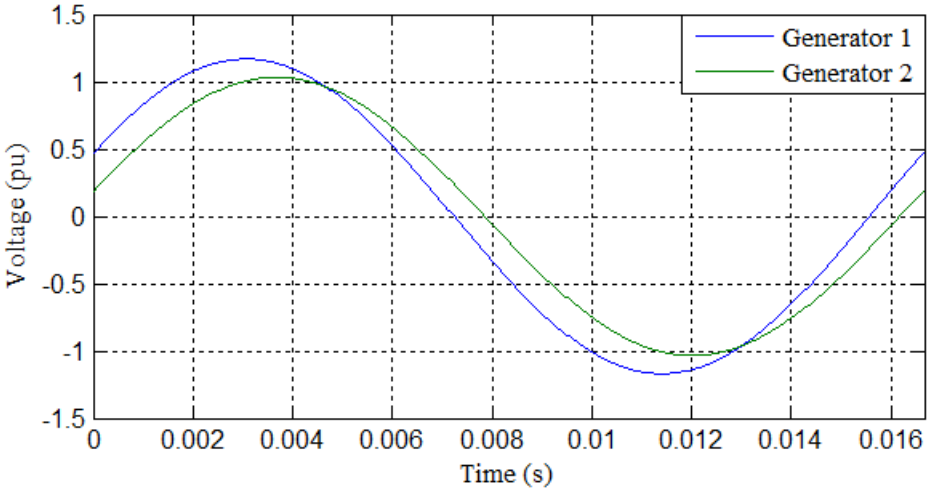

Fig. 4.5 Generation condition

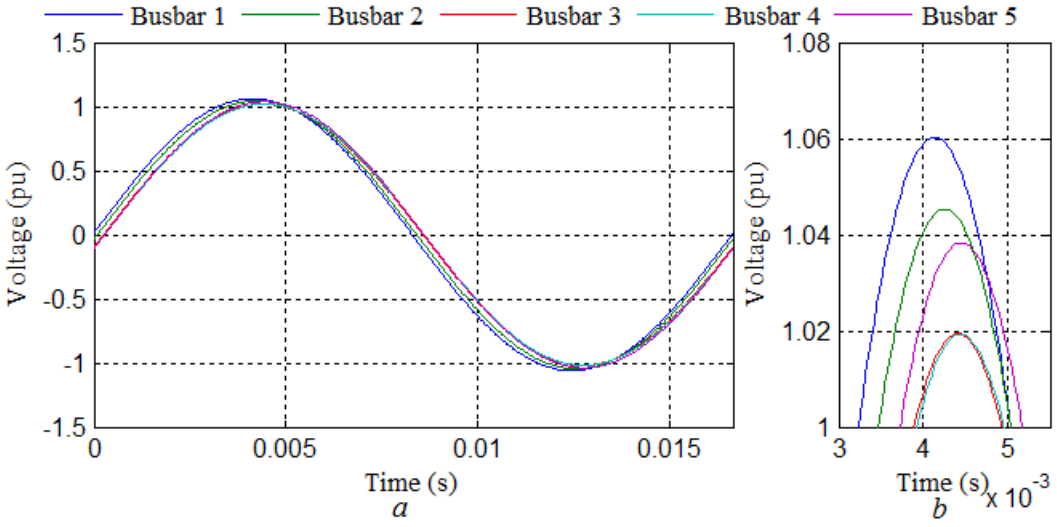

Fig. 4.6 Voltage at all busbars for steady state linear condition

Table 4.5 Power flow in the time and frequency domains

	Power Flow		**Time domain simulation**	
Busbar	**|Voltage| (pu)**	**Angle (degree)**	**|Voltage| (pu)**	**Angle (degree)**
1	1.060	0.000	1.06	0.000
2	1.045	-2.565	1.045	-2.56
3	1.019	-5.955	1.019	-5.95
4	1.019	-6.637	1.019	-6.63
5	1.038	-6.791	1.038	-6.79

4.4.2 Power system simulation with nonlinear load

A nonlinear load is connected at busbar 5. The nonlinear load has been described in Section 2.3.1.6. The resistive load is increased to R_L = 1.25, i.e. P_L = 0.8. According to (2.15) the firing angle is computed for an active power of 0.6, resulting in α = 66.17º or 3.1 milliseconds. Fig. 4.7 shows the bus voltage and current at the nonlinear load. Please observe how the distorted current causes harmonic distortion at busbar 5.

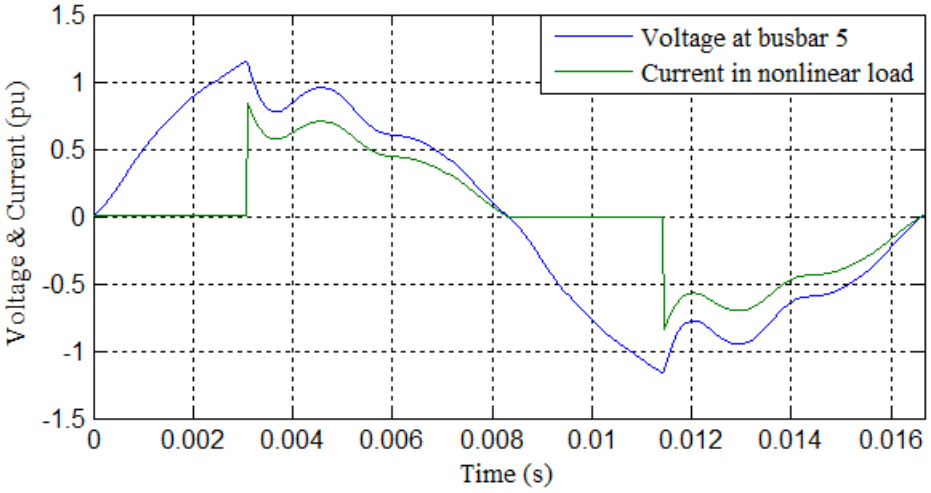

Fig. 4.7 Current in nonlinear load and distorted voltage at busbar 5

Not only the harmonic distortion is in the voltage at busbar 5 but also throughout the entire network, as shown in Fig. 4.8. However, from Fig. 4.8 it can be observed that the greatest distortion is in the busbar where the nonlinear load is connected, i.e. for this particular case, busbar 5.

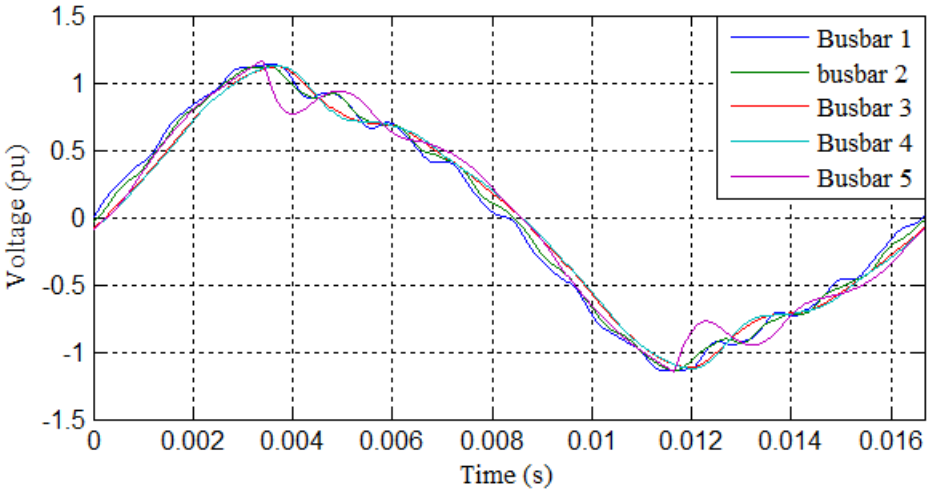

Fig. 4.8 Harmonic propagation through the entire network

4.4.3 Measuring process

The measurement data, voltage and current sampled waveforms, have been obtained by time domain simulation. In order to apply the proposed algorithm, data taken from measurements have been contaminated by the addition of random noise. The sampling frequency is F_S = 50000 samples per second. For instance, Fig. 4.9 shows the sending end line current and busbar voltage waveforms in line 1-3 and at busbar 1, respectively, with 1% of noise.

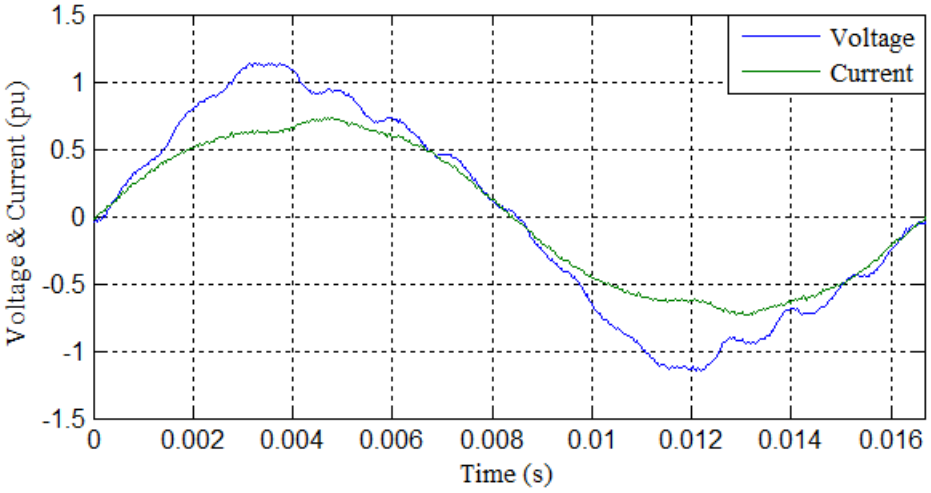

Fig. 4.9 Voltage at busbar 1 and sending end line current 1-3 measurements with noise of 1%

4.4.4 Filter based on Fourier transform

To show the effect of using noisy measurements, waveforms shown in Fig. 4.9 have been used to determine the voltage at busbar 3 using (4.22). As expected, due to the differentiation process, the computed signal shows significant noise, as shown in Fig. 4.10. To prevent the above, the filter based on Fourier transform has been applied to noisy measurements before TDHSE process is evaluated. For illustrative purposes, Fig. 4.11 shows how the noise has been reduced in the measurements for voltage at busbar 1 and sending current 1-3, which has been corrupted with 5% of noise. The measurements have been smoothed.

To evaluate the performance of the filtering process, the added noise level has been varied from 1 to 5%. The root-mean-square deviation (RMSD) has been used to compare differences between waveforms without noise and filtered measurements. Table 4.6 gives the RMSD for several noise levels; it can be observed from Table 4.6 how noise is mitigated. The remaining error will be mitigated using the TDHSE described next.

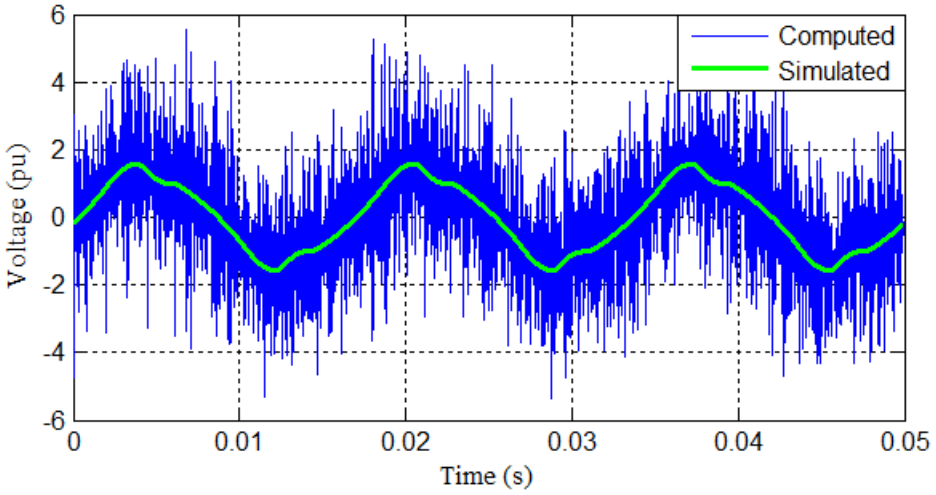

Fig. 4.10 Computed bus voltage 3 showing an increased noise due to the differentiation process

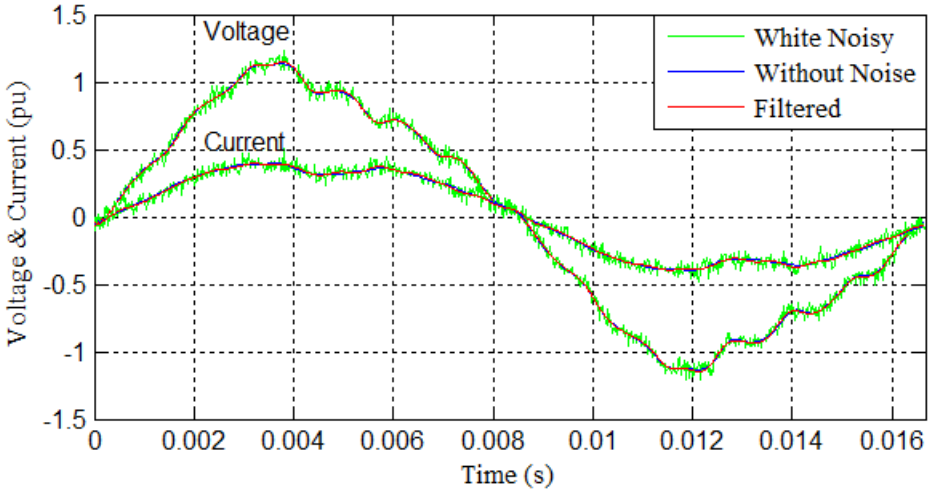

Fig. 4.11 Voltage at busbar 1 and sending end line current 1-3 filtered with noise of 5%

Table 4.6 Performance of the filter

Noise Level (%)	RMSD Busbar 1	RMSD Line 1-3
1	0.0052	0.0023
2	0.0061	0.0036
3	0.0075	0.0050
4	0.0090	0.0065
5	0.0107	0.0080

4.4.5 Time domain harmonic state estimation

Three case studies are conducted. The minimum number of measurements must be equal to the state variables to be full observable the power system under study, i.e. the properly determined condition since each measurement is related to a state variable. The measuring system can be configured in different ways that generates full observability. Thus, two particular properly determined measurement sets are selected, among others. The third case study is for an over-determined condition, i.e. there are more measurements than state variables, and this condition generates redundancy in measurements.

4.4.5.1 *Case study 1: Properly determined condition 1*

For this particular case study, two measuring devices have been chosen for voltages and three for currents. In order to compare the results, the added noise will be kept constant with the level noise set to 3%. The first combination to study the effect of the measuring devices placement is identified with black colour in Fig. 4.3. Since two devices are set for voltages, the selected state variables according to (4.24) have been partitioned into six states variables, but using only two measuring devices. Hence, the resulting **H** is a 9×9 matrix. Fig. 4.12(*a*), Fig. 4.12(*b*), and Fig. 4.12(*c*) show the simulated and the estimated voltage at unmonitored busbars 2, 3, and 4, respectively. A close agreement between responses has been achieved.

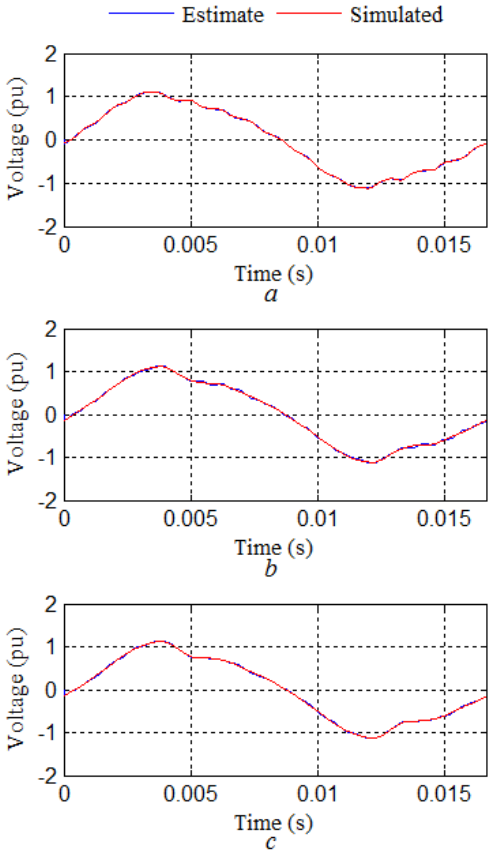

Fig. 4.12 Voltage at unmonitored busbars: (*a*) busbar 2, (*b*) busbar 3, and (*c*) busbar 4

Fig. 4.13 shows the detail of the spectra for the simulated and the estimated waveforms for the unmonitored busbar voltages. The THD shown in Table 4.7 indicates that the proposed TDHSE and the simulated values are in close agreement. The maximum difference between the simulated and the estimated responses is 0.08% presented in voltage at busbar 4.

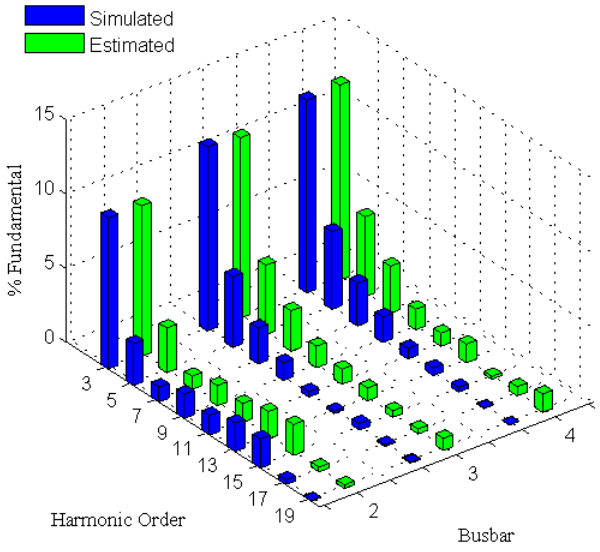

Fig. 4.13 Spectra for voltage at unmonitored busbar 2 for black measurement set

Table 4.7 THD for unmonitored busbars using the black measurement set

Busbar	Simulated THD (%)	Estimated THD (%)	Absolute Error	Relative Error (%)
2	11.2456	11.1317	0.0117	0.1
3	13.7957	13.4989	0.0385	0.2
4	14.7079	14.4959	0.0876	0.5

4.4.5.2 *Case study 2: Properly determined condition 2*

This case study is similar to case study conducted in Section 4.4.5.1. The difference is the placement of the measuring devices. The combination to study the effect of measuring devices placement is identified with green colour in Fig. 4.3. The measuring device identified with green and black colour is no considered. Fig. 4.12 shows the estimated voltage at unmonitored busbars (*a*), (*b*), and (*c*) for busbar 1, 2 and 5, respectively. A close agreement has been again achieved, which demonstrates the potential of the proposed TDHSE methodology. The Fig. 4.13 shows the detail of the spectra for the simulated and the estimate harmonic state evaluated in the unmonitored busbars. The THD is shown in Table 4.8. The maximum difference between the simulated and the estimated responses is 0.29% presented in voltage at busbar 5. It appears that although the accuracy depends on measuring locations, the difference between the black and green sets was of 0.2%.

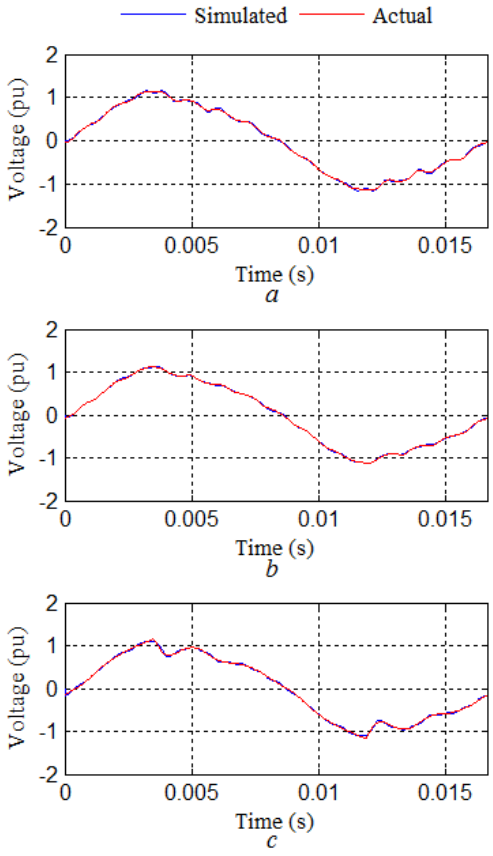

Fig. 4.14 Voltage at unmonitored busbars: (*a*) busbar 1, (*b*) busbar 2, and (*c*) busbar 5

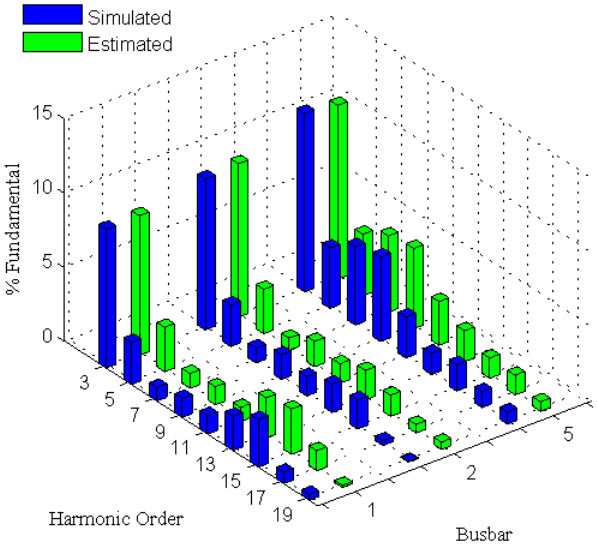

Fig. 4.15 Spectra for voltage at unmonitored busbar 2 using green measurement set

Table 4.8 THD for unmonitored busbars using the green measurement set

Busbar	Simulate	Estimated	Absolute Error	Relative Error (%)
1	10.7733	10.9156	0.1815	1.68
2	11.2456	11.2954	0.1520	1.35
5	15.5756	15.0563	0.2958	1.89

4.4.5.3 *Case study 3: An over-determined condition*

Fig. 4.4 shows one additional measuring device to the green set to generate an over-determined condition, i.e. $m > n$. The resulting **H** is a 10×9 matrix. Table 4.8 shows and compares the THD for the properly determined and over-determined condition. Using the over-determined condition, the TDH error for unmonitored busbar 1 has been lightly increased, 0.06%. However, The TDH errors for busbars 2 and 5 have been decreased, from 0.15 to 0.03 and for 0.29 to 0.01, respectively.

Table 4.9 THD for unmonitored busbars using the green-black measurement set

Busbar	Simulated	Properly Estimated	Properly Absolute Error	Relative Error (%)	Over Estimated	Over Absolute Error	Relative Error (%)
1	10.7733	10.9156	0.1815	1.68	10.9823	0.2482	2.30
2	11.2456	11.2954	0.1520	1.35	11.1804	0.0369	0.32
5	15.5756	15.0563	0.2958	1.89	15.3715	0.0194	0.12
Average	12.5315	12.4224	0.2098	1.67	15.5114	0.0201	0.82

4.5 Conclusions

A methodology in the time domain harmonic to estimate the voltage waveforms at unmonitored buses of power networks using filtered measurements based on Fourier transform has been proposed, and the Fourier transform has been applied to the estimate waveforms to explicitly obtain the harmonic state. The performance of the proposed methodology has been validated through direct comparison of the estimated waveforms against the simulated response. In all the analysed cases a close agreement between the estimated and the simulated response has been achieved; thus, demonstrating the potential of the TDHSE methodology.

The proposed methodology does not require an accurate previous knowledge of the harmonic sources nor of initial conditions. It only needs of a snapshot of voltage and current during at time interval of interest to estimate the harmonic state.

Although the accuracy of estimation depends on device placement, the error due to location has been relatively small, i.e. for the analysed cases it has been kept below 0.2%.

It has been demonstrated that the proposed TDHSE methodology has an accurate performance using a limited number of measuring devices.

Chapter 5 Harmonic state estimation in unbalanced power networks based on the optimal number of meters and the half-wave symmetry property

5.1 Introduction

This chapter describes a time domain methodology for HSE in three-phase unbalanced power systems. The proposed methodology is formulated to analyse the unbalanced operation of three-phase power networks including nonlinear loads. It takes into account the optimal number of measuring devices and exploits the property of half-wave symmetry in voltage and current waveforms to significantly reduce the computational effort of the solution process. The results obtained are validated through direct comparison against those obtained by the SimPowerSystems toolbox of Simulink®.

5.2 HSE in the discrete-time domain

The complete scheme for the HSE solution in the time domain is shown in Fig. 5.1. A concise description of the functional blocks is as follows: The measurement matrix relates measurements to state variables. It is developed using a three-phase network to analyse the unbalanced operation of power systems including nonlinear loads. The measuring process takes into account the optimal number of measuring devices to obtain full observability. Data are waveform samples; however, data may be corrupted by noise. A filter based on the FFT is applied for noise mitigation. To exploit the feature of symmetry, the voltage and current waveforms are sampled only during half-cycle. The TDHSE uses the measurement equation and the least square criterion to minimise the estimation error. In order to change from time domain to frequency domain, the FFT is used. To apply FFT, the feature of half-wave symmetry is used to obtain an estimated complete cycle.

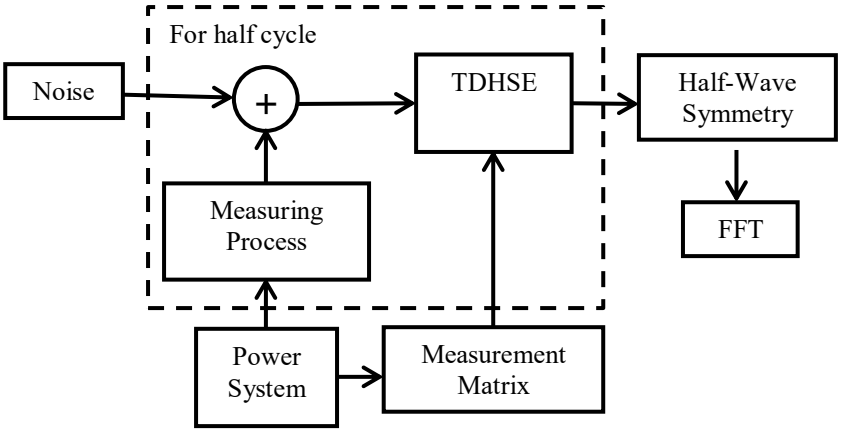

Fig. 5.1 Complete scheme for the time domain HSE problem

5.2.1 Measurement matrix

HSE is based on the mathematical relationship between state variables and measurements in a power network using a limited number of measuring devices as it is defined in (1.15).

The matrix **H** is said to be over-determined if $m > n$, under-determined if $m < n$, or properly determined if $m = n$ [Jeffrey 2010].

If the matrix **H** is over-determined, a well-known method to solve (1.15) is the classic WLS method as the criterion for performance optimization. The WLS method minimises the sum of the squared deviations from actual measurements of estimated state [Abbas et al. 2012], [Rakpenthai *et al.* 2013]. The estimated vector $\hat{\mathbf{x}}$ is defined in (4.11) [Abur and Exposito 2004].

If the matrix **H** is under-determined, the SVD gives a solution using the pseudo-inverse [Rad *et al.* 2013], [Nguyen et al. 2010], i.e. **H** can be factorised using SVD.

In Chapter 4, the elements more frequently analysed in power systems to form the measurement equation, such as medium and long transmission lines, as well as transformer and linear loads, have been analysed for single-phase networks. The mathematical formulation is now extended to represent three-phase unbalanced power networks.

5.2.1.1 *Transmission line modelled as an equivalent π-circuit*

Fig. 5.2 shows a general scheme for two buses, s and r, connected through a transmission line. The transmission line is usually modelled by a distributed parameters model, but it can be represented by an equivalent π-circuit as there is only interest in the behaviour at input and output ends of the line. The transmission line model includes the following parameters: the self and mutual resistances **R**, self and mutual inductances **L**, self and mutual capacitances **C** and the self and mutual admittances **G**, required to build the equivalent π-cicuit [Grainger and Stevenson 1996].

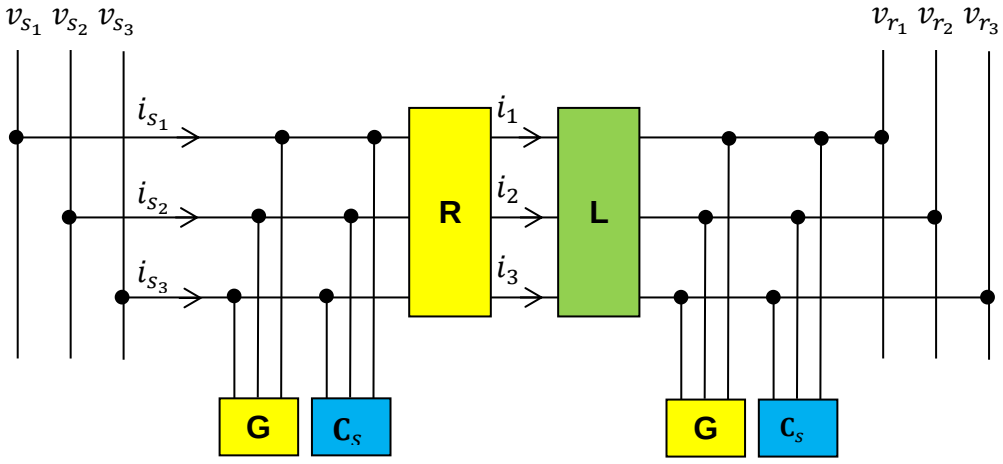

Fig. 5.2 Transmission line modelled as an equivalent π-circuit

The series branch current, $\mathbf{i} \in \mathbb{R}^{3\times3}$ in the RL components, and the shunt currents, $\mathbf{i}_G$ and $\mathbf{i}_C \in \mathbb{R}^{3\times3}$ in the $\mathbf{G}$ and $\mathbf{C}$ components, respectively, are not possible measurements as they are physically not available. However, by applying circuit theory in the continuous-time, the busbar voltages $\mathbf{v}_s$ and $\mathbf{v}_r \in \mathbb{R}^{3\times3}$, can be related as,

$$\mathbf{v}_s - \mathbf{v}_r = \mathbf{R}\mathbf{i} + \mathbf{L}\mathbf{i}' \tag{5.1}$$

where $\mathbf{v}_s = \begin{bmatrix} v_{s_1} \\ v_{s_2} \\ v_{s_3} \end{bmatrix}$, $\mathbf{v}_r = \begin{bmatrix} v_{r_1} \\ v_{r_2} \\ v_{r_3} \end{bmatrix}$, $\mathbf{R} = \begin{bmatrix} R_{11} & R_{12} & R_{13} \\ R_{21} & R_{22} & R_{23} \\ R_{31} & R_{32} & R_{33} \end{bmatrix}$, $\mathbf{i} = \begin{bmatrix} i_1 \\ i_2 \\ i_3 \end{bmatrix}$, $\mathbf{L} = \begin{bmatrix} L_{11} & L_{12} & L_{13} \\ L_{21} & L_{22} & L_{23} \\ L_{31} & L_{32} & L_{33} \end{bmatrix}$ and $\mathbf{i}' = \begin{bmatrix} i_1' \\ i_2' \\ i_3' \end{bmatrix}$.

By applying the Kirchhoff current law (KCL) at bus *s*, the sending end current $\mathbf{i}_s$ is defined as,

$$\mathbf{i}_s = \mathbf{i} + \mathbf{i}_\mathrm{G} + \mathbf{i}_\mathrm{C} \tag{5.2}$$

where $\mathbf{i}_s = \begin{bmatrix} i_{s_1} \\ i_{s_2} \\ i_{s_3} \end{bmatrix}$, $\mathbf{i}_\mathrm{G} = \begin{bmatrix} i_{\mathrm{G}_1} \\ i_{\mathrm{G}_2} \\ i_{\mathrm{G}_3} \end{bmatrix}$ and, $\mathbf{i}_\mathrm{C} = \begin{bmatrix} i_{\mathrm{C}_1} \\ i_{\mathrm{C}_2} \\ i_{\mathrm{C}_3} \end{bmatrix}$.

The continuous-time current $\mathbf{i}_\mathrm{C}$ in the capacitor $\mathbf{C}_s$, connected at busbar *s*, is given by,

$$\mathbf{i}_\mathrm{C} = \mathbf{C}_s\mathbf{v}_s' \tag{5.3}$$

where $\mathbf{C}_s = \begin{bmatrix} C_{11} & C_{12} & C_{13} \\ C_{21} & C_{22} & C_{23} \\ C_{31} & C_{32} & C_{33} \end{bmatrix}$, and, $\mathbf{v}_s' = \begin{bmatrix} v_{s_1}' \\ v_{s_2}' \\ v_{s_3}' \end{bmatrix}$.

By applying the Ohm's law, the continuous-time current through an admittance $\mathbf{G}$ connected at busbar *s* is given by,

$$\mathbf{i}_\mathrm{G} = \mathbf{G}\mathbf{v}_s \tag{5.4}$$

where $\mathbf{G} = \begin{bmatrix} G_{11} & G_{12} & G_{13} \\ G_{21} & G_{22} & G_{23} \\ G_{31} & G_{32} & G_{33} \end{bmatrix}$.

Hence, substituting (5.3) and (5.4) in (5.2) and solving for $\mathbf{i}$ gives,

$$\mathbf{i} = \mathbf{i}_s - \mathbf{G}\mathbf{v}_s - \mathbf{C}_s\mathbf{v}_s' \tag{5.5}$$

Please notice (5.5) is now left as a function of available measurements. The derivative of (5.5) is,

$$\mathbf{i}' = \mathbf{i}_s' - \mathbf{G}\mathbf{v}_s' - \mathbf{C}_s\mathbf{v}_s'' \tag{5.6}$$

Substitution of (5.5) and (5.6) in (5.1) gives,

$$(\mathbf{I} + \mathbf{RG})\mathbf{v}_s + (\mathbf{RC}_s + \mathbf{LG})\mathbf{v}_s' + \mathbf{LC}_s\mathbf{v}_s'' - \mathbf{v}_r = \mathbf{R}\mathbf{i}_s + \mathbf{L}\mathbf{i}_s' \tag{5.7}$$

where $\mathbf{I} \in \mathbb{R}^{3\times3}$ is the identity matrix.

To obtain the discretised measurement equation it is necessary to consider the samples *k*, the previous *k*-1, and the subsequent *k*+1. By applying (4.12) and (4.13) to discretise (5.7) leads to,

$$(\mathbf{I} + \mathbf{RG})\mathbf{v}_s^k + \frac{(\mathbf{RC}_s+\mathbf{LG})(\mathbf{v}_s^{k+1}-\mathbf{v}_s^{k-1})}{2T_\mathrm{S}} + \frac{\mathbf{LC}_s(v_s^{k+1}-2\mathbf{v}_s^k+\mathbf{v}_s^{k-1})}{T_\mathrm{S}^2} - \mathbf{v}_r^k = \mathbf{R}\mathbf{i}_S^k + \frac{\mathbf{L}(\mathbf{i}_S^{k+1}-\mathbf{i}_S^{k-1})}{2T_\mathrm{S}} \tag{5.8}$$

Reordering (5.8) gives,

$$\mathbf{c1}_{s-r}\mathbf{v}_s^k + \mathbf{c2}_{s-r}\mathbf{v}_s^{k+1} + \mathbf{c3}_{s-r}\mathbf{v}_s^{k-1} - \mathbf{v}_r^k = \mathbf{b1}_s\mathbf{i}_s^k + \mathbf{b2}_s\mathbf{i}_s^{k+1} + \mathbf{b3}_s\mathbf{i}_s^{k-1} \tag{5.9}$$

where $\mathbf{c1}_{1,s-r} = \mathbf{I} + \mathbf{RG} - \frac{2\mathbf{LC}_s}{T_S^2}$, $\mathbf{c2}_{s-r} = \frac{\mathbf{RC}_s}{2T_S} + \frac{\mathbf{LG}}{2T_S} + \frac{\mathbf{LC}_s}{T_S^2}$, $\mathbf{c3}_{s-r} = \frac{\mathbf{LC}_s}{T_S^2} - \frac{\mathbf{RC}_s}{2T_S} - \frac{\mathbf{LG}}{2T_S}$, $\mathbf{b1}_s = \mathbf{R}$, $\mathbf{b2}_s = \mathbf{L}/2T_S$, and $\mathbf{b3}_s = -\mathbf{L}/2T_S$. The sub-index $s-r$ of the coefficients: **c1, c2,** and **c3** is associated with the sending end and receiving end of the transmission line. The sub-index s of the coefficients: **b1, b2,** and **b3** is associated with the sending end bus voltage.

If the sending end bus *s* is the instrumented busbar of the transmission line, the measurements are the sending end voltage $\mathbf{v}_{zs}$ and the sending end current $\mathbf{i}_{zs}$**.** This condition gives a properly determined measurement equation,

$$\begin{bmatrix} \mathbf{b1}_s\mathbf{i}_{zs}^k + \mathbf{b2}_s\mathbf{i}_{zs}^{k+1} + \mathbf{b3}_s\mathbf{i}_{zs}^{k-1} \\ \mathbf{v}_{zs}^k \\ \mathbf{v}_{zs}^{k+1} \\ \mathbf{v}_{zs}^{k-1} \end{bmatrix} = \begin{bmatrix} \mathbf{c1}_{s-r} & \mathbf{c2}_{s-r} & \mathbf{c3}_{s-r} & -\mathbf{I} \\ \mathbf{I} & \mathbf{0} & \mathbf{0} & \mathbf{0} \\ \mathbf{0} & \mathbf{I} & \mathbf{0} & \mathbf{0} \\ \mathbf{0} & \mathbf{0} & \mathbf{I} & \mathbf{0} \end{bmatrix} \begin{bmatrix} \mathbf{v}_s^k \\ \mathbf{v}_s^{k+1} \\ \mathbf{v}_s^{k-1} \\ \mathbf{v}_r^k \end{bmatrix} \tag{5.10}$$

where $\mathbf{z} = \begin{bmatrix} \mathbf{b1}_s\mathbf{i}_{zs}^k + \mathbf{b2}_s\mathbf{i}_{zs}^{k+1} + \mathbf{b3}_s\mathbf{i}_{zs}^{k-1} \\ \mathbf{v}_{zs}^k \\ \mathbf{v}_{zs}^{k+1} \\ \mathbf{v}_{zs}^{k-1} \end{bmatrix}$, $\mathbf{H} = \begin{bmatrix} \mathbf{c1}_{s-r} & \mathbf{c2}_{s-r} & \mathbf{c3}_{s-r} & -\mathbf{I} \\ \mathbf{I} & \mathbf{0} & \mathbf{0} & \mathbf{0} \\ \mathbf{0} & \mathbf{I} & \mathbf{0} & \mathbf{0} \\ \mathbf{0} & \mathbf{0} & \mathbf{I} & \mathbf{0} \end{bmatrix}$, and $\mathbf{x} = \begin{bmatrix} \mathbf{v}_s^k \\ \mathbf{v}_s^{k+1} \\ \mathbf{v}_s^{k-1} \\ \mathbf{v}_r^k \end{bmatrix}$. Please notice that matrices $\mathbf{I}$ and $\mathbf{0} \in \mathbb{R}^{3\times3}$ are the identity and zero matrices, respectively.

5.2.1.2 *Transmission line modelled as lumped parameter*

If the admittance $\mathbf{G}$ is neglected, the line transmission can be represented by a more simplified model. Hence, the coefficients in (5.9) are simplified. Please notice that for this case, these coefficients are parameters $\in \mathbb{R}^{3\times3}$. The resulting coefficients are:

$\mathbf{c1}_{s-r} = \mathbf{I} - \frac{2\mathbf{LC}_s}{T_S^2}$, $\mathbf{c2}_{s-r} = \frac{\mathbf{RC}_s}{2T_S} + \frac{\mathbf{LC}_s}{T_S^2}$, $\mathbf{c3}_{s-r} = \frac{\mathbf{LC}_s}{T_S^2} - \frac{\mathbf{RC}}{2T_S}$, $\mathbf{b1}_s = \mathbf{R}$, $\mathbf{b2}_s = \mathbf{L}/2T_S$, and $\mathbf{b3}_s = -\mathbf{L}/2T_S$.

5.2.1.3 *Short transmission line*

For these devices, the capacitance $\mathbf{C}_s$ and the admittance $\mathbf{G}$ are omitted. Hence, the coefficients are simplified as follows,

$\mathbf{c1}_{s-r} = \mathbf{I}$, $\mathbf{c2}_{s-r} = \mathbf{0}$, $\mathbf{c3}_{s-r} = \mathbf{0}$, $\mathbf{b1}_s = \mathbf{R}$, $\mathbf{b2}_s = \mathbf{L}/2T_S$, and $\mathbf{b3}_s = -\mathbf{L}/2T_S$.

Rewriting (5.9) with the new coefficients gives,

$$\mathbf{v}_s^k - \mathbf{v}_r^k = \mathbf{b1}_s\mathbf{i}_s^k + \mathbf{b2}_s\mathbf{i}_s^{k+1} + \mathbf{b3}_s\mathbf{i}_s^{k-1} \tag{5.11}$$

5.2.1.4 *Current in a load connected at busbar s*

If the load is modelled as a resistance $\mathbf{R}_L$ connected in parallel to an inductance $\mathbf{L}_L$ supplied by $\mathbf{v}_s$**,** and $\mathbf{i}_L$ is the current in the load**,** the equation that relates the load current and the supplying voltage is,

$$\mathbf{i}_L' = \frac{\mathbf{v}_s'}{\mathbf{R}_L} + \frac{\mathbf{v}_s}{\mathbf{L}_L} \tag{5.12}$$

By applying (4.14) to discretise (5.12) gives,

$$\mathbf{c4}_s\mathbf{v}_s^k + \mathbf{c5}_s\mathbf{v}_s^{k+1} + \mathbf{c6}_s\mathbf{v}_s^{k-1} = \mathbf{i}_L^{k+1} - \mathbf{i}_L^{k-1} \tag{5.13}$$

where $\mathbf{c4}_s = 2T_S/\mathbf{L}_L$. $\mathbf{c5}_s = 1/\mathbf{R}_L$, $\mathbf{c6}_s = -1/\mathbf{R}_L$.

If the load is modelled by a resistance $\mathbf{R}$ connected in series to an inductance $\mathbf{L}$, (5.11) can be extended to model the load. If $\mathbf{v}_r = \mathbf{0}$ and $\mathbf{i}_s = \mathbf{i}_L$ in (5.11), it yields,

$$\mathbf{v}_s^k = \mathbf{b1}_s\mathbf{i}_L^k + \mathbf{b2}_s\mathbf{i}_L^{k+1} + \mathbf{b3}_s\mathbf{i}_L^{k-1} \tag{5.14}$$

5.2.1.5 *Current in a capacitors bank connected at busbar s*

The current in a capacitors' bank $\mathbf{C}_s$ connected at busbar *s* can be obtained using (5.3). By applying (4.12) to discretise (5.3) gives,

$$\mathbf{v}_s^{k+1} - \mathbf{v}_s^{k-1} = \mathbf{b4}_s\mathbf{i}_{C_s}^k \tag{5.15}$$

where $\mathbf{b4}_s = 2T_S/\mathbf{C}_s$ and $\mathbf{i}_{C_s}$ is the current in the capacitors' bank, which can be measured.

5.2.1.6 *Line current when busbar voltages are known*

In the frequency domain, if all busbar voltages are known, the total network can be determined. In the time domain, this premise is also true. This is the reason to take the bus voltages as state variables. The series current in a transmission line of Fig. 5.2 can be determined by solving (5.1) for $\mathbf{i}$ using a numerical method such as the Euler method, i.e.

$$\mathbf{i}^k = \left(\mathbf{R} + \frac{\mathbf{L}}{T_S}\right)^{-1}\left(\mathbf{v}_s^k - \mathbf{v}_r^k + \frac{\mathbf{L}}{T_S}\mathbf{i}^{k-1}\right) \tag{5.16}$$

Since $\mathbf{i}^{k-1}$ is not known, it can be initialized to zero and apply the numerical integration for a few cycles, to obtain a better initial approximation. The shunt current in a transmission line can be also determined by discretising (5.3) and (5.4), i.e.

$$\mathbf{i}_C^k = \frac{\mathbf{C}_s}{2T_S}(\mathbf{v}_s^{k+1} - \mathbf{v}_s^{k-1}) \tag{5.17}$$

$$\mathbf{i}_G^k = \mathbf{G}\mathbf{v}_s^k \tag{5.18}$$

Finally, the sending end current can be determined through the discretised form of (5.2), i.e.

$$\mathbf{i}_s^k = \mathbf{i}^k + \mathbf{i}_C^k + \mathbf{i}_G^k \tag{5.18}$$

5.2.2 Measuring process

The measuring process consists in the capture of voltage and current waveforms. The measuring devices can be data acquisition (DAQ) systems. The number of channels of DAQ systems is practically unlimited since they can be connected in cascade. Since HSE deals with a limited number of measuring devices, an algorithm to optimise this limited number must be used. Data may be corrupted by noise, making necessary the use of a filter for its mitigation. These two issues are described next.

***5.2.2.1** Optimal number of measuring devices*

Power quality meters have been used for HSE assessment. To optimise their number, several contributions in the frequency domain have been reported [Saxena *et al.* 2014], [Almeida and Kagan 2013], [Eldery *et al.* 2006]. Since the proposed methodology is formulated in the time domain, an optimisation algorithm must be suggested. The reported algorithms to obtain full observability in the frequency domain can be exploited [Korres *et al*. 2014], [Koutsoukis *et al.* 2013], [Rashidi 2013], [Saha et al. 2012], [Mahari and Seyedi 2013], [Müller and Castro 2016], [Gou 2008]; therefore, the concept can be extended to the time domain. The approaches to analyse the observability are the numerical analysis [Korres *et al*. 2014], [Koutsoukis *et al.* 2013], and the topological analysis [Koutsoukis *et al.* 2013], [Rashidi 2013]. The topological analysis approach can be summarised in the following rules [Rashidi 2013], [Saha *et al.* 2012], [Mahari and Seyedi 2013], [Müller and Castro 2016]:

Rule 1: Installation of a measuring device in a given bus makes itself and other buses incident to that bus observable [Rashidi 2013], [Saha *et al.* 2012], [Mahari and Seyedi 2013], [Müller and Castro 2016], [Gou 2008].

Since TDHSE uses voltage and current waveforms as measurements, conventional measurements such as injection current and power flow are not used in methodologies formulated in the time domain. However, particularly, there are two additional rules that incorporate the pseudo-measurement of zero injection bus (ZIB) [Koutsoukis *et al.* 2013], [Rashidi 2013], [Saha et al. 2012], [Mahari and Seyedi 2013], [Müller and Castro 2016]. A ZIB is a bus that does not inject current into the system. These additional rules to obtain observability are as follows,

Rule 2: If only one bus is unobservable among a ZIB and its entire incident buses, the unobservable bus will also be identified as observable by applying the KCL at the ZIB. Currents in the time domain can be computed using (5.16), (5.17), and (5.18).

Rule 3: If the entire incident buses to m connected unobservable ZIBs are observable, the ZIBs can be observable by applying KCL.

The mathematical formulation that satisfies the rule of observability number 1 can be formulated as a problem of ILP as follows [Gou 2008],

$$\mathbf{Min} \sum_{\mathbf{i=1}}^{\mathbf{n}} \mathbf{d_i}$$

$$S.T. \mathbf{Ad} \geq \mathbf{b} \tag{5.19}$$

where n is the number of busbars and d_i is a binary variable with entries are

$$d_i = \begin{cases} 1, & \text{if bus } i \text{ is instrumented} \\ 0, & \text{otherwise} \end{cases}$$

The matrix A is formed using the line data of the bus, i.e.

$$a_{ij} = \begin{cases} 1, & \text{if } i = j \\ 1, & \text{if } i \text{ and } j \text{ are adjacents} \\ 0, & \text{otherwise} \end{cases}$$

The vector $\mathbf{d} \in \mathbb{R}^n$ contains each possibility of monitoring the n buses, i.e. $\mathbf{d} = [d_1\ d_2 \cdots d_n]^{\mathrm{T}}$.

The vector $\mathbf{b} \in \mathbb{R}^n$ contains the number of times that a bus is observed. The basic case, when each bus must be observable at least once, corresponds to $\mathbf{b} = [1\ 1 \cdots 1]^{\mathrm{T}}$.

The number of measuring devices can be reduced further if the ZIB and rules of observability number 2 and 3 are taken into account. In order to apply (5.19) when a ZIB is taken into account, the topological observability must be modified. The modification consist in join the ZIB with one incident to it, and modifies the new constrains defined in matrix A.

5.2.2.2 *Half-wave symmetry property*

In order to exploit the half-wave symmetry property, the waveforms are sampled only for a half-cycle instead of a complete cycle. That means that if a cycle is divided into *N* samples it is only necessary to take *N*/2 samples.

Let $\mathbf{z}_{\mathrm{h}}$ be the half-cycle sampled measurement. By exploiting the half wave symmetry in voltage and current waveforms, a completed cycle can be formed as follows,

$$\mathbf{z} = \mathbf{z}_{\mathrm{h}} \cup -\mathbf{z}_{\mathrm{h}} \tag{5.20}$$

As a consequence, the time needed to take the measurement set is reduced by approximately 50% as it only samples half cycle of the waveform.

5.2.2.3 *Filter based on Fourier transform*

Measurements are commonly contaminated by noise. Noise affects differently each harmonic owing to harmonics are of different magnitude. To mitigate the noise, a filter based on FFT, explained in Section 4.2.3, is used. The filtering is applied to each measurement.

5.2.3 Noise

The simulated response of the analysed test systems was obtained with the SimPowerSystems toolbox of Simulink®. The selected measurements have been contaminated by adding random values with normal distribution, zero mean, and different variance levels. The added noise affects differently the estimation of each harmonic as harmonic levels are of different magnitudes. The signal noise ratio (SNR) is a quantity that compares the signal level to the noisy environment. For instance, if the noise is 1%, harmonics whose level is 10% will have a SNR of -46.08 dB whereas harmonics of 0.5% will have a SNR of 13.86 dB, i.e. the magnitude of the noise is twice the magnitude of the signal. Even more, if two noisy measurements are used to estimate a third quantity, the noise in the estimated quantity is the result of multiplication of the noisy levels of the corresponding measurements.

The accuracy of an approximated method can be evaluated in terms of the error of the method [Hoffman 2001]. There are two ways to define the error: absolute error and relative error. The absolute error is defined as,

$$absolute\ error = |exact\ value - approximated\ value| \tag{5.21}$$

The absolute error does not take into account the magnitude of the quantity under study. When the numbers that will be compared widely differ from each other, the relative error is the best choice for this purpose. The relative error is defined as,

$$relative\ error = \frac{|exact\ value - approximated\ value|}{exact\ value} \tag{5.22}$$

The relative error can be declared directly or as a percentage.

5.3 Test systems

5.3.1 Modified Lower South Island of New Zealand

The modified Lower South Island of New Zealand test system is shown in Fig. 5.3. The test system data are reported in [Watson & Arrillaga 2007]. One bus has been instrumented to obtain a full observability, i.e. the properly determined condition. This condition is shown in Fig. 5.3. A three-phase harmonic current source is injected at bus T220. The harmonic current components are given in Table 5.1.

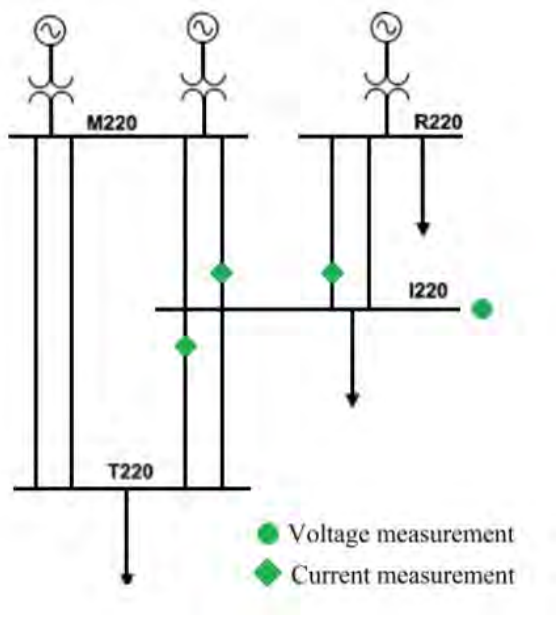

Fig. 5.3 Modified Lower South Island of New Zealand

Table 5.1 Harmonic current injection

h	Peak value (A)	Phase sequence
5	4	-
7	2	+
11	1	-
13	0.5	+

5.3.2 Modified IEEE 14-bus

To evaluate the robustness of the proposed methodology, the modified IEEE 14-bus system, shown in Fig. 5.4 has been also selected as test system. Positive sequence data is taken from [IEEE 2016] while the zero sequence data is given in Appendix B. The measuring devices and their placement to obtain a full observability are shown in Fig. 5.4 as a green set. This condition corresponds to the determined case. According to the available measuring devices, more can be added to have redundancy and thus reduce the estimation error. For illustrative purposes, an additional set of measuring devices, marked as a red set, has been added to obtain an over-determined case. This set is also shown in Fig. 5.4 and identified as additional measurements.

In order to add nonlinear loads, an AC-AC converter has been used. The AC-AC converter is controlled by the firing angle α; hence, the load current is a nonlinear load connected to busbar 4.

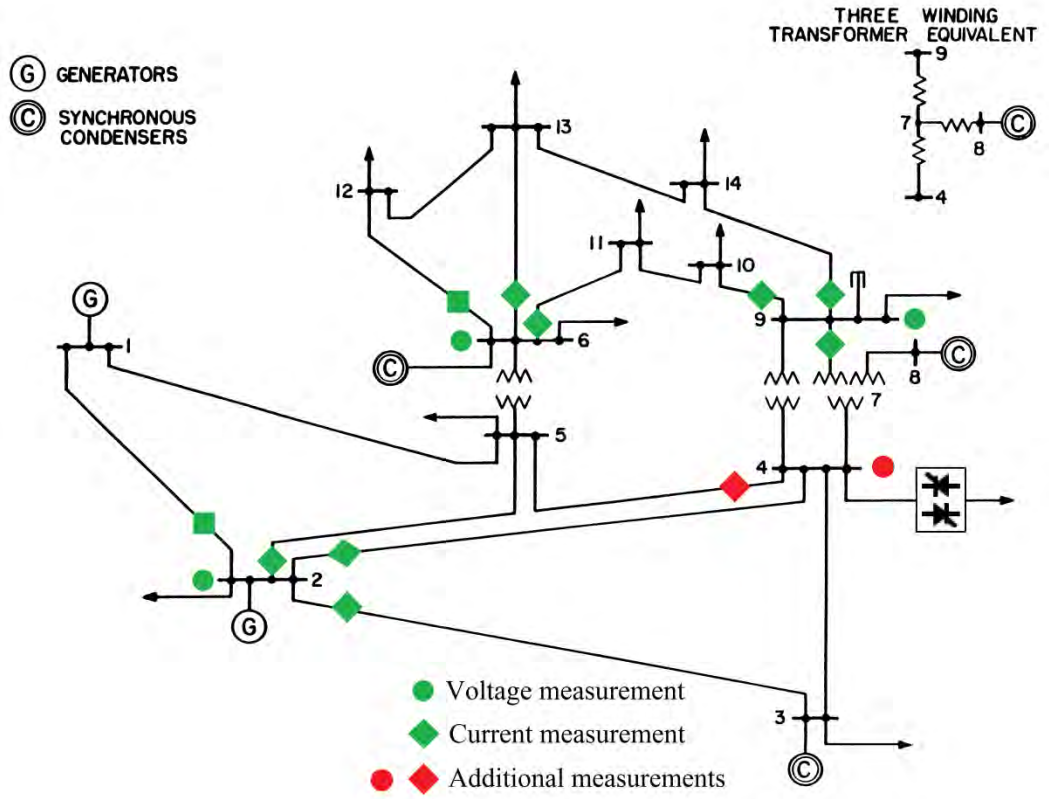

Fig. 5.4 Modified IEEE 14-bus system

5.4 Case studies

5.4.1 Case study 1: Comparative analysis of the proposed method

This case study has been performed in the test system shown in Fig. 5.3.

5.4.1.1 *Optimal placement of measuring devices*

By applying (5.18) to the test system, the resulting instrumented busbar is I220. The number of measuring devices to obtain full observability is 12, i.e. the four three-phase measuring devices shown in Fig. 5.3. This represents a significant saving in the instrumented resources with respect to the case study reported in [Medina and Cisneros-Magaña 2012] where the harmonic state was obtained using 27 measuring devices. It represents a reduction of 55% in the number of measuring devices.

5.4.1.2 *Measuring process*

The added noise in the measurements has a standard deviation of 0.3. The fundamental frequency is $f = 50$ Hz. The sample frequency is $F_S = 25{,}600$ samples per second, i.e. 256 samples per half period. According to the proposed methodology, voltage and current waveforms have been sampled during half period. Fig. 5.5 shows the sampled three-phase waveforms of the noisy sending end current in line I220–T220, which are identified in black.

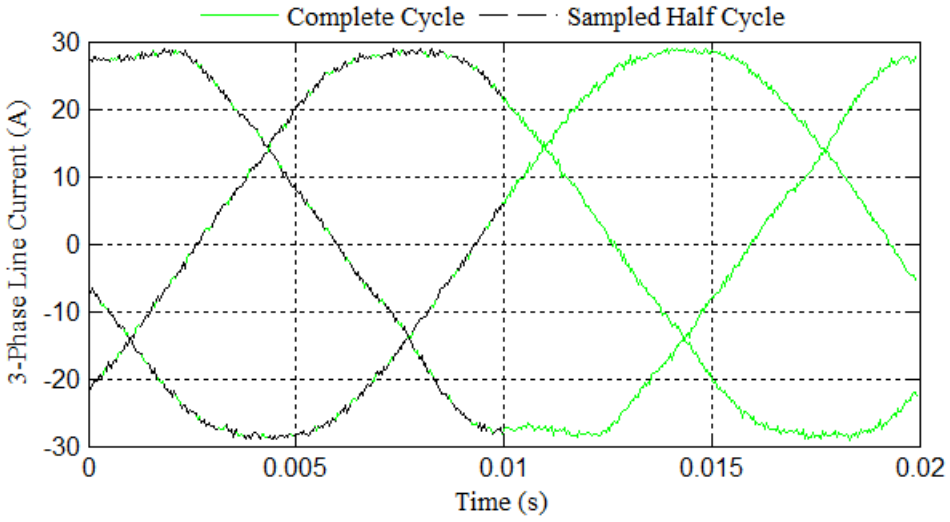

Fig. 5.5 Half cycle is sampled for sending end current in line I220–T220

A complete cycle is formed. The first half cycle is obtained by direct measurements, i.e. by sampling the electric quantities. The second half cycle is generated by applying the half-wave symmetry property by using (5.20) as shown in Fig. 5.6. Now, the filter based on Fourier for a half cycle can be applied. The sending end current waveforms in line I220-T220 is shown in Fig. 5.7. The noise has been mitigated from 0.3 to 0.03, i.e. ten times.

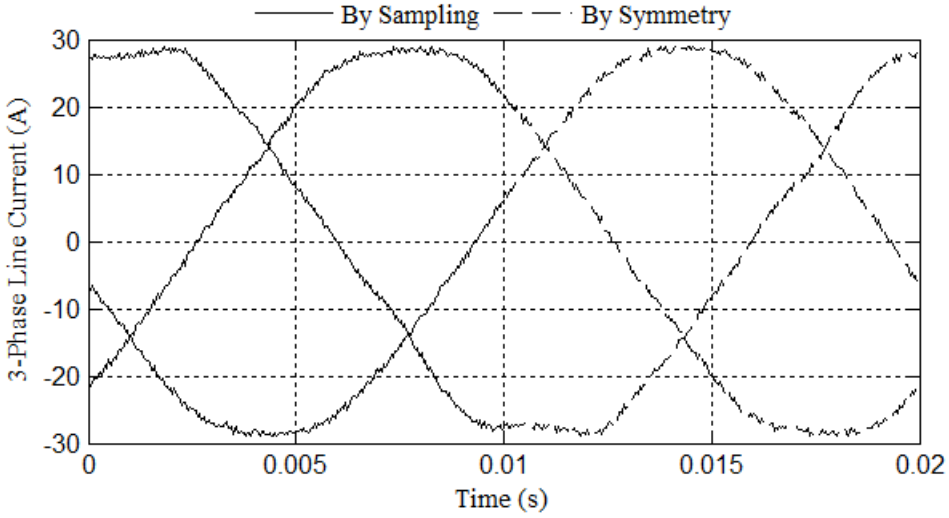

Fig. 5.6 A complete cycle is formed for sending end current in line I220–T220

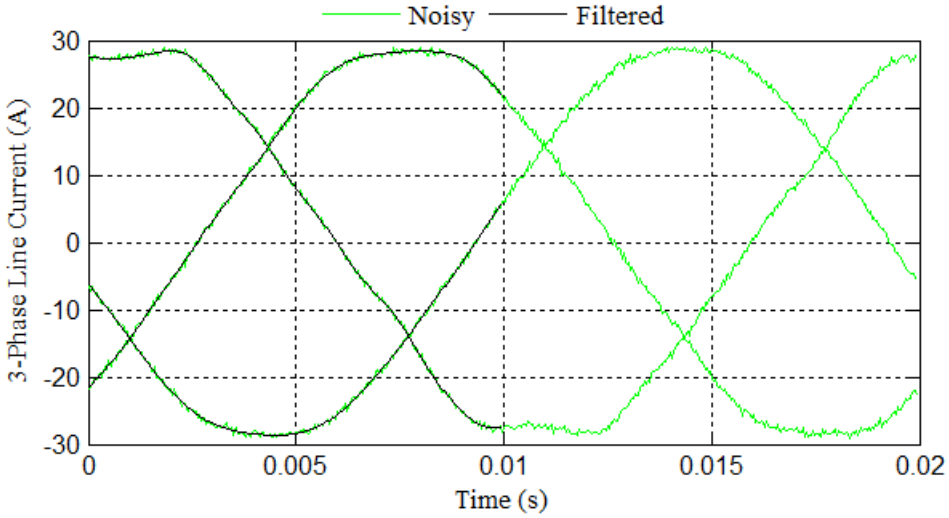

Fig. 5.7 Half cycle is filtered for sending end current in line I220–T220

5.4.1.3 *TDHSE by exploiting half-wave symmetry property*

An unbalanced harmonic source, defined in Table 5.1 is connected at busbar T220. However, the proposed methodology does not need knowledge of the harmonic injection: hence it is assumed that methodology does not have knowledge about harmonic sources.

The estimation for the unmonitored current waveforms uses the half-wave symmetry property. Hence, the estimated waveforms consist of two parts: First, it is solved with (1.15) using half-wave filtered measurements. Second, by exploiting the half wave symmetry in voltage and current waveforms, a completed cycle can be formed using (3.7). Hence, the non-monitored branch current I220–T220 line has been estimated using (5.15). Finally, by applying the FFT, the harmonic content is obtained.

The harmonic contents in the estimated waveforms are compared against those obtained from the SimPowerSystems toolbox of Simulink®, taken as simulated values, and against the obtained with the method reported in in [Medina and Cisneros-Magaña 2012]. Good agreement between responses is observed, which verifies the accuracy of the proposed method for HSE. Table 5.2 shows the resulting error on the THD evaluation. The THD obtained with the proposed methodology is compared to the TDHs obtained by the method reported in in [Medina and Cisneros-Magaña 2012] and the simulated (reference) power system response. Using (5.21), the absolute error of THD is computed. The maximum difference for the THD between the simulated response and the response obtained using the proposed method is 0.0625.

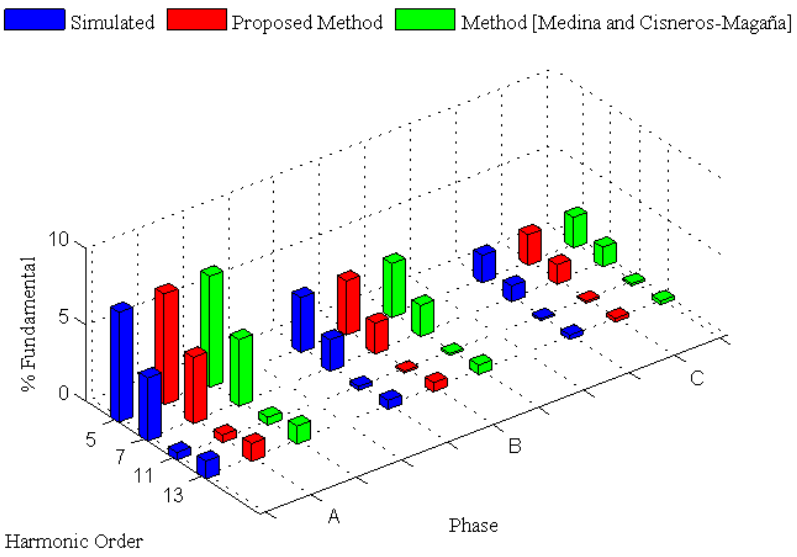

Fig. 5.8 Comparative harmonic spectra for sending end current in line I220–T220

Table 5.2 Comparative THD absolute error

Phase	Simulated	Proposed Method	Method [Medina and Cisneros-Magaña 2012]	Error Proposed Method	Error Method [Medina and Cisneros-Magaña 2012]
A	8.3695	8.4161	8.4225	0.0466	0.0530
B	4.1848	4.2466	4.2500	0.0619	0.0652
C	2.0924	2.1549	2.1554	0.0625	0.0630

5.4.2 Case study 2: Balanced load condition

The purpose of this case study is to test the proposed method with a balanced load condition. The modified IEEE 14-bus test system shown in Fig. 5.4 has been selected. The test system operates with a properly and over determined condition.

5.4.2.1 Balanced harmonic injection

The linear load placed at bus 4 has been replaced by a nonlinear load consisting of thyristors controlled AC-AC converter. The firing angles are 90 degrees to generate a wide range of harmonics; the nonlinear load is assumed to be balanced. For illustrative purposes, Fig. 5.9 shows the current waveforms in the nonlinear load connected at bus 4 and Fig 5.10 the resulting voltage waveform. Please notice from Fig. 5.10 that the firing angles are approximately 90 degrees. As a result of the nonlinear load, the voltage waveforms at busbar 4 are highly distorted, as shown in Fig. 5.10.

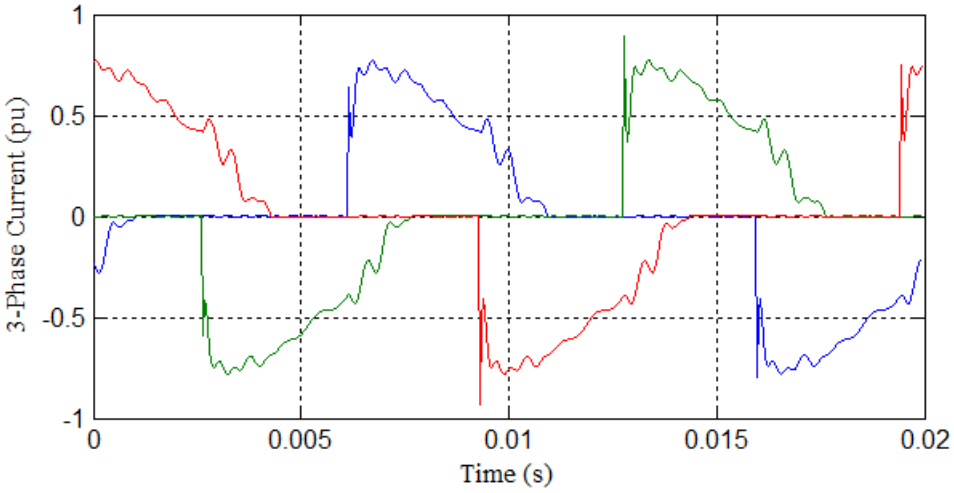

Fig. 5.9 Balanced three-phase current waveforms in nonlinear load connected at busbar 4

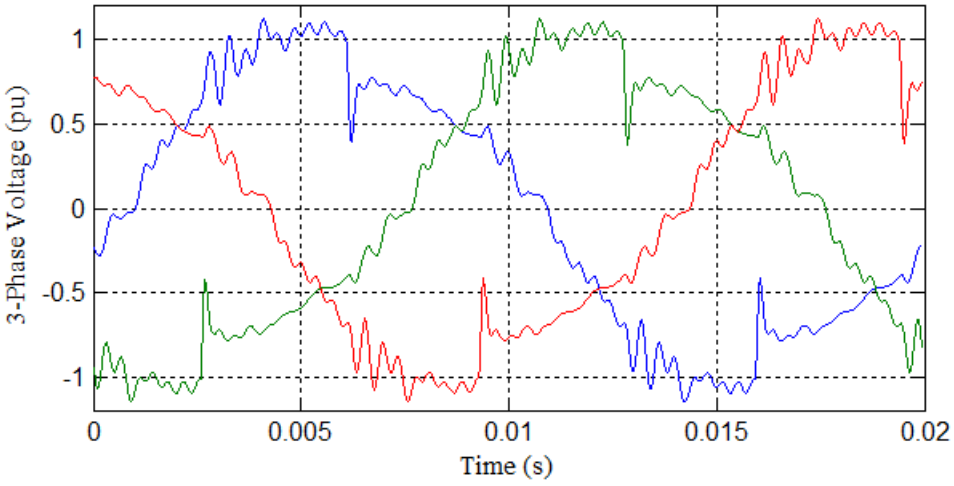

Fig. 5.10 Balanced three-phase voltage waveforms at busbar 4

5.4.2.2 The measuring process under a properly determined condition

This case study is conducted using the minimum number of measuring devices, i.e. the properly determined condition. The number of measuring devices is the optimal, i.e. the minimal number that forms the properly determined condition. This condition is shown in Fig. 5.4 as the green colour set.

The measurements taken from the measuring devices have been contaminated by adding 1% of random noise. This noise generates different inaccuracies for each harmonic. For illustrative purposes, Fig. 5.11 shows the resulting harmonic content with and without noise for voltage at busbar 2. Since a balanced condition is assumed, only one phase is shown. Table 5.3 details the generated inaccuracies in each harmonic of interest for this measurement. The maximum absolute error between harmonic magnitudes without and with noise is 0.25 presented in harmonic 5.

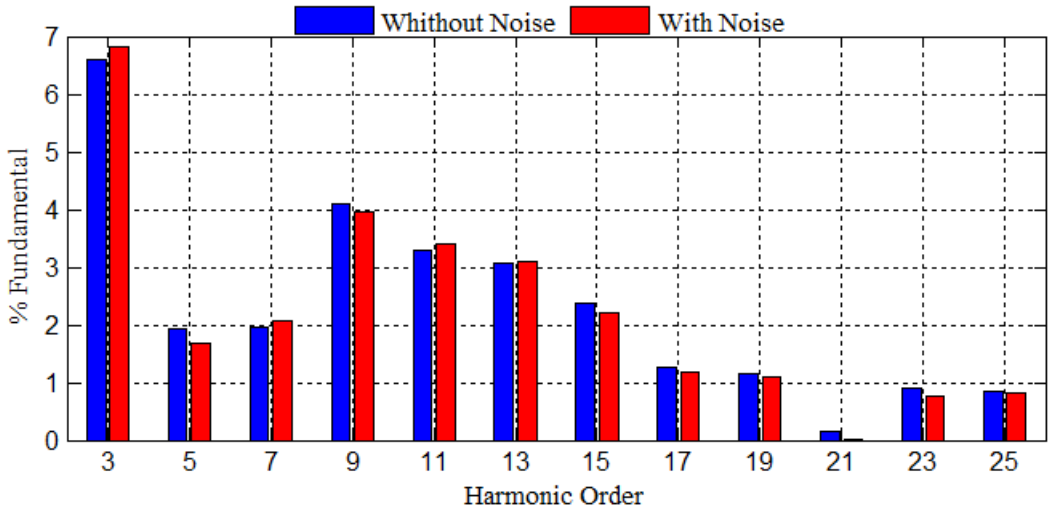

Fig. 5.11 Spectra for balanced voltage at busbar 2

Table 5.3 Inaccuracies generated owing to 1% of noise

Harmonic order	Without noise (%)	With noise (%)	Absolute Error
3	6.5917	6.8168	0.2251
5	1.9301	1.6791	0.2510
7	1.9591	2.0794	0.1203
9	4.1091	3.9637	0.1455
11	3.2993	3.3981	0.0988
13	3.0644	3.0870	0.0226
15	2.3676	2.2036	0.1639
17	1.2692	1.1751	0.0941
19	1.1472	1.1110	0.0361
21	0.1623	0.0202	0.1421
23	0.9156	0.7537	0.1619
25	0.8436	0.8316	0.0120

To select the harmonics of interest, the filter based on FFT is used. For illustrative purposes, Fig. 5.12 shows the contaminated three-phase voltage waveforms at busbar 2 and their respective filtered

waveforms. The contaminated three-phase sending end line current waveforms in line 2-3 as well as their respective filtered waveforms are shown in Fig. 5.13. The noise has been mitigated from 1% to 0.2%. In order to exploit the half-wave symmetry of the waveforms, only the half period of the waveforms have been sampled and filtered.

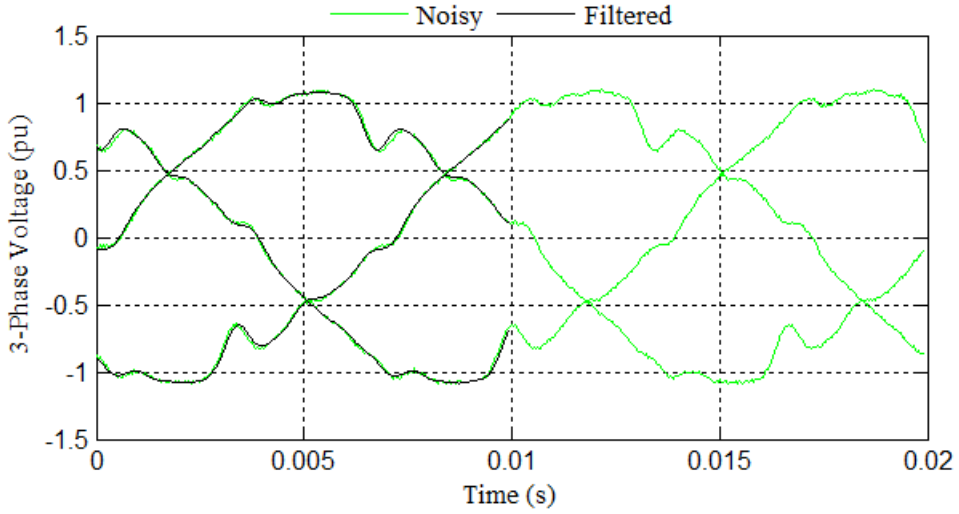

Fig. 5.12 Balance three-phase voltage waveforms at busbar 2

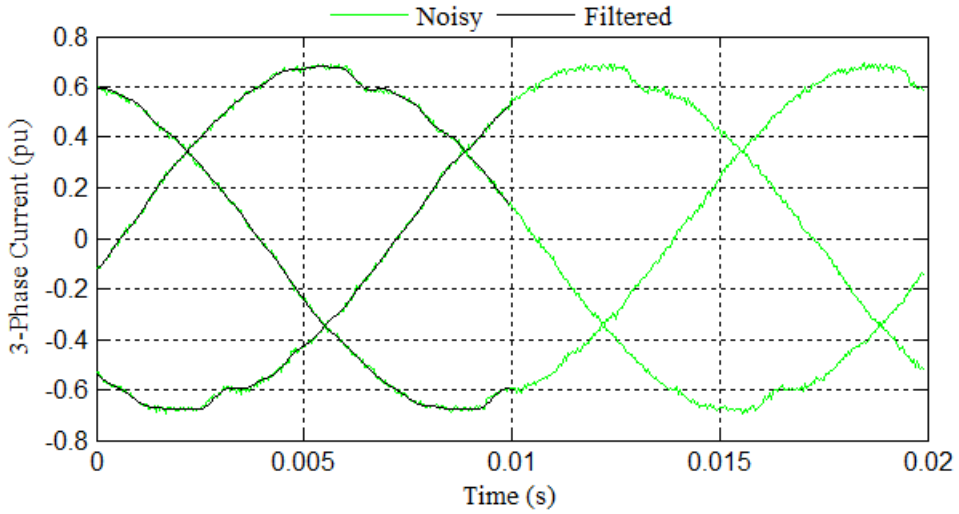

Fig. 5.13 Balanced three-phase sending end current waveforms in line 2–3

5.4.2.3 *TDHSE under a properly determined condition*

Using the minimal number of measuring devices, the properly determined condition is obtained. The matrix $\mathbf{H}_c \in \mathbb{R}^{57\times57}$ is formed as follows,

$$\mathbf{H}_c = \begin{bmatrix} \mathbf{H_1} & \mathbf{0} \in \mathbb{R}^{21\times18} & \mathbf{0} \in \mathbb{R}^{21\times18} \\ \mathbf{0} \in \mathbb{R}^{18\times21} & \mathbf{H_2} & \mathbf{0} \in \mathbb{R}^{18\times18} \\ \mathbf{0} \in \mathbb{R}^{18\times21} & \mathbf{0} \in \mathbb{R}^{18\times18} & \mathbf{H_3} \end{bmatrix} \tag{5.23}$$

where:

$$\mathbf{H_1} = \begin{bmatrix} \mathbf{I} & \mathbf{0} & \mathbf{0} & \mathbf{0} & \mathbf{0} & \mathbf{0} & \mathbf{0} \\ \mathbf{0} & \mathbf{I} & \mathbf{0} & \mathbf{0} & \mathbf{0} & \mathbf{0} & \mathbf{0} \\ \mathbf{0} & \mathbf{0} & \mathbf{I} & \mathbf{0} & \mathbf{0} & \mathbf{0} & \mathbf{0} \\ \mathbf{c1}_{1-2} & \mathbf{c2}_{1-2} & \mathbf{c3}_{1-2} & -\mathbf{I} & \mathbf{0} & \mathbf{0} & \mathbf{0} \\ \mathbf{c1}_{2-3} & \mathbf{c2}_{2-3} & \mathbf{c3}_{2-3} & \mathbf{0} & -\mathbf{I} & \mathbf{0} & \mathbf{0} \\ \mathbf{c1}_{2-4} & \mathbf{c2}_{2-4} & \mathbf{c3}_{2-4} & \mathbf{0} & \mathbf{0} & -\mathbf{I} & \mathbf{0} \\ \mathbf{c1}_{2-5} & \mathbf{c2}_{2-5} & \mathbf{c3}_{2-5} & \mathbf{0} & \mathbf{0} & \mathbf{0} & -\mathbf{I} \end{bmatrix}$$

$$\mathbf{H_2} = \begin{bmatrix} \mathbf{I} & \mathbf{0} & \mathbf{0} & \mathbf{0} & \mathbf{0} & \mathbf{0} \\ \mathbf{0} & \mathbf{I} & \mathbf{0} & \mathbf{0} & \mathbf{0} & \mathbf{0} \\ \mathbf{0} & \mathbf{0} & \mathbf{I} & \mathbf{0} & \mathbf{0} & \mathbf{0} \\ \mathbf{c1}_{6-11} & \mathbf{c2}_{6-11} & \mathbf{c3}_{6-11} & -\mathbf{I} & \mathbf{0} & \mathbf{0} \\ \mathbf{c1}_{6-12} & \mathbf{c2}_{6-12} & \mathbf{c2}_{6-12} & \mathbf{0} & -\mathbf{I} & \mathbf{0} \\ \mathbf{c1}_{6-13} & \mathbf{c2}_{6-13} & \mathbf{c3}_{6-13} & \mathbf{0} & \mathbf{0} & -\mathbf{I} \end{bmatrix}$$

$$\mathbf{H_3} = \begin{bmatrix} \mathbf{I} & \mathbf{0} & \mathbf{0} & \mathbf{0} & \mathbf{0} & \mathbf{0} \\ \mathbf{0} & \mathbf{I} & \mathbf{0} & \mathbf{0} & \mathbf{0} & \mathbf{0} \\ \mathbf{0} & \mathbf{0} & \mathbf{I} & \mathbf{0} & \mathbf{0} & \mathbf{0} \\ \mathbf{c1}_{7-9} & \mathbf{c2}_{7-9} & \mathbf{c3}_{7-9} & -\mathbf{I} & \mathbf{0} & \mathbf{0} \\ \mathbf{c1}_{9-10} & \mathbf{c2}_{9-10} & \mathbf{c3}_{9-10} & \mathbf{0} & -\mathbf{I} & \mathbf{0} \\ \mathbf{c1}_{9-14} & \mathbf{c2}_{9-14} & \mathbf{c3}_{9-14} & \mathbf{0} & \mathbf{0} & -\mathbf{I} \end{bmatrix}$$

Please note that matrices $\mathbf{0}$ and $\mathbf{I} \in \mathbb{R}^{3\times3}$ are the zero and identity matrices, respectively.

By using (5.23) in (4.12) the waveform are estimated. Then, by applying the FFT to estimated waveforms, the harmonic content is obtained. The harmonic content for the simulated and the estimated harmonic, named properly estimated, at unmonitored busbar 5, is shown in Fig. 5.14. Since a balanced condition is assumed, only one phase is shown. Table 5.4 gives the properly estimated error for the HSE. The maximum difference is 0.32% for the 23-*th* harmonic. However, the average error is 0.14%. This estimated error can be reduced using the over-determined estimation as will be shown in the next section.

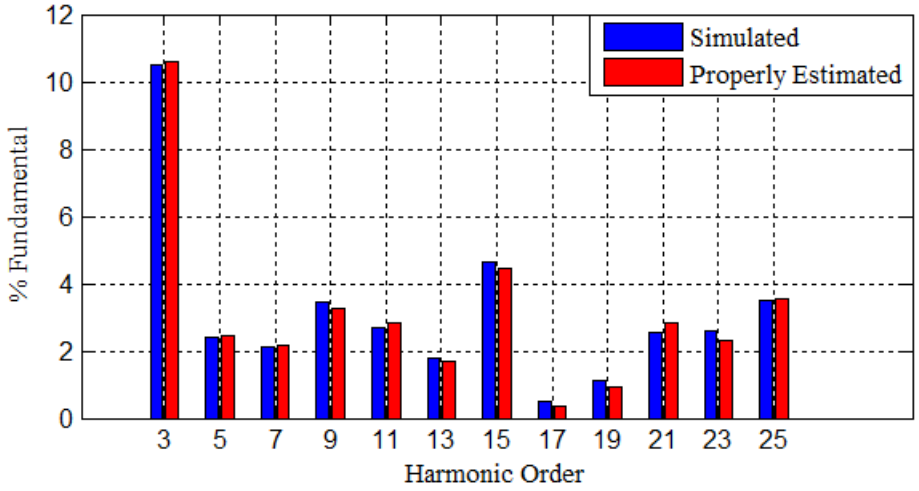

Fig. 5.14 HSE in balanced voltage at unmonitored busbar 5 under a properly determined condition

Table 5.4 Harmonic content in voltage at unmonitored busbar 5 using a properly determined condition

Harmonic order	Simulated	Properly Estimated	Absolute Error
3	10.5011	10.5872	0.0861
5	2.4184	2.4692	0.0508
7	2.1295	2.1500	0.0205
9	3.4754	3.2742	0.2012
11	2.6772	2.8180	0.1408
13	1.7664	1.7037	0.0627
15	4.6518	4.4312	0.2206
17	0.4864	0.3517	0.1347
19	1.1127	0.9329	0.1798
21	2.5275	2.8453	0.3178
23	2.6181	2.2943	0.3238
25	3.5194	3.5501	0.0307

5.4.2.4 *TDHSE under an over-determined condition*

Two measuring devices have been added at busbar 4, as shown in Fig. 5.4. The additional measuring devices are the measurements of the receiving end current of line 4-5 and the voltage at bus 4, marked as a red set. The over–determined condition forms the matrix $\mathbf{H_o} \in \mathbb{R}^{63\times57}$ is,

$$\mathbf{H_o} = \begin{bmatrix} \mathbf{H_1} & \mathbf{0} \in \mathbb{R}^{21\times18} & \mathbf{0} \in \mathbb{R}^{21\times18} \\ \mathbf{0} \in \mathbb{R}^{18\times21} & \mathbf{H_2} & \mathbf{0} \in \mathbb{R}^{18\times18} \\ \mathbf{0} \in \mathbb{R}^{18\times21} & \mathbf{0} \in \mathbb{R}^{18\times18} & \mathbf{H_3} \\ \mathbf{H_4} & \mathbf{0} \in \mathbb{R}^{6\times18} & \mathbf{0} \in \mathbb{R}^{6\times18} \end{bmatrix} \tag{5.24}$$

where:

$$\mathbf{H_4} = \begin{bmatrix} \mathbf{0} & \mathbf{0} & \mathbf{0} & \mathbf{0} & \mathbf{0} & \mathbf{I} & \mathbf{0} \\ \mathbf{c1}_{4-5} & \mathbf{c2}_{4-5} & \mathbf{c3}_{4-5} & \mathbf{0} & \mathbf{0} & \mathbf{0} & -\mathbf{I} \end{bmatrix}$$

Using (5.24) in (4.11), the TDHSE for an over-determined condition is solved. In order to compare results with the properly determined condition, the voltage at busbar 5 will be again analysed. The harmonic content for the simulated and the estimated harmonic, for an over-estimated condition at unmonitored busbar 5 is shown in Fig. 5.15. A close agreement between the harmonic content obtained with the different methods is observed. Table 5.5 gives the estimated error for the over-determined condition for the TDHSE assessment. The maximum difference is 0.13% for the 11-*th* harmonic. The average estimated error has been 0.04%.

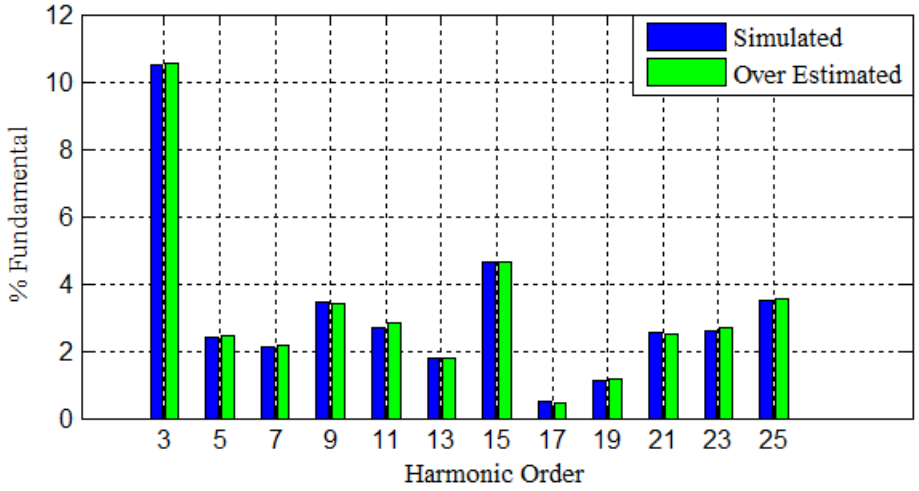

Fig. 5.15 HSE in balanced voltage at unmonitored busbar 5 under an over-determined condition

Table 5.5 Absolute error for TDHSE at unmonitored busbar 5 using an over-determined condition

Harmonic order	Sinulated	Over Estimated	Absolute Error
3	10.5011	10.5351	0.0340
5	2.4184	2.4699	0.0515
7	2.1295	2.1582	0.0287
9	3.4754	3.3884	0.0870
11	2.6772	2.8138	0.1366
13	1.7664	1.7756	0.0092
15	4.6518	4.6315	0.0203
17	0.4864	0.4510	0.0354
19	1.1127	1.1446	0.0319
21	2.5275	2.4984	0.0291
23	2.6181	2.6717	0.0536
25	3.5194	3.5379	0.0185

5.4.2.5 *Comparison of the TDHSE under properly and over-determined conditions*

In order to compare the responses of the TDHSE under properly and over determined conditions, both harmonic spectra are shown in Fig. 5.16. It can be observed that the TDHSE assessment is closer to the simulated response when the over-determined condition is used. Table 5.6 gives detailed information about both responses. The maximum difference is reduced from 0.32 to 0.13. Even more, the average error is reduced from 0.14 to 0.04, which demonstrates the potential of the proposed TDHSE methodology.

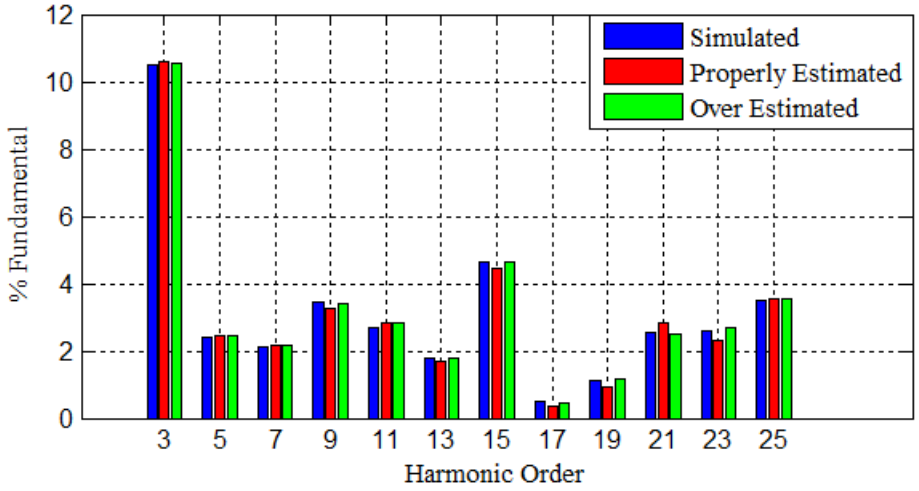

Fig. 5.16 HSE in balanced voltage at busbar 5

Table 5.6 The estimate error comparison of the TDHSE at unmonitored busbar 5

Harmonic order	Simulated	Properly Estimated	Over Estimated	Properly Absolute Error	Over Absolute Error
3	10.5011	10.5872	10.5351	0.0861	0.0340
5	2.4184	2.4692	2.4699	0.0508	0.0515
7	2.1295	2.1500	2.1582	0.0205	0.0287
9	3.4754	3.2742	3.3884	0.2012	0.0870
11	2.6772	2.8180	2.8138	0.1408	0.1366
13	1.7664	1.7037	1.7756	0.0627	0.0092
15	4.6518	4.4312	4.6315	0.2206	0.0203
17	0.4864	0.3517	0.4510	0.1347	0.0354
19	1.1127	0.9329	1.1446	0.1798	0.0319
21	2.5275	2.8453	2.4984	0.3178	0.0291
23	2.6181	2.2943	2.6717	0.3238	0.0536
25	3.5194	3.5501	3.5379	0.0307	0.0185

5.4.3 Case study 3: Unbalanced load condition

The purpose of this case study is to show the performance of the proposed method under unbalanced operation conditions. The modified IEEE 14-bus test system shown in Fig. 5.4 has been selected.

5.4.3.1 *Unbalanced harmonic injection*

The linear load placed at bus 4 has been replaced by a nonlinear load consisting of a thyristors controlled AC-AC converter. The firing angles are 90 degrees to create a powerful and wide range of harmonics. The nonlinear load is assumed to be balanced. The nonlinear load at bus 4 has been disconnected from phase C to

introduce unbalance in the power system. Fig. 5.17 shows the current waveforms in the nonlinear load placed at busbar 4. The firing angles are approximately 90 degrees. As a result of the nonlinear load, the voltage waveforms at busbar 4 are highly distorted, as shown in Fig. 5.18. In addition, voltage of phase C at busbar 4 is distorted due to magnetic coupling.

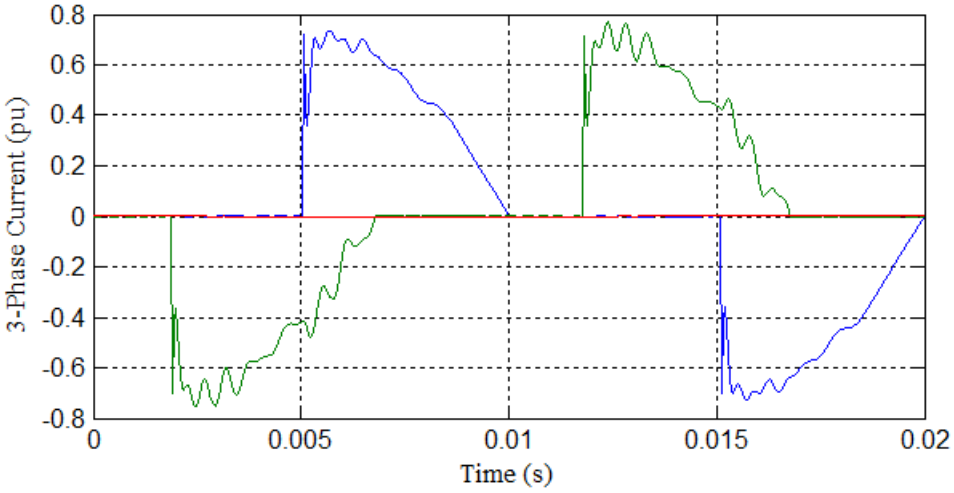

Fig. 5.17 Unbalanced three-phase current waveforms in nonlinear load connected at busbar 4

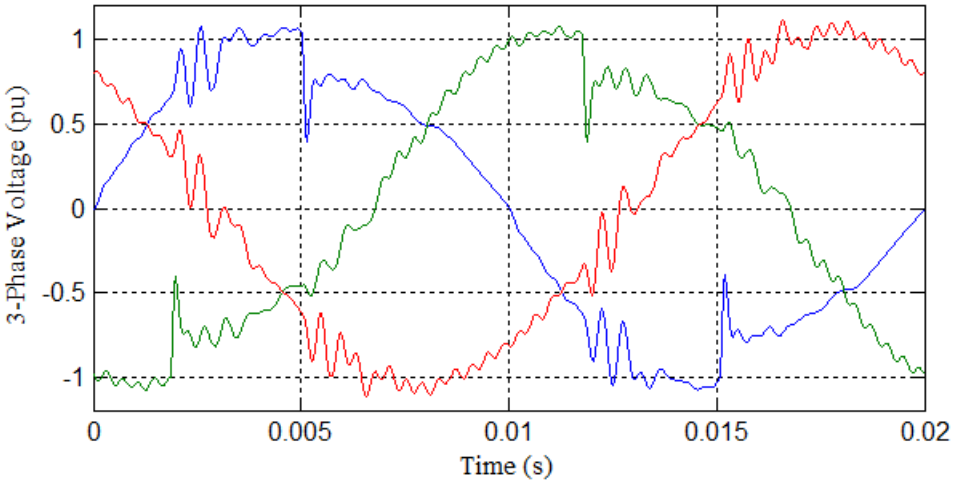

Fig. 5.18 Unbalanced three-phase voltage waveforms at busbar 4

5.4.3.2 *The measuring process under an over determined condition*

Two measuring devices have been added at bus 4, as shown in Fig. 5.4. The additional measuring devices are the measurements at the receiving end current in line 4-5 and the voltage at busbar 4, marked as a red set. The measurements taken from these measuring devices have been contaminated by adding 1% of random noise. This noise generates different inaccuracies for each harmonic. For illustrative purposes, Fig. 5.19 shows the resulting harmonic content for voltage at busbar 2.

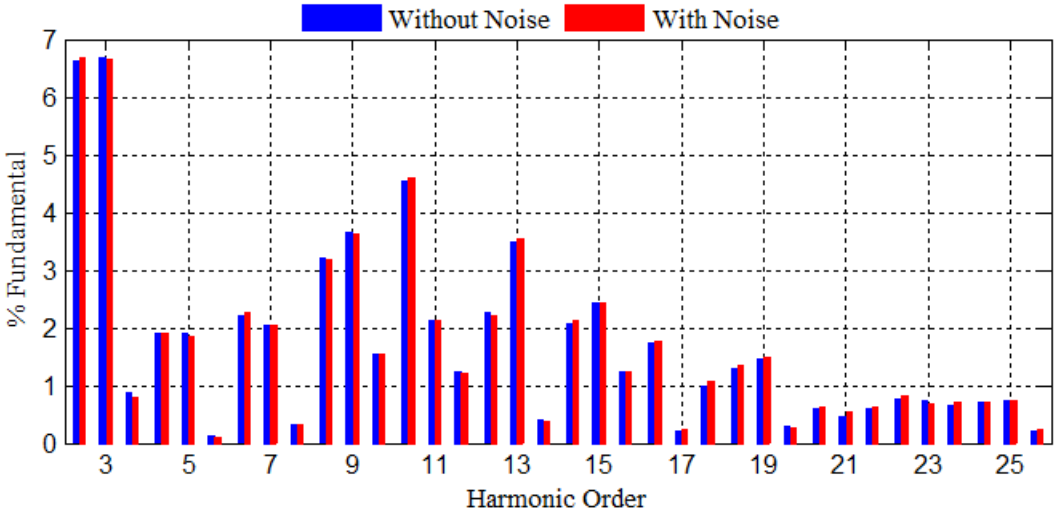

Fig. 5.19 Spectra for three-phase voltage at busbar 2

To select the harmonics of interest, the filter based on FFT is used. Fig. 5.20 shows the contaminated and unbalance three-phase voltage waveforms at busbar 2 and their respective filtered waveforms. The contaminated and unbalanced three-phase sending end line current waveforms in line 2-3 as well as their respective filtered waveforms are shown in Fig. 5.21. The noise has been mitigated from 1% to 0.25%. Filtered waveforms contain only the harmonics of interest, which are altered by the added noise. In order to exploit the half-wave symmetry of the waveforms, only the half period of the waveforms have been sampled and filtered.

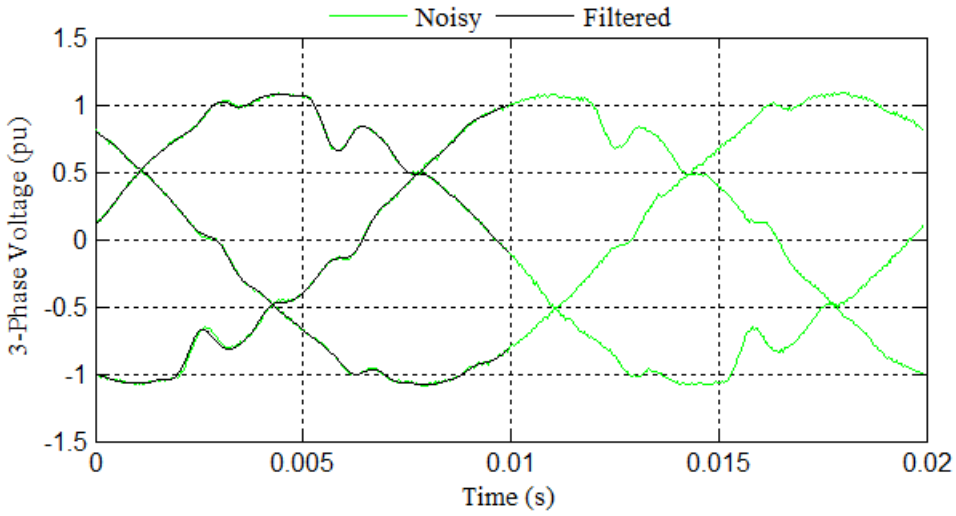

Fig. 5.20 Unbalanced three-phase voltage waveforms at busbar 2

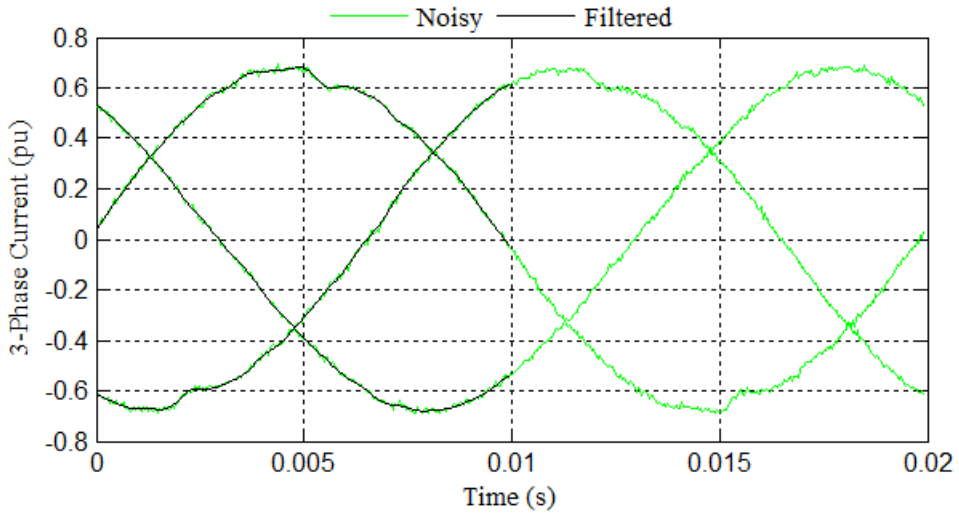

Fig. 5. 21 Unbalanced three-phase sending end current waveforms in line 2–3

5.4.3.3 *TDHSE under a properly determined condition*

By applying (5.23) in (4.12), the unbalanced three-phase harmonic state is evaluated. The harmonic content for the simulated and the estimated harmonic, named properly estimated, at unmonitored busbar 5 is shown in Fig. 5.22. Since an unbalanced condition is assumed, the three phases are shown for each harmonic order of interest. Table 5.7, 5.8, and 5.9 give detailed information about the estimated error. It can be noticed that absolute error is small, e.g. the maximum absolute error is 0.68 for the 25th-harmonic in phase B.

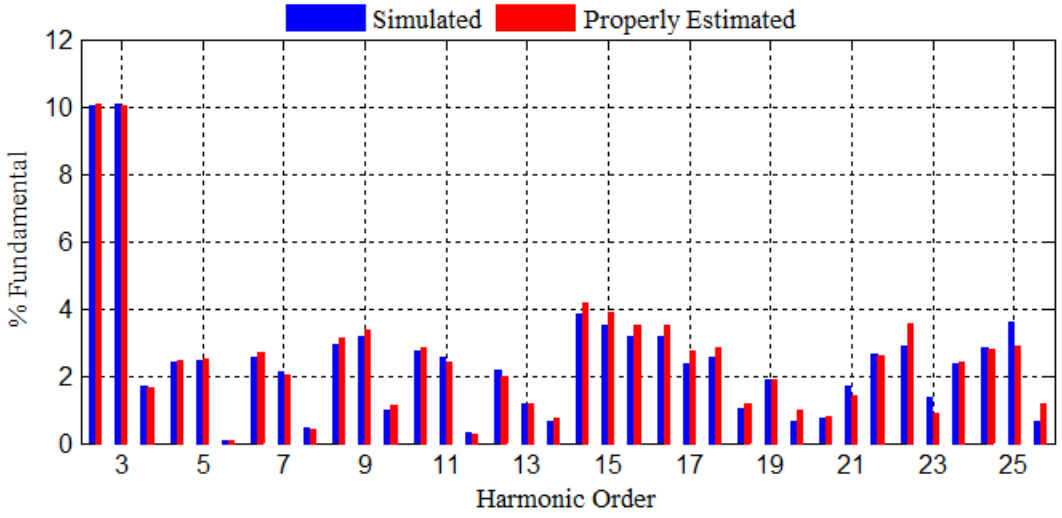

Fig. 5.22 Harmonic content in unbalanced voltage at unmonitored busbar 5

Table 5.7 Estimated error of phase A of unmonitored busbar 5 under properly determined conditions

Harmonic order	Simulated	Properly Estimate	Absolute Error
3	10.0322	10.0835	0.0513
5	2.4181	2.4497	0.0316
7	2.5565	2.7000	0.1436
9	2.9055	3.1188	0.2133
11	2.7544	2.8456	0.0913
13	2.1441	1.9715	0.1726
15	3.8259	4.1833	0.3575
17	3.1735	3.5176	0.3441
19	1.0202	1.1565	0.1363
21	0.7590	0.8054	0.0464
23	2.9000	3.5695	0.6694
25	2.8308	2.8086	0.0222

Table 5.8 Estimated error of phase B of unmonitored busbar 5 under properly determined conditions

Harmonic order	Simulated	Properly Estimate	Absolute Error
3	10.0728	10.0471	0.0257
5	2.4678	2.5160	0.0482
7	2.1251	2.0387	0.0864
9	3.1769	3.3735	0.1966
11	2.5258	2.3987	0.1271
13	1.1536	1.1869	0.0333
15	3.5034	3.8607	0.3573
17	2.3388	2.7145	0.3757
19	1.8763	1.8801	0.0038
21	1.7087	1.4240	0.2847
23	1.3578	0.8819	0.4759
25	3.5715	2.8832	0.6883

Table 5.9 Estimated error of phase C of unmonitored busbar 5 under properly determined conditions

Harmonic order	Simulated	Properly Estimate	Absolute Error
3	1.6956	1.6525	0.0431
5	0.0639	0.0939	0.0300
7	0.4325	0.4218	0.0106
9	0.9612	1.1400	0.1788
11	0.3297	0.2685	0.0611
13	0.6234	0.7172	0.0938
15	3.1557	3.4953	0.3396
17	2.5613	2.8541	0.2928
19	0.6605	0.9834	0.3229
21	2.6281	2.6078	0.0203
23	2.3385	2.4282	0.0897
25	0.6291	1.1885	0.5594

5.4.3.4 *TDHSE under an over-determined condition*

By using (5.24) in (4.11), the TDHSE is again solved. The voltage at busbar 5 is analysed. The harmonic content for the simulated and the estimated harmonic under an over-estimated condition at unmonitored busbar 5 is shown in Fig. 5.23. A close agreement between the estimated harmonic content and the simulated is observed. Table 5.10, 5.11, and 5.12 give the absolute estimate error for the over-estimated harmonic state at voltages of phases A, B, and C, respectively. The maximum error was 0.23 presented in 25-th harmonic in voltage of phase B.

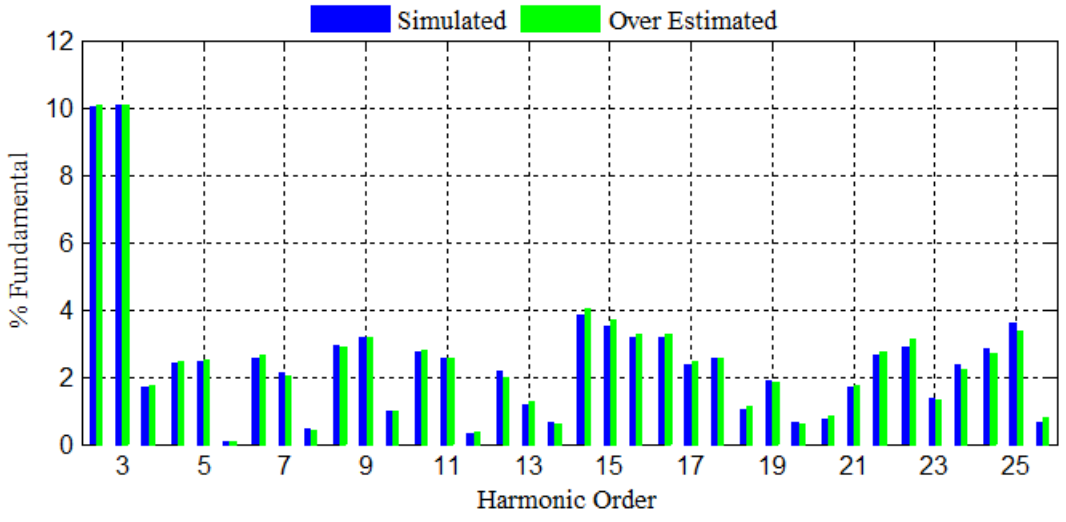

Fig. 5.23 Harmonic content in unbalanced voltage at unmonitored busbar 5

Table 5.10 Estimated error of phase A of unmonitored busbar 5 under over-determined conditions

Harmonic order	Simulated	Over Estimate	Absolute Error
3	10.0322	10.0700	0.0378
5	2.4181	2.4736	0.0555
7	2.5565	2.6455	0.0891
9	2.9055	2.9023	0.0032
11	2.7544	2.7823	0.0279
13	2.1441	1.9999	0.1442
15	3.8259	4.0326	0.2068
17	3.1735	3.2469	0.0734
19	1.0202	1.0966	0.0764
21	0.7590	0.8156	0.0566
23	2.9000	3.0996	0.1996
25	2.8308	2.6750	0.1559

Table 5.11 Estimated error of phase B of unmonitored busbar 5 under over-determined conditions

Harmonic order	Simulated	Over Estimate	Absolute Error
3	10.0728	10.0929	0.0201
5	2.4678	2.5118	0.0440
7	2.1251	2.0379	0.0872
9	3.1769	3.1781	0.0012
11	2.5258	2.5701	0.0443
13	1.1536	1.2484	0.0948
15	3.5034	3.6674	0.1641
17	2.3388	2.4603	0.1215
19	1.8763	1.8202	0.0561
21	1.7087	1.7393	0.0306
23	1.3578	1.2909	0.0669
25	3.5715	3.3402	0.2313

Table 5.12 Estimated error of phase C of unmonitored busbar 5 under over-determined conditions

Harmonic order	Simulated	Over Estimate	Absolute Error
3	1.6956	1.7364	0.0409
5	0.0639	0.0741	0.0102
7	0.4325	0.4164	0.0160
9	0.9612	0.9593	0.0019
11	0.3297	0.3591	0.0294
13	0.6234	0.6131	0.0103
15	3.1557	3.2461	0.0903
17	2.5613	2.5459	0.0154
19	0.6605	0.6040	0.0565
21	2.6281	2.7569	0.1288
23	2.3385	2.2034	0.1351
25	0.6291	0.8004	0.1714

5.4.2.5 *Comparison of the TDHSE under properly and an over-determined conditions*

Fig. 2.24 shows a comparison between the TDHSE under a properly and an over determined condition against the simulated system response. It can be observed how the over estimation has improved the TDHSE assessment solution. It can be notice that the maximum absolute error has decreased from 0.66 to 0.23 presented in 25-*th* harmonic in voltage of phase B.

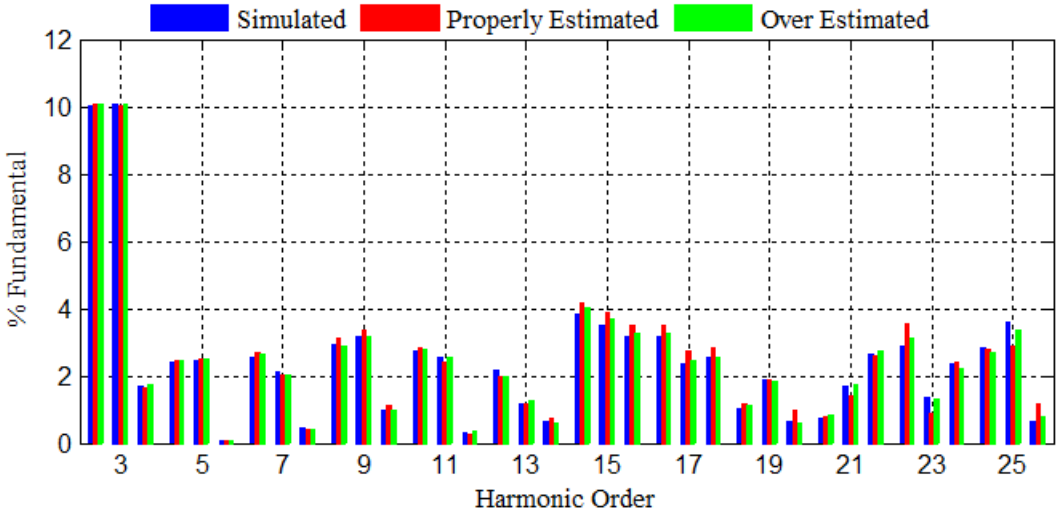

Fig. 5.24 Harmonic content in unbalanced voltage at unmonitored busbar 5

5.5 Conclusion

A time domain methodology for harmonic state estimation assessment (TDHSE) based on optimal number of meter and the principle of half-wave symmetry property has been proposed. It can be applied in both balanced and unbalanced three-phase power systems.

A method based on topological analysis to obtain the optimal number of measuring devices and their appropriate placement to evaluate the HSE in the time domain has been proposed. This allows cost savings of instrumentation.

By taking advantage of the half-wave symmetry property in the waveforms of voltage and current, the execution time to evaluate the HSE in the time domain has been reduced by approximately 50% as only half period is sampled and processed.

The results indicate that using the critically-determined condition, the estimation error can be acceptable for harmonics whose magnitude is larger than the noise level.

Besides, the results suggest that the accuracy of the HSE, including harmonics whose magnitude is small compared to the noise level, can be improved if the over-determined condition is used.

The proposed methodology does not require of an accurate previous knowledge of the harmonic sources nor of a procedure for the determination of precise initial state conditions.

Chapter 6 Transient state estimation based on numerical derivatives, the optimal number of measuring devices, and filtered measurements

6.1 Introduction

The transient state estimation (TSE) is used to locate the disturbance location in order to quickly correct the problem. Another aim of the TSE is to determine the peak voltages that can damage any component of the power system. This chapter describes a methodology for transient state estimation in power systems. The proposed methodology is formulated using numerical derivative methods instead of integration to relate the state variables to measurements. It does not require knowledge of the steady state to establish the pre-disturbance time interval. The method uses an optimal measuring system based on topological analysis to obtain full observability. The adverse effect of noisy measurements in the estimation solution is mitigated using an infinite impulse response filter. A transient index is introduced to estimate the fault location. The transient state estimation is assessed using two power test systems. The results are validated through direct comparison against those obtained by simulation using SimPowerSystems toolbox of Simulink®.

6.2 Proposed TSE methodology

The main stages for the proposed TSE methodology are follows:

- Develop the mathematical model for the power system.
- Determine the optimal measuring system.
- Design the filter to mitigate the noise in measurements during TSE
- Apply the proposed methodology for TSE.

6.2.1 Mathematical formulation to TSE problem

The proposed mathematical formulation to TSE problem is given as follows. Let us,

$$\mathbf{x} = \mathbf{H}^{-1}\mathbf{z} + \mathbf{e} \tag{6.1}$$

The idea is to determine the state variables as a function of measurement quantities. The measurement matrix will not be inverted, instead $\mathbf{H}^{-1}$ is directly developed based on parameter of the power system.

The power system is modelled by an ODE set. However, it can be transformed into difference equations if time t is discretised as in (4.1), i.e. $t[k] = kT_S$.

Numerical derivatives are needed to transform the ODE set into difference equations. In this research work, the three-point midpoint formula is used as it generates an error $O(T_S^2)$ [Burden and Fires 2011]. The formulas for this purpose have been defined in (4.14) and (4.15).

The most possible cases in power systems where the state variables can be related to measurements are the following:

6.2.1.1 Two busbars connected through a transmission line

The transmission line is represented by an equivalent π-model, as shown in Fig. 5.2, as there is only interest in behaviour at the sending and receiving ends of the line.

From Fig. 5.2, it is assumed that busbar *s* is monitored and busbar *r* is unmonitored. Hence, (5.9) can be solved for $\mathbf{v}_r$ as,

$$\mathbf{v}_r^k = \mathbf{c}1_{s-r}\mathbf{z}_{\mathbf{v}_s}^k + \mathbf{c}2_{s-r}\mathbf{z}_{\mathbf{v}_s}^{k+1} + \mathbf{c}3_{s-r}\mathbf{z}_{\mathbf{v}_s}^{k-1} + \mathbf{b}1_s\mathbf{z}_{\mathbf{i}_s}^k + \mathbf{b}2_s\mathbf{z}_{\mathbf{i}_s}^{k+1} + \mathbf{b}3_s\mathbf{z}_{\mathbf{i}_s}^{k-1} \tag{6.2}$$

where $\mathbf{c}1_{s-r} = \mathbf{I} + \mathbf{RG} - 2\mathbf{LC}/T_S^2$, $\mathbf{c}2_{s-r} = (\mathbf{RC} + \mathbf{LG})/2T_S + \mathbf{LC}/T_S^2$,

$\mathbf{c}3_{s-r} = \mathbf{LC}/T_S^2 + (\mathbf{RC} + \mathbf{LG})/2T_S$, $\mathbf{b}1_s = -\mathbf{R}$, $\mathbf{b}2_s = \mathbf{L}/2T_S$, and $\mathbf{b}3_s = -\mathbf{L}/2T_S$.

It should be noticed that after three samples, i.e. $k-1$, k, and $k+1$, the *k-th* value of the associated state variables can be estimated. The estimation process finishes when all *N* samples of the time interval are analysed.

The busbar voltages taken as state variables do not require of an initial state. An initial value is required for the measurement, so the first three samples define the initial condition. Hence, there is no computational effort to determine the steady state.

Once $\mathbf{v}_r$ is determined, the receiving end current $\mathbf{i}_r$ can be defined as follows,

$$\mathbf{i}_r = \mathbf{i} + \mathbf{i}_{Gr} + \mathbf{i}_{Cr} \tag{6.3}$$

Solving for **i** from (5.2) gives,

$$\mathbf{i} = \mathbf{i}_s - \mathbf{i}_{Gs} - \mathbf{i}_{Cs} \tag{6.4}$$

Substituting (6.4) in (6.3) yields,

$$\mathbf{i}_r = \mathbf{i}_s - \mathbf{i}_{Gs} - \mathbf{i}_{Cs} + \mathbf{i}_{Gr} + \mathbf{i}_{Cr} \tag{6.5}$$

Discretising (6.15) and ordering gives,

$$\mathrm{i}_r^k = \mathrm{i}_s^k - \mathrm{G}\mathbf{v}_s^k + \mathrm{G}\mathbf{v}_r^k - \mathrm{C}(\mathbf{v}_s^{k+1} - \mathbf{v}_s^{k-1})/\mathbf{2}T_S + \mathrm{C}(\mathbf{v}_r^{k+1} - \mathbf{v}_r^{k-1})/\mathbf{2}T_S \tag{6.6}$$

Since $\mathbf{i}_r$ depends on state variables, it is named a dependent variable.

6.2.1.2 Two busbars connected through a transformer

To analyse the transformer, it is necessary to refer the equivalent circuit to either the primary side of the transformer or its secondary side. Fig. 2.11 shows the simplified transformer equivalent circuit referred to the primary side. The modelling can be extended to the three phase transformer using a matrix notation for the transformer parameters, as shown in Fig. 6.1. The transformer model includes the following parameters: the relation of the ideal turns ratio *a*; the winding resistance, both primary and secondary windings, $\mathbf{R_1}$ and $\mathbf{R_2}$, respectively; and the leakage inductance of primary and secondary windings, $\mathbf{L_1}$ and $\mathbf{L_2}$. The state variables are the voltages at the input $\mathbf{v}_s$ and output $\mathbf{v}_r$ of the transformer.

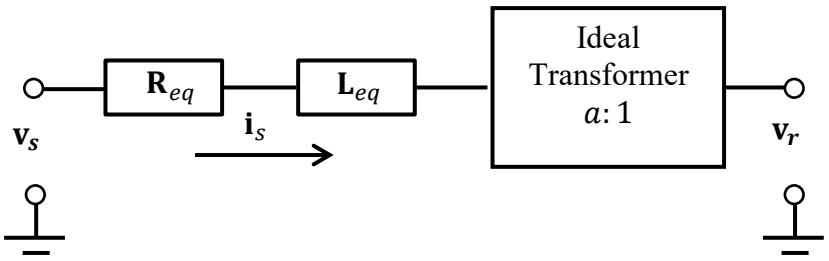

Fig. 6.1 Three-phase transformer modelled by impedance and an ideal transformer

The equation in the continuous time that represents the three-phase transformer is,

$$\mathbf{v}_s - a\mathbf{v}_r = \mathbf{R}_{\mathrm{eq}}\mathbf{i}_{\mathrm{s}} + \mathbf{L}_{\mathrm{eq}}\mathbf{i}'_{\mathrm{s}} \tag{6.7}$$

where $\mathbf{R_{eq}} = \mathbf{R_1} + \boldsymbol{a}^2\mathbf{R_2}$ and $\mathbf{L_{eq}} = \mathbf{L_1} + \boldsymbol{a}^2\mathbf{L_2}$.

Solving for $\mathbf{v}_r$ in (6.7) gives,

$$\mathbf{v}_r = a^{-1}\left(\mathbf{v}_s - \mathbf{R}_{\mathrm{eq}}\mathbf{i}_{\mathrm{T}} + \mathbf{L}_{\mathrm{eq}}\mathbf{i}'_{\mathrm{s}}\right) \tag{6.8}$$

It is assumed that the primary side of the transformer is instrumented. Let $\mathbf{z}_{\mathbf{v}_s}$ be the busbar voltage and $\mathbf{z}_{\mathbf{i}_s}$ the transformer current measurements. Hence, (21) is now,

$$\mathbf{v}_r = a^{-1}\left(\ \mathbf{z}_{\mathbf{v}_s} - \mathbf{R}_{\mathrm{eq}}\mathbf{z}_{\mathbf{i}_s} + \mathbf{L}_{\mathrm{eq}}\mathbf{z}'_{\mathbf{i}_s}\right) \tag{6.9}$$

By applying (4.14) and (4.15) to discretise (6.9) result in,

$$\mathbf{v}_r^k = a^{-1}\left(\mathbf{z}_{\mathbf{v}_s}^k - \mathbf{R}_{\mathrm{eq}}\mathbf{z}_{\mathbf{i}_s}^k + \mathbf{L}_{\mathrm{eq}}\left(\mathbf{z}_{\mathbf{i}_s}^{k+1} - \mathbf{z}_{\mathbf{i}_s}^{k-1}\right)/2T_{\mathrm{S}}\right) \tag{6.10}$$

6.2.2 Measuring system

6.2.2.1 Optimal measuring system

The optimal measuring system is one that uses the minimal number of measuring devices and their placement, so that full observability can be obtained. Each instrumented busbar requires a communication channel. Hence, it is not trivial to place the device anywhere, e.g. Fig. 6.2 shows two measuring devices placed at busbar *s*, one for busbar voltage and one for the sending end line current. This placement generates one communication channel. On the other hand, if the same devices are placed as shown in Fig. 6.3, the number of communication channels is now two since busbars *s* and *r* are distant from each other.

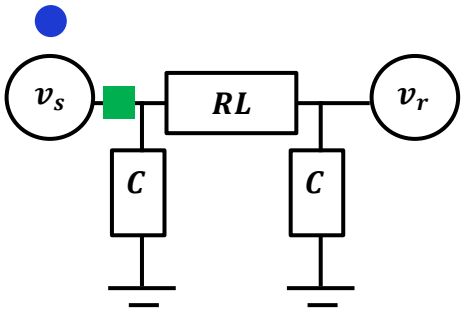

Fig. 6.2 Measuring device placement uses one communication channel

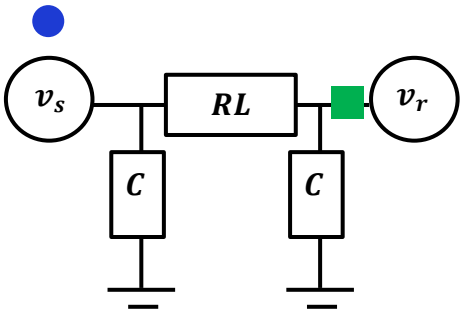

Fig. 6.3 Measuring device placement uses two communication channels

The methods to assess TSE [Yu and Watson 2007], [Cisneros-Magaña and Medina 2013], [Farzanehrafat and Watson 2013], [Watson and Farzanehrafat 2014], [Cisneros-Magaña *et al.* 2014] have not used an optimal measuring system. There are no explicitly reported methods to obtain the optimal measuring system to assess TSE. However, there are several contributions to obtain full observability in the frequency domain using phasor quantities [Korres *et al*. 2014], [Koutsoukis et al. 2013], [Rashidi 2013], [Saha et al. 2012], [Mahari and Seyedi 2013], [Müller and Castro 2016], [Gou 2008]. These contributions can be exploited extending the concept to the time domain as it has been described in Section 5.2.2.1.

6.2.2.2 *Saving index*

An analytical way to analyse the effectiveness of the instrumentation used is through a proposed index, named saving index η_{sa}, defined as follows:

$$\eta_{sa} = \frac{n}{mn_{ch}} \tag{6.11}$$

where n_e is the number of states variables that the measuring system can determine; m is number of measuring devices and n_{ch} the number of communication channels used by the measuring system.

The saving index can be used to compare two sets of measurements, e.g. for the measuring system shown in Fig. 6.2, the resulting saving index results is $\eta_{sa1} = 1/1/1 = 1$ while the saving index for the measuring system shown in Fig. 6.3 is $\eta_{sa2} = 1/1/2 = 0.5$, which implies that the first measuring system is more efficient, i.e. two times for this particular case, when is compared against the second.

6.2.2.3 *Filtering of noisy measurements during TSE*

Measurements are unfortunately contaminated by noise. In [Cisneros-Magaña and Medina 2013], an over-determined solution is used to compensate the adverse effect of noisy measurements. As an alternative, a digital filter is proposed to mitigate the noise of the measurements.

Digital filters can be classified into finite impulse response (FIR) and infinite impulse response (IIR) filters, respectively. FIR and IIR filters each have advantages and disadvantages, and neither is best in all

situations. In this research work, an IIR filter is proposed due to the fact that its design is generally easier than the one needed for IIR filter [Parks and Burrus 1987], [Madisetti 2010].

The IIR filter of order $M-1$ can be defined by

$$\tilde{z}^k = \sum_{i=2}^{M} a_i \, \tilde{z}^{k-i} + \sum_{j=1}^{M} b_j \, z^{k-j} \tag{6.12}$$

It is required to take M samples and set to zero the first M-1 outputs to generate the first filtered measurement.

The sample frequency F_S should be considered. According to Nyquist theorem, the F_S must be at least the double of the frequency of interest. However, it is recommended that F_S be ten times over the cut-off frequency; hence,

$$F_S = 20hf \tag{6.13}$$

The techniques to design an IIR filter can be found in the open literature, e.g. [Parks and Burrus 1987], [Madisetti 2010].

6.2.3 Process flowchart of the proposed TSE methodology

Fig. 6.4 shows the flowchart for the solution process of the proposed methodology. The first step is the design of the optimal measuring system. A method in the time domain to find the optimal measuring system has been described in Section 5.2.2.1. Once measuring system is defined, the second step is to define the inverse measurement matrix using (6.2) and (6.10). The design of the optimal measuring system and the inverse measurement matrix are previous conditions to run the iterative section shown in Fig. 6.4 to find the solution for the TSE assessment.

The iterative process starts setting the sample counter k to 1. Then, a measurement $\boldsymbol{z}[k]$ is taken from the power network. The measurement is contaminated by noise; hence, the IIR filter defined by (6.11) is applied. The first estimation is generated after M measurements. Please notice that the initial state is determined by the first and second samples. The iterative process continues until N samples are processed.

After state variables are determined, the dependent variables are computed. The fault location must be identified. A systematic procedure to identify the fault location is given as follows:

The rms voltage during the pre-disturbance time interval and the rms voltage during the transient time interval of voltages per phase at all busbars are compared. The location, where the maximum difference is detected will be a good indication of the fault occurrence. Because there are different voltage areas in a power system, this difference is redefined as,

$$T_i = \left(V_{pf} - V_{tr}\right)/V_{pf} \tag{6.14}$$

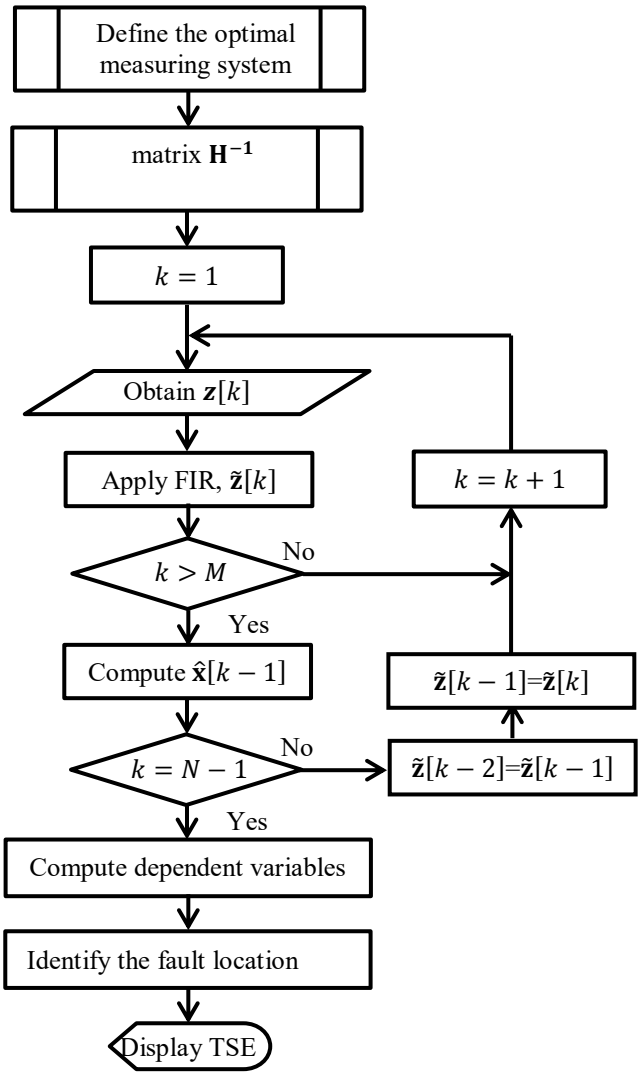

Fig. 6.4 Transient state estimation flowchart

6.3 Test systems

6.3.1 Modified IEEE 14-bus test system

The modified IEEE 14-bus test system is proposed to validate and compare the previous case studies of TSE assessment. Fig. 6.5 shows the single line diagram of such test system where the best placement of measuring devices is indicated. Their parameters are reported in [IEEE 2016] where base values of 100MVA and 230KV are assumed. However, for unbalanced cases, the zero sequence data given in Appendix A are needed.

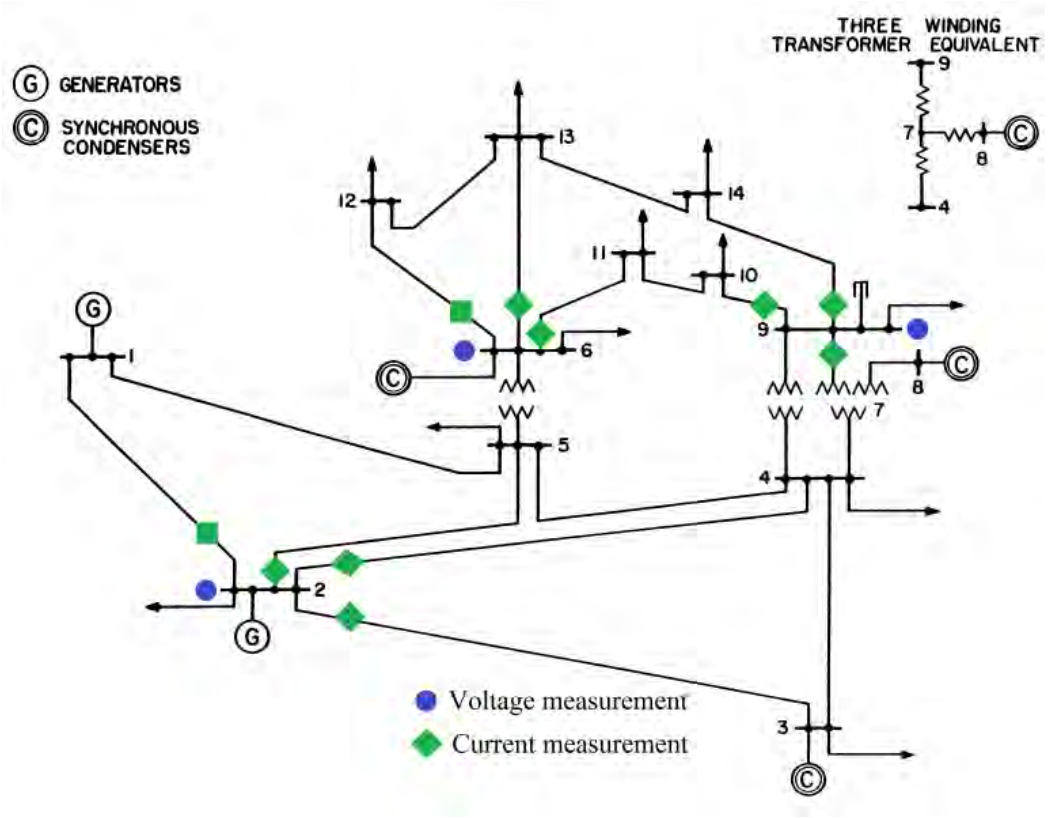

Fig. 6.5 Modified IEEE 14-bus [IEEE 2016]

6.3.2 Modified New Zealand test system

The 11 kV distribution network of New Zealand is the test system used to validate as well as to compare the proposed methodology to previous case studies for TSE assessment. Fig. 6.6 shows the single line diagram of such test system where the best placement of measuring devices is indicated. Their positive and zero sequence parameters are reported in [Watson and Farzanehrafat 2014].

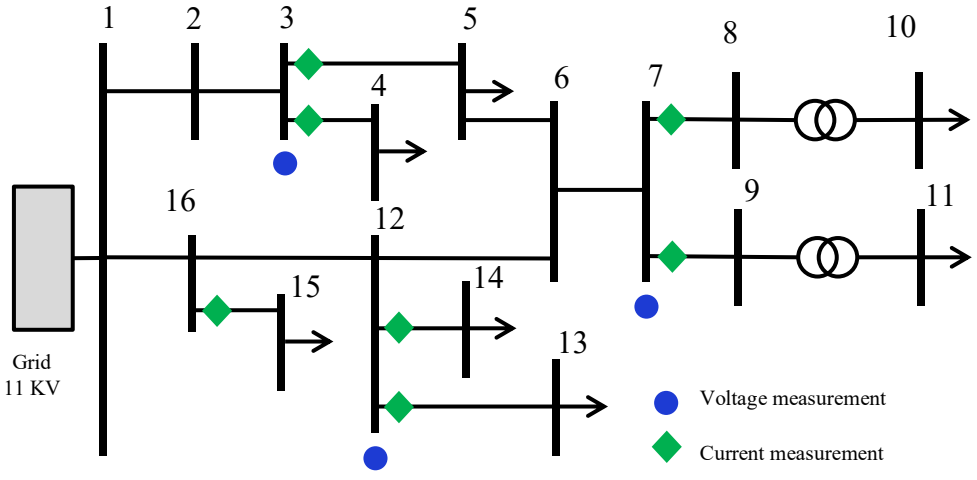

Fig. 6.6 New Zealand distribution network [Watson and Farzanehrafat 2014]

6.4 Results

6.4.1 Saving resources

The main objective in this case study is to evaluate the saving resources in the instrumentation of the power system when an optimal measuring system is implemented to obtain full observability.

6.4.1.1 *Measuring system for the modified IEEE 14-bus test system*

By applying (5.19) to the test system shown in Fig. 6.5 and considering the busbar 7 as a ZIB, the resulting instrumented busbars to obtain full observability are 2, 6, and 9 as indicated in Fig. 6.5. As expected, this result agrees with those obtained in [Mahdi et al. 2011], [Saha et al. 2012], [Mahari and Seyedi 2013].

To compare the efficiency of the measuring devices placement shown in Fig. 6.2 against the case reported in [Cisneros-Magaña and Medina 2013] the saving index is used. Using (6.11), the saving index is computed. The detailed data is given in Table 6.1. Using the proposed methodology the saving index is improved from 0.18 to 0.35, i.e. the resources are 94% more efficient respect to the case reported in [Cisneros-Magaña and Medina 2013].

Table 6.1 Comparative between proposed and prior placements [Cisneros-Magaña and Medina 2013]

Item	[Cisneros-Magaña and Medina 2013]	Proposed
No. of measurements	33	39
No. of communication channels	5	3
Estimated busbar voltages	30	42
Saving index	**0.18**	**0.35**

6.4.1.2 *Measuring system for modified New Zealand distribution test system*

By applying (5.19) to the test system shown in Fig. 6.6 and considering the busbar 2, 3, 6, 7, 9, 12, and 15 as ZIBs, the resulting instrumented busbars to obtain full observability are 3, 7, 12 and 15 as shown in Fig. 4(*b*).

This placement configuration is compared against the case reported in [Watson and Farzanehrafat 2014]. The comparison criterion is the saving index. By using (6.11), the saving index is computed. The detailed data is given in Table 6.2. Please note that using the proposed methodology, the resulting number of communication channels has been reduced from 6 to 4. The saving index is increased from 0.18 to 0.35, i.e. the resources are optimised around 81% more than the case reported in [Watson and Farzanehrafat 2014].

Table 6.2 Comparative between proposed and prior placements [Watson and Farzanehrafat 2014]

Item	[Watson and Farzanehrafat 2014]	Proposed
No. of measurements	36	30
No. of communication channels	6	4
Estimated busbar voltages	48	48
Saving index	**0.22**	**0.4**

6.4.2 Filtering process

The main objective of case study is to show the performance of the IIR filter implemented to mitigate the noise in the measurements. According to (6.12) and considering $h = 50$ and $f = 50$, the sampled frequency is $F_S = 50{,}000$ samples per second; thus, the maximum measurable frequency is 25,000 Hz. Then, the cut-off frequency corresponding to the maximum frequency of interest is 2,500 Hz which is ten times less than $F_S/2$. The order of IIR filter has been set to $M - 1 = 5$.

The reference values for the test systems shown of Fig. 6.5 and Fig. 6.6 have been taken from simulations using SimPowerSystems toolbox of Simulink®. In both test systems, a transient is caused through the application of a short-circuit on phase A at busbar 5. The measurements taken from the simulation are contaminated by adding noise with normal distribution where the maximum deviation is 5%. Fig. 6.7 shows the noisy three-phase voltage measurement at busbar 2 in the modified IEEE 14-bus test system of Fig. 6.5.

By using (6.12), the noisy measurements have been filtered; the corresponding filtered measurements are shown in Fig. 6.8. The RMSD is used to compare the noise in noisy and filtered waveforms. The noise level in filtered measurements has been reduced from 5 to 0.5%, approximately.

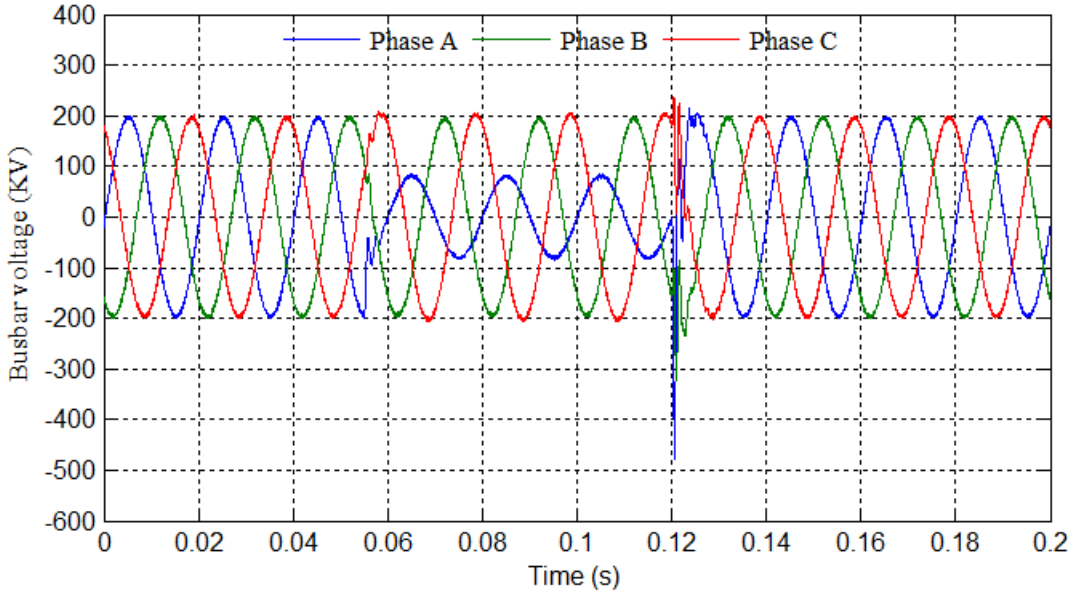

Fig. 6.7 Noisy voltage at busbar 2 in the modified IEEE 14-bus test system

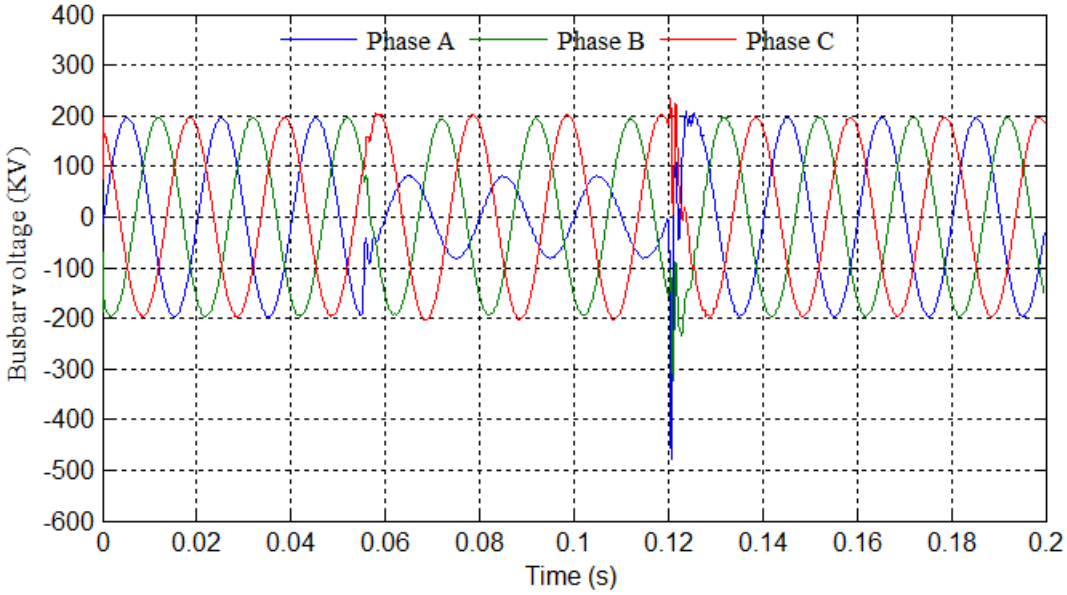

Fig. 6.8 Filtered voltage at busbar 2 in the modified IEEE 14-bus test system

6.4.3 Evaluation of the TSE under an asymmetric fault

The main objective of this case study is to estimate the TSE at unmonitored busbars and by inspection of the busbars, to identify the cause of the transients.

6.4.3.1 *TSE assessment using the modified IEEE 14-bus test system*

A case of a short-circuit fault in phase A of busbar 5 is evaluated and the results are compared against those obtained with SimPowerSystems tool of Simulink®. The short-circuit fault starts at 0.055 s and ends at 0.12 s, causing a long transient. Using (6.2) and (6.8) for the filtered measurements taken according Fig. 6.5, 13 three-phase busbar voltages can be determined. Using (5.15), (5.16), (5.17), and considering busbar 7 as ZIB, the voltage at busbar 8 is estimated.

The TSE assessments for phases A, B and C at unmonitored busbar 5 are shown in Fig 6.9(*a*), 6.9(*b*) and 6.9(*c*), respectively. Variations on phase A affect phases B and C due to magnetic coupling can be observed. An important issue in power quality analysis is to determine the maximum variations in current and voltage that can damage some electrical network component as well as the activation of protections. Fig. 6.9(*d*), 6.9(*e*), and 6.9(*f*) show that the maximum variations occur between 0.118 and 0.126 s. The peak voltage in phase A is $-1{,}012$ KV which presents an error of 1.1% when is compared against the simulated value.

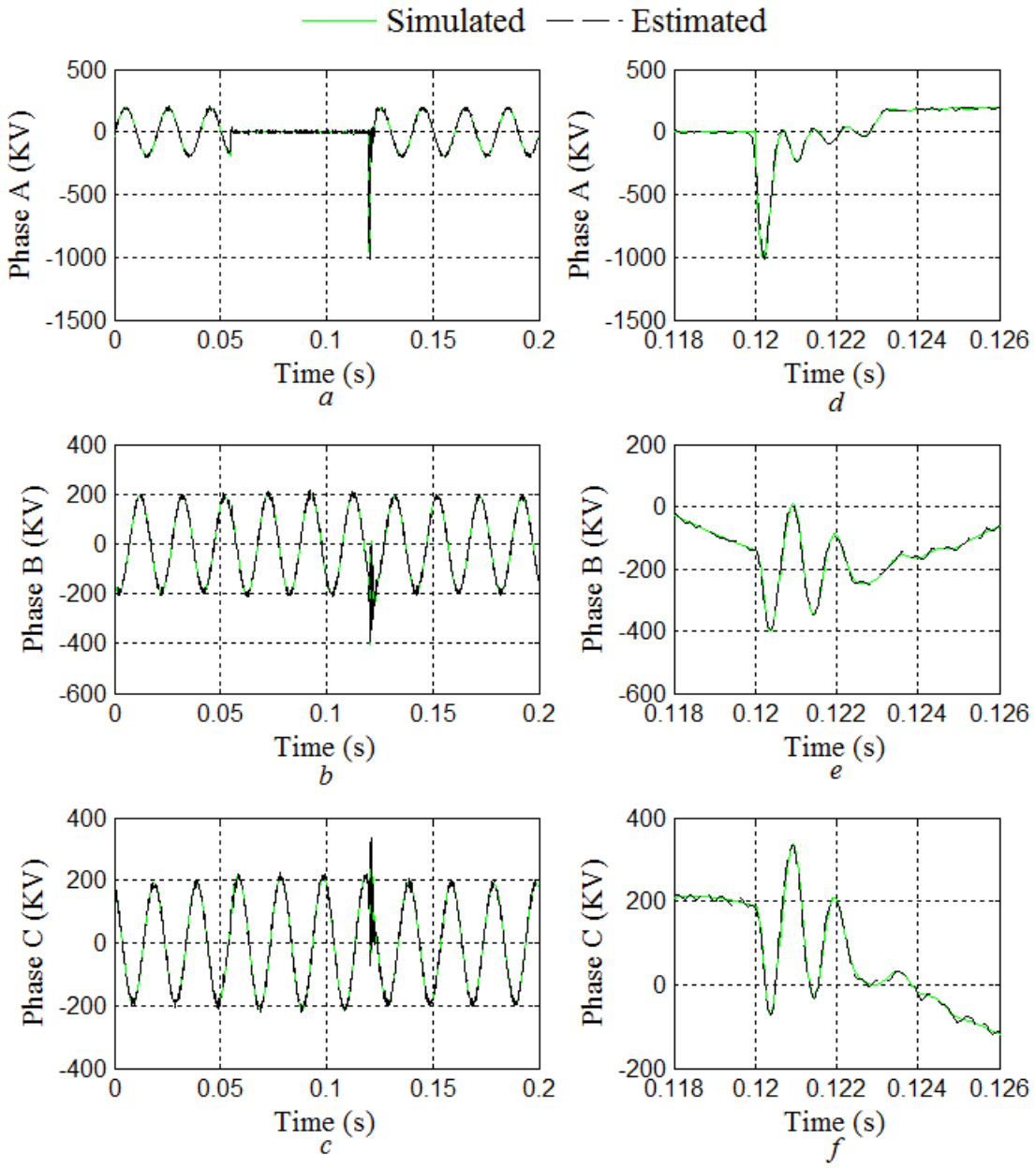

Fig. 6.9 Proposed TSE at busbar voltage 5 in the 14-bus test system. The completed time intervals under study are shown in (*a*), (*b*), and (*c*) while, the details of transients are shown in (*d*), (*e*) and (*f*)

The main objective of TSE assessment is to identify the fault location. Each busbar is divided in three nodes, e.g. the busbar 1 is formed by nodes 1, 2, and 3; busbar 2 by nodes 4, 5, and 6 and so on. Using (6.13), the T_i for each node voltage is computed. Fig. 6.10 shows the resulting forty two indices. The maximum T_i is 0.9556 corresponding to node 13 (phase A of busbar 5). Then, it can be estimated that the fault location occurred in phase A of busbar 5.

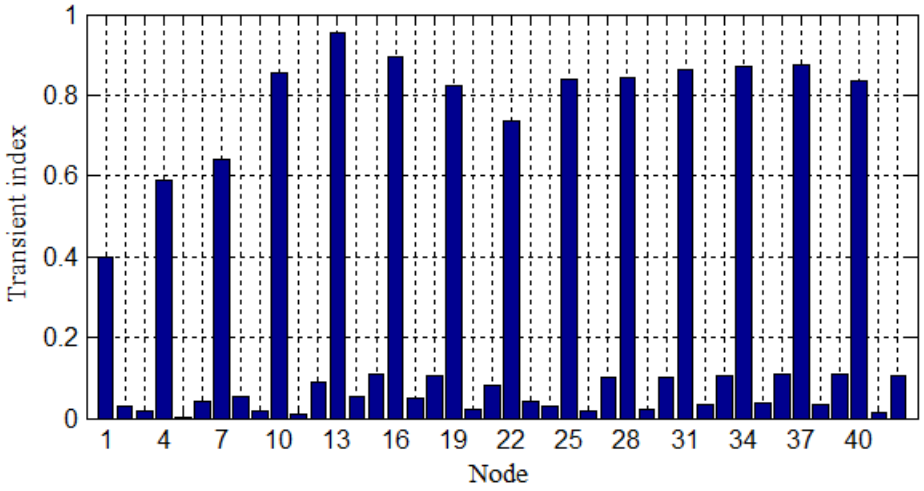

Fig. 6.10 Fault location in the 14-bus test system by using the $\boldsymbol{T_i}$

6.4.3.2 *TSE assessment using the modified New Zealand test system*

The conditions for the modified New Zealand test system are similar to these of modified IEEE 14-bus test system. By applying the proposed methodology, the busbar voltages are estimated. For illustrative purposes, the estimated busbar voltages at unmonitored busbars 5, 11, and 16 are shown in Fig. 6.11, 6.12 and 6.13, respectively.

Fig. 6.11 shows the three-phase TSE assessment per phase at unmonitored busbar 5. Fig 6.11(*a*), 6.11(*b*) and 6.11(*c*) show the TSE assessment in phases A, B, and C, respectively. It can be observed how variations on phase A affect to phases B and C due to magnetic coupling. Figs. 6.11(*d*), 6.11(*e*), and 6.11(*f*) show in detail maximum variations occur between 0.11 and 0.14 s. For this case, the selected node voltages do not present significant peak values. Please observe the agreement between the results obtained by the proposed methodology (estimated) and those obtained by SimPowerSystems toolbox of Simulink® (simulated). The estimated error is around 0.01%.

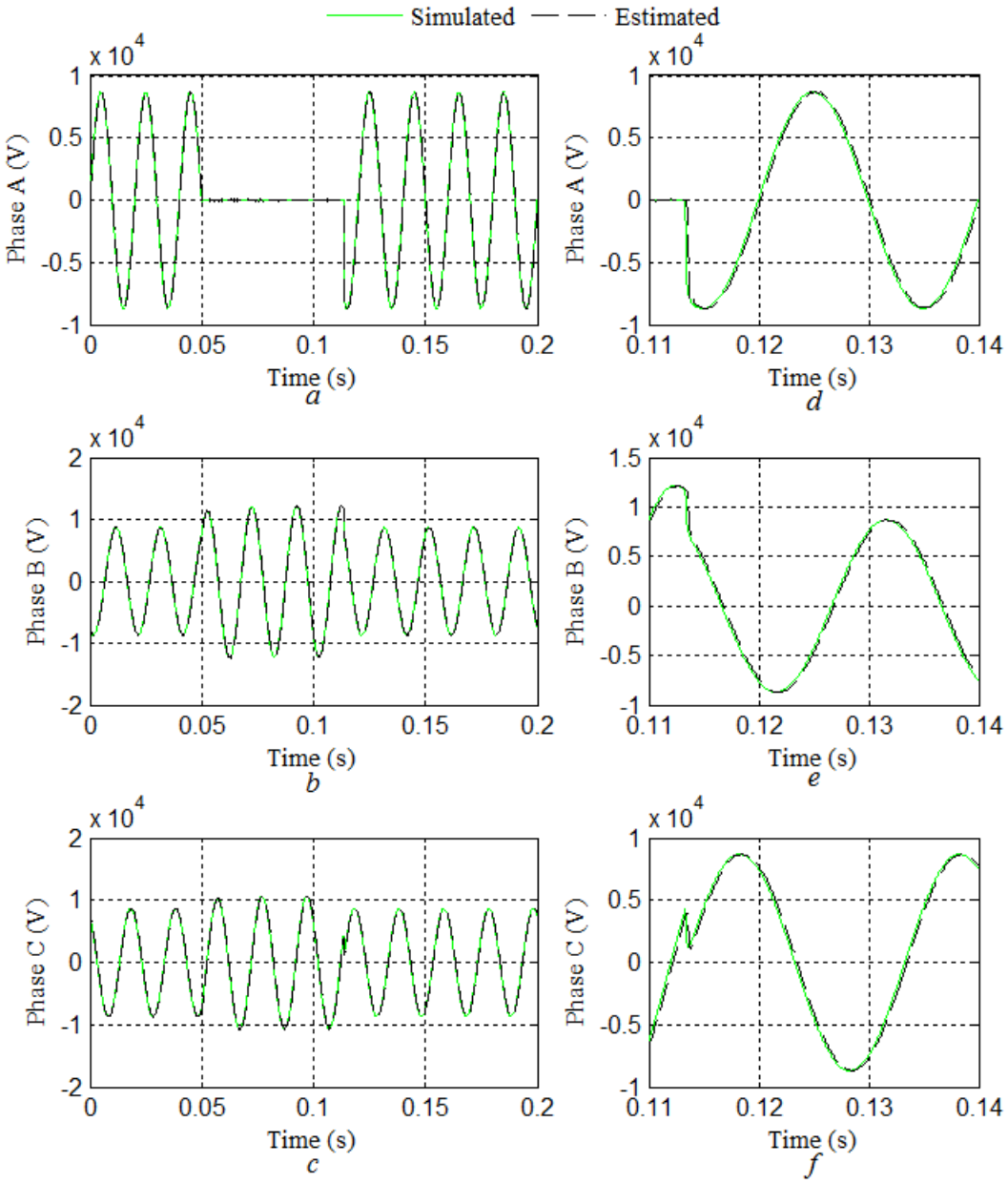

Fig. 6.11 Proposed TSE at busbar voltage 5 in the 16-bus test system. The completed time intervals under study are shown in (*a*), (*b*), and (*c*) while, the details of transients are shown in (*d*), (*e*) and (*f*).

Fig. 6.12 shows the three-phase TSE assessment at unmonitored busbar 11. Please note that this busbar is the low-voltage side of the transformer. The TSE assessment agrees well with the results obtained by SimPowerSystems toolbox of Simulink®. The estimated error is negligible, approximately 0.5%.

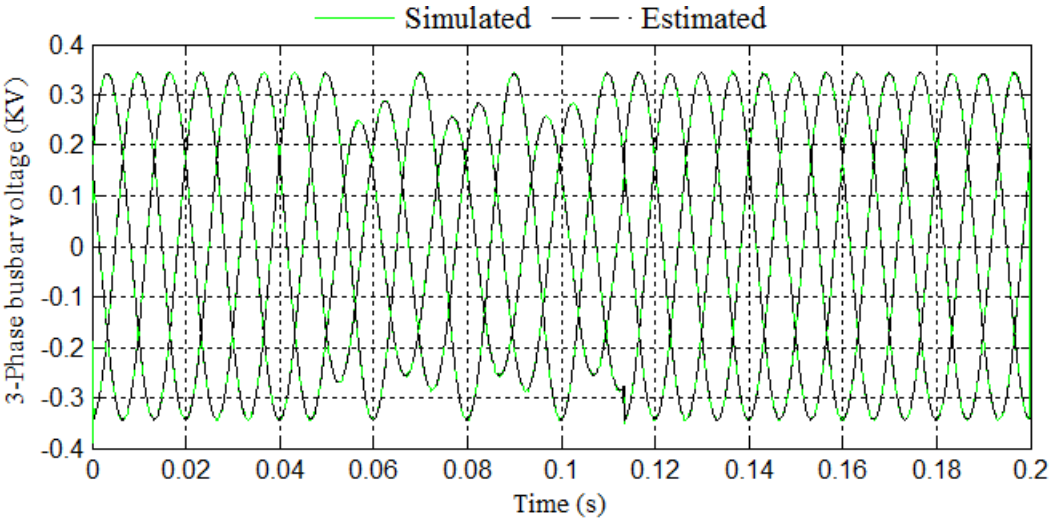

Fig. 6.12 Proposed TSE assessment in unmonitored busbar 11

The busbar 16 is only instrumented with a current meter. An additional voltage meter could be used to measure the voltage. However, using the observability rules, the voltage at busbar 16 is estimated as shown in Fig. 6.13. An excellent agreement between the estimated and the simulated responses has been obtained.

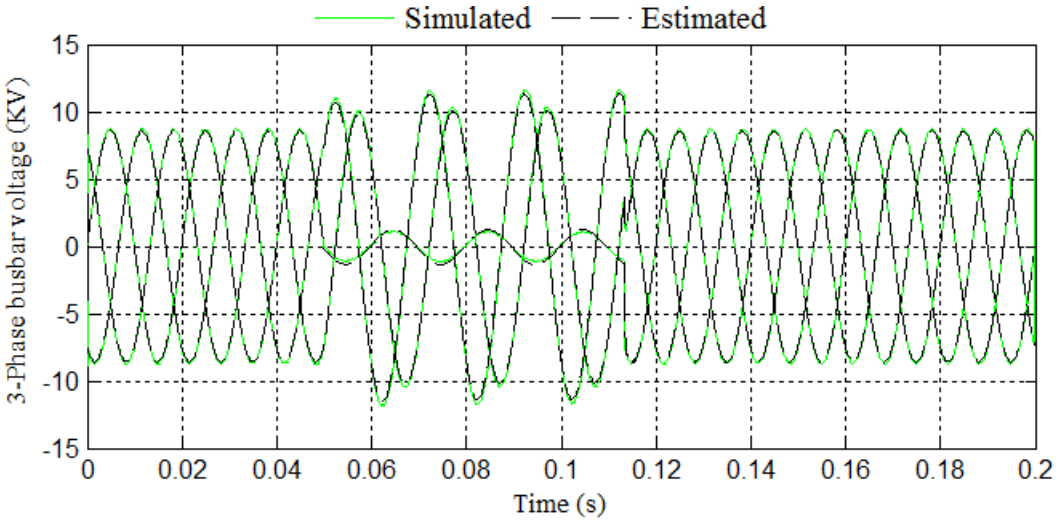

Fig. 6. 13 Proposed TSE assessment in unmonitored busbar 16

The fault location is estimated using (6.13) to obtain T_i. These indices are shown in Fig. 6.14. The maximum T_i is 0.9942 corresponding to node 13, which corresponds to phase A of busbar 5. Thus, it can be suggested that the fault location is on phase A at busbar 5.

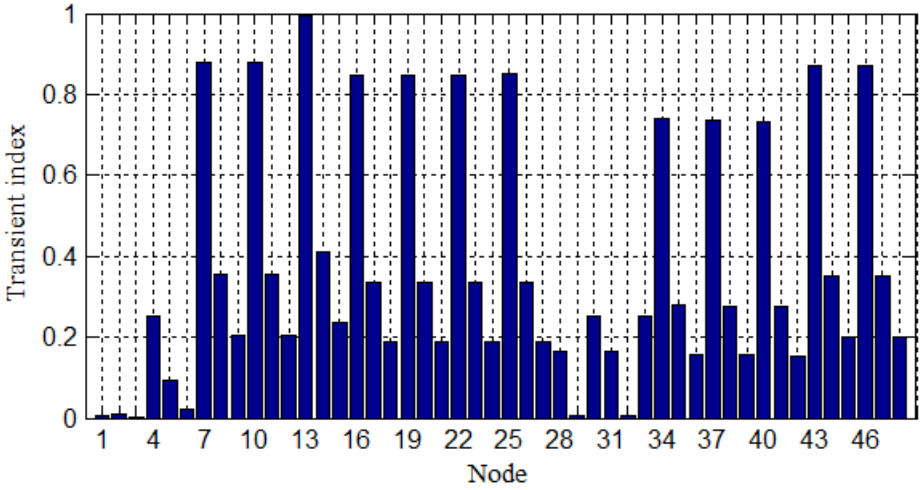

Fig. 6.14 Fault location in the 16-bus test system by using the T_i

6.5 Conclusions

A methodology based on numerical derivative methods for transient state estimation has been proposed. It does not require of a precise determination of the pre-disturbance time interval. Thus, allowing a considerable reduction in the computational effort for the TSE assessments.

A method based on time domain topological analysis to obtain the optimal number of monitoring devices for TSE assessment has been proposed. The saving index has been introduced as a criterion to compare the efficiency between two different sets of measuring systems.

The adverse effects of noisy measurement conditions in the TSE assessment have been effectively mitigated using an IIR filter.

The transient index has been introduced as a good tool to estimate the fault location. The tool has been successfully applied in two test systems.

The results obtained with the proposed TSE methodology have been successfully validated through direct comparison against the simulated system responses obtained with SimPowerSystems of Simulink®. A close agreement between responses has been obtained for all the analysed cases.

Chapter 7 General conclusions and future research

7.1 General conclusions

This thesis has reported innovative time domain power quality state estimation.

A scale-down test system laboratory set-up has been developed to conduct research in the field of estimation of energy quality. The prototype incorporates linear and nonlinear loads to conduct studies in the harmonic state estimation field.

The time domain harmonic state estimation based on the Kalman filter and using partial experimental measurements has been proposed. The methodology can properly estimate the harmonic state in a power network under balanced and unbalanced operation conditions.

A method to find the steady-state solution using the Kalman filter has been proposed. Hence, the computational effort to determine the initial state is considerably reduced.

A methodology based on numerical derivative methods to estimate the time domain harmonic state in power systems has been proposed, which does not require of an initial state. The methodology accuracy is increased when redundant measurements are added to the measuring system.

The half-wave symmetry in voltage and current waveforms has been exploited to reduce the computational effort necessary to achieve the TDHSE solution since only half cycle is processed instead of a complete cycle.

A method based on topological analysis to determine the optimal number of monitoring devices to obtain full observability in the time domain has been proposed. In addition, an index named saving index has been introduced as a criterion to compare the efficiency between two different sets of measuring systems.

A methodology based on numerical derivative methods to estimate the transient state has been proposed. The methodology does not require having knowledge of steady state to establish the pre-disturbance time interval, which reduces the computational effort needed to achieve the steady state solution. In addition, the methodology has introduced an index named transient index as a good tool to identify the fault occurrence.

7.2 Future research

In reference to the research work reported in this thesis, the author proposes the following directions for future research:

1) An experimental 5-bus test system laboratory set-up has been developed. The measurements have been taken through a digital oscilloscope. However, the number of channels is limited to four. Another disadvantage is the fact that digital oscilloscopes do not storage data during an interval time. Therefore, a solution for these disadvantages is to incorporate power quality meters to the experimental test system. Power quality meters can capture and store current and voltage waveforms, i.e. in the time domain. Hence, these measurements can be used to conduct HSE and TSE assessment in the time domain.

2) The OPAL-RT equipment offers the industry's most complete, open and highest-performance real-time digital simulation solution for power systems. The OPAL-RT equipment can be used together with the experimental 5-bus test laboratory set-up to conduct research in real-time. Hence, the natural next step can be to develop the methodologies for time domain HSE and TSE in real-time.

3) Time domain HSE and TSE have been conducted in this research work. Another way to continue this research is to extend the developed methodologies to the field of voltage sag state estimation (VSSE) since sag can be considered a kind of transient.

4) Renewable wind power has become important, being an alternative to reduce or substitute the conventional electrical generation sources. The number of wind farms has been increasing in the world. Increased penetration of wind power introduces adverse conditions such as: loss of synchronism, voltage collapse, load shedding, large deviations in voltage and/or frequency, introducing flicker and harmonics, high transmission and distribution losses, over loading and increased power oscillation. Hence, it is important to incorporate wind generation to power system and to apply the developed methodologies to HSE and TSE assessment under wind power generation. There is a wind turbine module available in laboratory; so, it is feasible to incorporate this module to the developed experimental test system to conduct research in this issue.

5) Incorporate the effect of renewable energy sources to power quality state estimation studies (HSE, TSE, and VSSE) off-line and real-time.

6) Validate the proposed methodologies using power test systems larger than ones used in this research work in order to verify its robustness.

Appendices

A. Verification of parameters of the experimental 5-bus test system

The experimental 2-bus test system, shown in Fig. A.1, is assembled in the laboratory and simulated using OrCAD® 17.2-2016 Lite which is free software [OrCAD 2016].

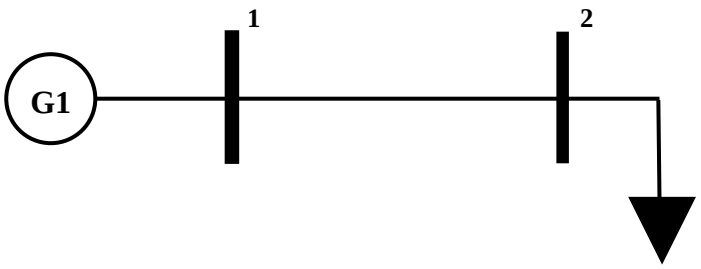

Fig. A.1 Basic 2-bus test system

A.1 Simulated response

The equivalent circuit for the basic 2-bus test system to be simulated in OrCAD® is shown in Fig. A.2. Please note that parameters found in Section 2.3.1 are used. The nodal voltage for the synchronous generator is set to 120 V (V_p=169.7 V) with $f = 60$ Hz. The simulated response is shown in Fig. A.3. From Fig. A.3, the phasor voltages at nodes 1 and 2 are obtained, which are given in Table A.1. As expected, there is a voltage drop across each series impedance since the system has no voltage compensation.

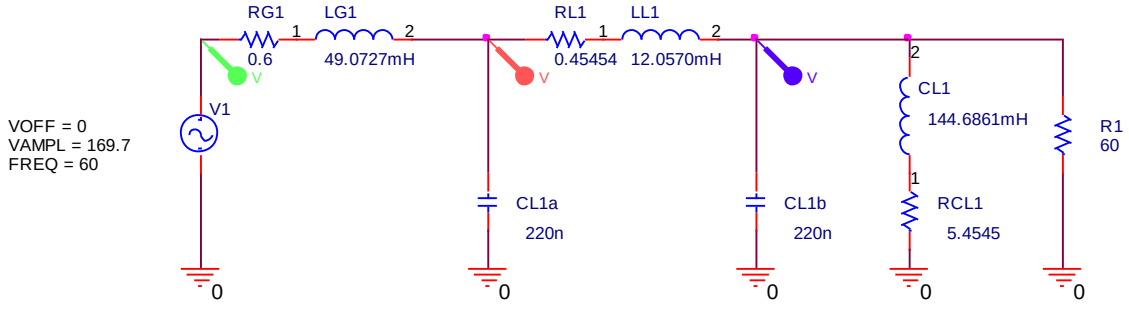

Fig. A.2 Equivalent circuit for basic 2-bus test system

Table A.1 Simulated node voltages

Node	Peak value	Rms value
1	124.3 V	$87.8\,\text{V} \angle -11.8°$
2	113.8 V	$80.4\,\text{V} \angle -15.8°$

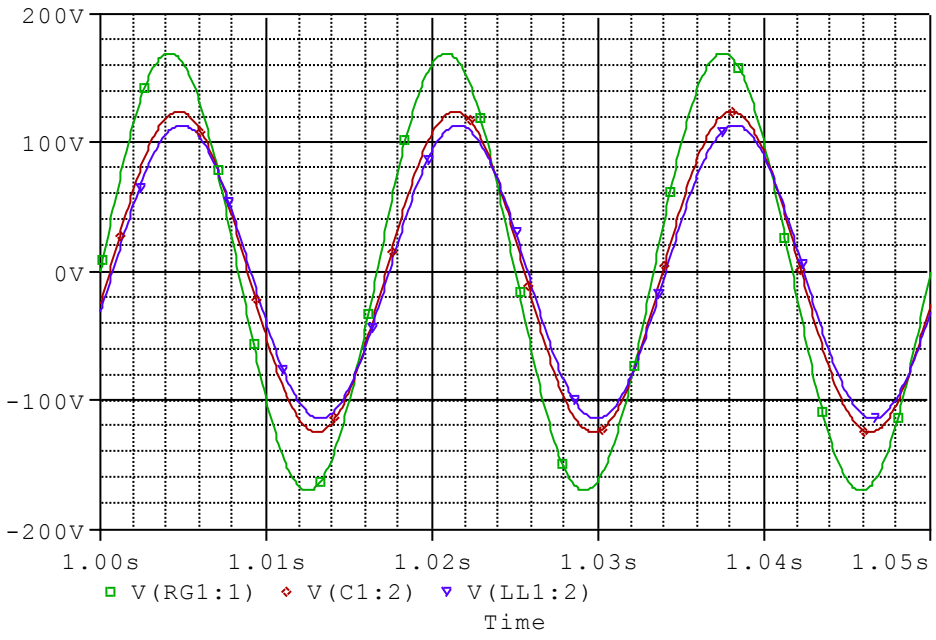

Fig. A.3 Simulated response for the basic 2-bus test system

A.2 Experimental response

Since it is not possible to measure the internal generator voltage, i.e. behind the synchronous reactance, the reading is taken in open circuit condition. Fig. A.4 shows the terminal generator voltage in open circuit condition. The excitation current is set to 0.8A to generate a peak voltage around of 170V. The frequency is maintained to 60 Hz.

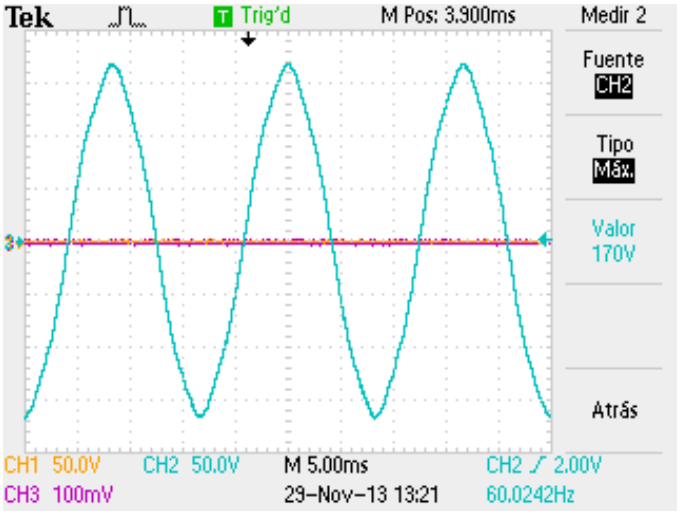

Fig. A.4 Experimental terminal generator voltage in open circuit condition

The generator is then charged through the transmission line according to the power network of Fig. A.1 The line current and voltages at nodes 1 and 2 are measured using the digital oscilloscope. The results are shown in Fig. A.5. Table A.2 summarises and compares the simulated and the experimental responses. The maximum error is 4.3 % which is within the manufacturer specifications set to +/- 5 %.

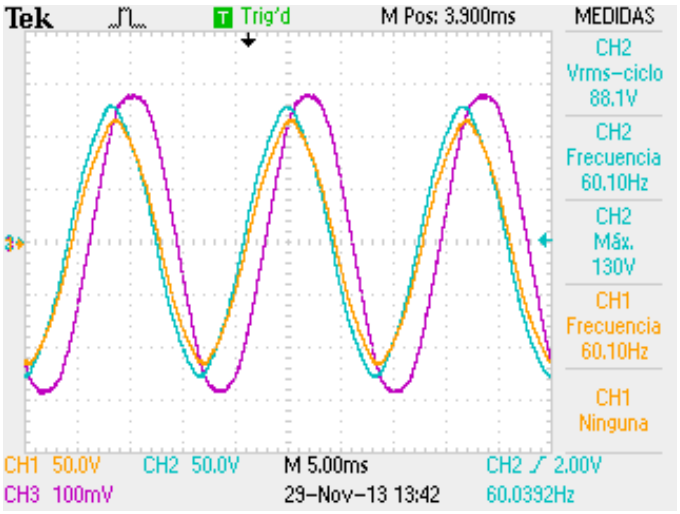

Fig. A.5 Measurements taken from basic 2-bus test system

Table A.2 Error for the experimental basic 2-bus test system response

Variable	**Simulate values**	**Experimental values**	**Error (%)**
V_1	124.1 V	130 V	3.4
V_2	113.8 V	118 V	4.3
I_{1-2}	2.94 A	2.84 A	3.5

B. Parameter data for IEEE 14-bus system

The analysis of three phase power networks under unbalanced operation condition requires of zero sequence data. Table B.1 shows the zero sequence data for the modified IEEE 14-bus data.

Table B.1 Zero sequence parameter for modified 14-bus test system

Line	R_0	L_0
1–2	0.048450	0.147925
1–5	0.135075	0.557600
2–3	0.117475	0.494925
2–4	0.145275	0.440800
2–5	0.142375	0.434700
3–4	0.167525	0.427575
4–5	0.033375	0.105275
4–7	0	0.209120
4–9	0	0.556180
5–6	0	0.252020
6–11	0.237450	0.497250
6–12	0.307275	0.639525
6–13	0.165375	0.325675
7–8	0	0.440375
7–9	0	0.275025
9–10	0.079525	0.211250
9–14	0.317775	0.675950
10–11	0.205125	0.480175
12–13	0.552300	0.499700
13–14	0.4227325	0.870050

References

[Abbas *et al*. 2012]

Abbas Ketabi, A., Reza, M., Nosratabadi, S.: 'Power quality meters placement using seeker optimization algorithm for harmonic state estimation', *Int. J. Elect. Power Energy Syst.*, Jan., 2012, **1**, (43), 141–149

[Abur and Exposito 2004]

Abur A., Exposito A. G., *Power System State Estimation: Theory and Implementation,* Marcel Dekker, USA, 2004.

[Acha and Madrigal 2001]

Acha E., Madrigal M., *Power Systems Harmonics Computer Modelling and Analysis,* John Wiley & Sons, 2001.

[Almeida and Kagan 2013]

Almeida, C., Kagan, N.: 'Harmonic state estimation through optimal monitoring systems', *IEEE Trans. Smart Grid*, 2013, **4**, (1), pp. 467–478

[Arefi *et al.* 2011]

Arefi A., Haghifam M.R., Fathi S.H., *Observability analysis of electric networks considering branch impedance*. International Journal of Electrical Power and Energy Systems, vol. 33, No. 4, May 2011, pp. 954-960.

[Arrillaga *et al.* 2000]

Arrillaga J., Watson N. R., Chen S., *Power System Quality Assessment,* John Wiley & Sons 2000.

[ATP 2002]

Prikler L., Hoidalen H. K., *ATPDRAW version 3.5 Users' Manual*, October 2002.

[Beides and Heydt 1991]

Beides H. M., Heydt G. T., *Dynamic state estimation of power system harmonics using Kalman filter methodology,* IEEE Trans. on Power Delivery, vol. 6, No. 4, Oct. 1991, pp. 1663-1670.

[Burden and Fires 2011]

Burden, R., Fires, J.: 'Numerical Analysis' (CENGAGE Learning, 2011 9th edn.)

References

[Chang *et al.* 2004]

Chang G., Hatziadoniu C., Xu W., Ribeiro P., Burch R., Grady W.M., Halpin M., Liu Y., Ranade S., Ruthman D., Watson N, Ortmeyer T., Wikston J., Medina A., Testa A., Gardinier R., Dinavahi V., Acram F., Lehn P., *Modeling Devices With Nonlinear Voltage-Current Characteristics for Harmonic Studies,* IEEE Trans. on Power Delivery, vol 19, No. 4, Oct. 2004, pp. 1802-1811.

[Chen *et al.* 2010]

Chen C.I., Chang, G.W., Hong R.C., Li H.M., *Extended real model of Kalman filter for time varying harmonic estimation,* IEEE Trans. on Power Delivery, vol. 25, No. 1, Jan. 2010, pp. 17-26.

[Cisneros-Magaña and Medina 2013]

Cisneros-Magaña R, Medina A., *Time domain transient state estimation using singular value decomposition Poincare map and extrapolation to the limit cycle*, Int J Electrical Power Energy Syst 2013; 53(1):810–817.

[Cisneros-Magaña *et al*. 2014]

Cisneros-Magaña, R., Medina, A., Segundo-Ramírez, J., *Efficient time domain power quality state estimation using the enhanced numerical differentiation Newton type method*, Int J of Electrical Power and Energy Systems, 2014; 63:414–422.

[Despalatovic *et al*. 2012]

M. Despalatovic, M. Jadric, B. Terzic, "Modeling of Saturated Synchronous Generator Based on Steady-State Operating Data", IEEE Trans. on Industry Applications, vol. 48 , No. 1, pp. 62-69, 2012.

[Du *et al.* 1996]

Du Z. P., Arrillaga J., Watson N. R., *Continuous harmonic state estimation of power systems,* IEE Proc. Gener., Transm. and Distrib., vol. 143, No. 4, July 1996, pp. 329-336.

[Dugan *et al.* 2002]

Dugan Roger C., McGranaghan Mark F., Santoso Surya, Wayne Beaty H., *Electrical Power Systems Quality* 2nd Edition, McGraw-Hill, 2002.

[Eldery *et al.* 2006]

Eldery, M., E., El-Saadany, E., Salama, A., *et al*.: 'A novel power quality monitoring allocation algorithm', *IEEE Trans. Power Deliv.*, 2006, **21**, (2), pp. 768–777

References

[EMTDC 2005]

EMTDC User's Guide, Manitoba HVDC Research Centre, Inc., Version 4.2.0, 4th printing, April 2005.

[EMTPTB 1981]

Electro-Magnetic Transients Program (EMTP) Theory Book, Branch of System Engineering Bonneville Power Administration, Portland, Oregon 97208-3621, USA, 1981.

[Farzanehrafat and Watson 2013]

Farzanehrafat A, Watson NR. Power quality state estimator for smart distribution grids. IEEE Trans on Power Sys 2013; 28(3):2183–2191.

[Ghahremani and Kamwa 2011]

Ghahremani E., Kamwa I., *Dynamic State Estimation in Power System by Applying the Extended Kalman Filter With Unknown Inputs to Phasor Measurements*, IEEE Trans. On Power Syst., vol. 26, no. 4, Nov. 2011, pp. 2556-2566.

[Grainger and Stevenson 1996]

Grainger John J., Stevenson William D., *Power System Analysis,* McGraw-Hill, 1996.

[Grewal and Andrews 2001]

Grewal M. S., y Andrews A.P., *Kalman Filtering: Theory and Practice using Matlab,* Second Edition, John Wiley & Sons, 2001.

[Gou 2008]

Gou, B.: 'Optimal Placement of PMUs by Integer Linear Programming', *IEEE Trans. Power Syst*., 2008, **23**, (3), pp. 1–2

[Hajian *et al.* 2011]

Hajian M., Ranjbar A.M., Amraee T., Mozafari B., *Optimal placement of PMUs to maintain network observability using modified BPSO algorithm*. International Journal of Electrical Power and Energy Systems, vol. 33, No. 1, January 2011, pp. 28-34.

[Heydt 1989]

Heydt G. T., *Identification of harmonic sources by a state estimation technique*, IEEE Trans. on Power Delivery, vol. 4, No. 1, Jan. 1989, pp. 569-576.

References

[Hoffman 2001]

Hoffman J.: 'Numerical Methods for Engineers and Scientists', (Marcel Dekker, Inc., 2001, 2nd edn.)

[IEEE 1992]

IEEE Recommended Practices and Requirements for Harmonic Control in Electrical Power Systems, IEEE Std. 519.

[IEEE 1995]

IEEE Recommended Practice for Monitoring Electric Power Quality, IEEE Std. 1159.

[IEEE 1996a]

Task Force on Harmonics, and Simulation, Modeling and simulation of the propagation of harmonics in electric power networks part I: concepts, models, and simulation techniques, IEEE Trans. on Power Delivery, 1996; 11: 452-465.

[IEEE 1996b]

Task Force on Harmonics, and Simulation, Modeling and simulation of the propagation of harmonics in electric power networks part II: sample systems and examples, IEEE Trans. on Power Delivery, 1996; 11 : 466-474.

[IEEE 2016]

IEEE Test Systems, Power Systems Test Case Archive.
http://www.ee.washington.edu/research/pstca
Accessed: February 20, 2017.

[Jeffrey 2010]

Jeffrey, A.: 'Matrix Operations for Engineers and Scientists: An Essential Guide in Linear Algebra' (Springer, 2010 1st edn.)

[Ketabi *et al*. 2011]

Ketabi A, Sheibani M R, Nosratabadi S M. Power quality meters placement using seeker optimization algorithm for harmonic state estimation. Electrical Power and Energy Systems 43 (2012) 141–149.

[Korres *et al*. 2014]

Korres, G., Manousakis, N., Xygkis, T., *et al*.: ' Optimal phasor measurement unit placement for numerical observability in the presence of conventional measurements using semi definite programming', *IET Gener. Transm. Distrib*., 2015, **9**, (15), pp. 2427–2436

References

[Koutsoukis *et al.* 2013]

Koutsoukis, N., Manousakis, N., Georgilakis, P., *et al.*: 'Numerical observability method for optimal phasor measurement units placement using recursive Tabu search method', *IET Gener. Transm. Distrib.*, 2013, **7**, (3), pp. 347–356

[Kundur 1994]

Kundur, P., *Power System Stability and Control,* McGraw-Hill, California, 1994.

[Kusko and Thompson 2007]

Kusko A., Thompson, M.T., *Power Quality in Electrical Systems,* McGraw-Hill, California, 2007.

[Farach et al. 1993]

Farach JE, Grady WM, Arapostathis A. An Optimal Procedure for Placing Sensors and Estimating the Locations of Harmonic Sources in Power Systems. IEEE Trans on Power Del. Vol 8 No.3 1993 pp 1303–1310.

[Festo 2015]

© 2015 Festo Didactic Inc

https://www.labvolt.com/solutions/6_electricity_new_energy/98-8013-00_2_kw_

Accessed: November 18, 2016.

[Ma and Girgis 1996]

Ma H. and Girigs A. A., *Identification and tracking of harmonic sources in a power system using a Kalman filter,* IEEE Trans. on Power Delivery, vol. 11, No. 3, 1996, pp. 1659-1665.

[Madisetti 2010]

Madisetti VK. Digital Signal Processing Fundamentals. 2nd ed. CRC Press; 2010.

[Madtharad *et al.* 2005]

Madtharad C., Premrudeepreechacharn S., Watson N. R., Saeng-Udom R., A*n Optimal Measurement Placement Method for Power System Harmonic State Estimation,* IEEE Trans. on Power Delivery, vol. 20, No. 2, April 2005, pp. 1514-1421.

References

[Mahdi et al. 2011]

Mahdi H, Ali MR, Turaj A, Babak M. Optimal placement of PMUs to maintain network observability using a modified BPSO algorithm. Int J Electrical Power Energy Syst 2011; 33(1):28–34.

[Mahari and Seyedi 2013]

Mahari, A., Seyedi H.: 'Optimal PMU placement for power system observability using BICA, considering measurement redundancy', *Electr. Power Syst. Res*., 2013, **103**, (1), pp. 78–85

[Matair *et al.* 2000]

Matair S. S., Watson N. R., Wong K. P., Pham V. L., Arrillaga J., *Harmonic state estimation: a method for remote harmonic assessment in a deregulated utility network*, Electric Utility Deregulation and Restructuring and Power Technologies, Proceedings DRPT 2000.

[Medina and Cisneros-Magaña 2012]

Medina, A., Cisneros-Magaña, R., *Time-domain harmonic state estimation based on the Kalman filter Poincaré map and extrapolation to the limit cycle*, IET Generation, Transmission & Distribution, vol. 6, pp. 1209-1217, 2012.

[Medina *et al.* 2003]

Medina, A., Ramos-Paz, A., Fuerte-Esquivel, C.R., *Periodic Steady State Solution of Electric Systems With Nonlinear Components Using Parallel Processing*, IEEE Trans. on Power Systems, vol. 18, No. 2, May 2003, pp. 963-965.

[Meliopoulos *et al.* 1994]

Meliopoulos A. P. S., Zhang F., Zelingher S., *Power system harmonic state estimation,* IEEE Trans. on Power Delivery, vol. 9, No. 3, July 1994, pp. 1701-1709.

[Moghadasian *et al.* 2010]

Moghadasian M., Mokhtari H., Baladi A., *Power System Harmonic State Estimation using WLS and SVD*; A practical Approach, IEEE 14th Int. Conf. on Harmonics and Quality of Power, ICHQP, 2010.

[Monticelli 1999]

Monticelli A., *State Estimation in Electric Power Systems: A Generalized Approach,* Kluwer Academic Publishers, USA, 1999.

References

[Moreno *et al.* 2009]

Moreno V. M. and Pigazo A., *Kalman Filter: Recent Advances and Applications*, In-Teh, I-Tech Education and Publishing KG, Vienna, Austria, 2009.

[Müller and Castro 2016]

Müller, H., Castro, C.: 'Genetic algorithm- based phasor measurement unit placement method considering observability and security criteria', *IET Gener. Transm. Distrib*., 2016, **10**, (1), pp. 270–280

[National Instrument 2016]

GPS Synchronization Architecture for Data Acquisition Devices

http://www.ni.com/white-paper/7023/en/

Accessed: February 20, 2017.

[Nguyen *et al*. 2010]

Nguyen, H., Yang, J. Choi, S.: 'On harmonic state estimation and the evaluation of harmonic power contribution from sources', Power and Ener. Soc, Gen. Meet., Minnesota, USA, Jul 2010, pp. 1–6

[Ogata 1995]

Ogata K., *Discrete-Time Control Systems,* Prentice-Hall, 2nd Ed., 1995.

[Ogata 2002]

Ogata K., *Modern Control Engineering,* Pearson Prentice Hall, 4th Ed., 2002.

[OrCAD 2016]

Cadence Design Systems, Inc. All rights Reserved.

http://www.orcad.com/products/orcad-lite-overview

Accessed: February 20, 2017.

[Parks and Burrus 1987]

Parks TW, Burrus CS. Digital Filter Design. John Wiley & Sons; 1987.

[PSCAD 2005]

Pscad User's Guide, Versión 4.2.0, Manitoba HVDC Research Centre Inc., Abril 2005.

References

[Rad *et al.* 2013]

Rad, M., Mokhtari, H., Karimi, H.: 'A new algorithm for optimal measurements placement, observability analysis and harmonic state estimation in power systems', Pow. Elect., Drive Sys. & Tech. Conf., Theran, Iran, Feb 2013, pp. 1–6

[Rakpentthai *et al.* 2013]

Rakpenthai, C., Uatrongjit, S., Watson N., Premrudeepreechacharn, S.: 'On harmonic state estimation of power system with uncertain network parameters', IEEE Trans. Power Syst., 2013, 28, (4), pp. 4828–4838

[Rashid 1993]

Rashid, H., Power Electronics: Circuits, Devices & Applications, Pearson Educations, 2nd ed. 1993, pp. 133-136.

[Rashidi 2013]

Rashidi, F., Abiri, E., Niknam T., *et al.*: 'Optimal placement of PMUs with limited number of channels for complete topological observability of power systems under various contingencies', *Int. J. Elect. Power Energy Syst.*, 2015, **1**, (67), pp. 125–137

[Ray and Subuchi 2012]

Ray, P.K., Subuchi, B., *Ensemble-Kalman-Filter-Based Power System Harmonic Estimation,* IEEE Trans. on Instrumentation and Measurement, 2012, vol. 61, No. 12, pp. 3216-3224.

[Saadat 1999]

H. Saadat, Power System Analysis, 1st ed., McGraw-Hill, 1999, pp. 189-240.

[Saini and Kapoor 2012]

Saini, MK., Kapoor, R., Classification of power quality events – A review, Electrical Power and Energy Systems, 2012; 43 : 11-19.

[Saha *et al.* 2012]

Saha Roy B.K., Sinha A.K., Pradhan A.K., *An optimal PMU placement technique for power system observability*. International Journal of Electrical Power and Energy Systems, vol. 42, No. 1, November 2012, pp. 71-77.

References

[Saxena *et al.* 2014]

Saxena, D., Bhaumik, S., Singh, S.: 'Identification of multiple harmonic sources in power system using optimally placed voltage measurement devices', *IEEE Trans. Ind. Elect*., 2014, **61**, (5), pp. 2483–492

[Segundo and Medina 2010]

Segundo-Ramírez J., Medina A., A*n Enhanced Process for Fast Periodic Steady State Solution of Nonlinear Systems by Poincaré Map and Extrapolation to the Limit Cycle*, International Journal of Nonlinear Sciences & Numerical Simulation, vol. 11, No. 8, 2010, pp. 659-668.

[Semlyen and Medina 1995]

Semlyen A., Medina A., *Computation of the Periodic Steady State in Systems with Nonlinear Components Using a Hybrid Time and Frequency Domain Methodology,* IEEE Trans. on Power Systems, vol. 10, No. 3, August 1995, pp. 1498-1504.

[Stagg and El-Abiad 1968]

G. W. Stagg, A.H. El-Abiad, Computer Methods in Power System Analysis, McGraw-Hill, New York, 1968, pp. 283-312.

[Suresh 2009]

Suresh K.: 'Electric Circuits and networks', (Pearson Education, 2009, 1st edn.)

[Vilchis-Rodríguez and Acha 2009]

D. S. Vilchis-Rodriguez, E. Acha, “A Synchronous Generator Internal Fault Model Based on the Voltage-Behind-Reactance Representation”, IEEE Trans. on Energy Conversion, vol. 24, No. 1, pp. 184-194, 2009.

[Watson 2010]

Watson N. R., *Power Quality State Estimation*, European Trans. Electrical Power; vol. 20, No 1, Jan. 2010, pp. 19-33.

[Watson and Ali 2014]

Watson NR, Ali F. Three-phase transient state estimation algorithm for distribution systems. IET Generation, Transmission & Distribution 2014; 8(10):1656–1666.

[Watson & Arrillaga 2007]

Watson N. R., Arrillaga J., *Power Systems Electromagnetic Transients Simulation,* IET Power and Energy Series 39, 2007.

References

[Yu *et al.* 2005]

Yu K. K. C., Watson N. R., Arrillaga J., *An Adaptive Kalman Filter for Dynamic Harmonic State Estimation and Harmonic Injection Tracking*, IEEE Trans. on Power Delivery, vol. 20, No. 2, April 2005, pp. 1577-1584.

[Yu and Watson 2007]

Yu K. K. C., Watson N. R., *An Approximate method for Transient State Estimation*, IEEE Trans. on Power Delivery, vol. 22, No. 3, July 2007, pp. 1680-1687.